

University of Alberta

RECEIVER DESIGNS FOR MULTIUSER INTERFERENCE COMMUNICATION SYSTEMS

by

Amirmasoud Rabiei



A thesis submitted to the Faculty of Graduate Studies and Research in partial fulfillment of the requirements for the degree of **Doctor of Philosophy**.

Department of Electrical and Computer Engineering

Edmonton, Alberta

Fall 2008



Library and
Archives Canada

Bibliothèque et
Archives Canada

Published Heritage
Branch

Direction du
Patrimoine de l'édition

395 Wellington Street
Ottawa ON K1A 0N4
Canada

395, rue Wellington
Ottawa ON K1A 0N4
Canada

Your file Votre référence
ISBN: 978-0-494-46407-6
Our file Notre référence
ISBN: 978-0-494-46407-6

NOTICE:

The author has granted a non-exclusive license allowing Library and Archives Canada to reproduce, publish, archive, preserve, conserve, communicate to the public by telecommunication or on the Internet, loan, distribute and sell theses worldwide, for commercial or non-commercial purposes, in microform, paper, electronic and/or any other formats.

The author retains copyright ownership and moral rights in this thesis. Neither the thesis nor substantial extracts from it may be printed or otherwise reproduced without the author's permission.

AVIS:

L'auteur a accordé une licence non exclusive permettant à la Bibliothèque et Archives Canada de reproduire, publier, archiver, sauvegarder, conserver, transmettre au public par télécommunication ou par l'Internet, prêter, distribuer et vendre des thèses partout dans le monde, à des fins commerciales ou autres, sur support microforme, papier, électronique et/ou autres formats.

L'auteur conserve la propriété du droit d'auteur et des droits moraux qui protègent cette thèse. Ni la thèse ni des extraits substantiels de celle-ci ne doivent être imprimés ou autrement reproduits sans son autorisation.

In compliance with the Canadian Privacy Act some supporting forms may have been removed from this thesis.

Conformément à la loi canadienne sur la protection de la vie privée, quelques formulaires secondaires ont été enlevés de cette thèse.

While these forms may be included in the document page count, their removal does not represent any loss of content from the thesis.

Bien que ces formulaires aient inclus dans la pagination, il n'y aura aucun contenu manquant.


Canada

**Humbly dedicated to the Commander of the Faithful,
Imam Ali (a.s.)**

Abstract

The ever growing demand for reliable, high-speed, wireless applications entails high transmission rates as well as small outage and average error probability. However, the limited available radio spectrum makes these goals difficult to achieve. Multiuser communication is a key technology to efficiently utilize radio resources through allocating time, frequency and space resources to different users. This thesis contributes to the performance analysis of the optimal multiuser receiver and optimal multiuser diversity receiver designs, as well as the design and analysis of intersymbol interference (ISI)-controlled cochannel interference (CCI) whitening receivers.

In the first part of this thesis, exact expressions for the bit error probability (BEP) of the jointly and individually optimal detectors (JOD and IOD) in a single-interferer additive white Gaussian noise (AWGN) channel are derived. The resulting BEP expressions are intuitive as they are decomposable into the BEP of a single-user binary phase-shift keying signal in an AWGN channel plus a term due to interference. It is also shown that the JOD is sensitive to carrier phase recovery errors and that its performance can dramatically degrade due to imperfect phase recovery. This part is concluded by deriving two multiuser receiver structures for space diversity reception of a signal distorted by multiple access interference and multipath fading. The proposed receivers minimize the BEP rather than maximizing the signal-to-noise-plus-interference-ratio (SINR), as does the optimum combining receiver.

The second part of this thesis focuses on the problem of CCI suppression using inter-

ference whitening in multiuser communication systems. It is shown that CCI whitening in synchronous channels degrades rather than enhances the performance in contrast to previously reported results. Then, asynchronous CCI whitening in fading environments is considered and the conditions under which this receiver can be used with benefit are studied. It is shown that ISI can make the whitening receiver inferior to the conventional matched filter receiver for many practical situations. The SINR-maximizing filter (SINRMF) is also derived for the ISI-impaired and ISI-free cases. In both cases, the SINRMF is shown to be composed of a whitening receiver followed by a discrete time filter that combats ISI. The optimum transmitter filter for ISI-free and ISI-impaired systems is also derived and its superiority over conventional systems employing a standard root raised-cosine filter is illustrated.

Acknowledgments

I would like to express my gratefulness and gratitude to my God Almighty for letting me learn and for continually blessing me in the long journey of learning.

I am sincerely grateful to my thesis supervisor, Dr. Norman C. Beaulieu, for his continuous guidance, encouragement and support both in my career and personal life. Working under his supervision at the *i*CORE Wireless Communications Laboratory was a great opportunity for me to improve my intellectual capacity and to develop my interpersonal skills.

I would like to thank Dr. Marco Chiani from Università di Bologna for being willing to read my thesis and be my external examiner. Special thanks are due to Dr. Chintha Tellambura, Dr. John Doucette, Dr. Masoud Ardakani and Dr. Sergiy Vorobyov for serving as my examination committee members.

I wish to sincerely thank Sharon Walker and Pavel Loskot for being a great source of encouragement, help and support. I would also like to thank Alireza Sameny, Parastoo Oruji, Mohsen Eslami, Iman Izadi and Tim Poon for their loyalty and warm friendship over the years. They were always there to listen and to offer words of comfort and encouragement when I needed them the most.

I would like to express my sincere appreciation to David Young for his valuable help with technical and personal issues. I was always impressed by his knowledge, selflessness and his continuous willingness to help. My thanks are also expressed to Reza Nikjah and Payam Dehghani for their fruitful technical discussions, and to my wonderful friends in Edmonton who never left me alone and made my Ph.D. such a memorable experience.

I am deeply indebted to my dearest parents and my brothers and sisters who made my studies possible by their prayers, love, encouragement, and spiritual support. There

has been no blessing greater than their outpouring love and their unwavering support throughout my lifetime.

Last but not least, I would like to thank my loving wife Simin, for her patience, understanding and true love. She has brightened my life in so many ways over the few months since we have started our life journey together.

This thesis was supported by an Alberta Ingenuity Graduate Student Scholarship and an Alberta Informatics Circle of Research Excellence (*i*CORE) Graduate Studentship. I greatly appreciate their financial support.

Table of Contents

1	Introduction	1
1.1	Background	1
1.2	Thesis Outline and Contributions	3
2	Overview of Multiuser Detection	7
2.1	Signal Model	7
2.2	Matched Filter Receiver	9
2.2.1	Conventional Matched Filter Receiver	9
2.2.2	Interference-Plus-Noise Whitening Matched Filter Receiver	10
2.3	Multiuser Detection	11
2.3.1	Linear MUD	11
2.3.1.1	Decorrelating Detector	12
2.3.1.2	MMSE Detector	13
2.3.1.3	Polynomial Expansion Detector	14
2.3.2	Nonlinear MUD	14
2.3.2.1	Optimum MUD	14
2.3.2.2	Decision-Driven MUD	16
3	Performance Analysis of Jointly and Individually Optimum Receivers	19
3.1	Error Probability of a Two-User Synchronous JOD in AWGN	20
3.1.1	Signal Model	21
3.1.2	BEP Derivation	22
3.1.3	Results and Discussion	25

3.2	BER of a Two-User Synchronous IOD in AWGN	30
3.2.1	Signal Model and Receiver Structure	30
3.2.2	BER Derivation	31
3.2.3	Results	35
3.3	BER of a Bandlimited Two-User JOD With Carrier Phase Error	38
3.3.1	System Model	39
3.3.2	BER Derivation	40
3.3.3	Results and Discussion	44
4	Two Multiuser Combining Receiver Diversity Structures	48
4.1	Signal Model and Optimum Combining	49
4.2	Better Than Optimum Combining	51
4.2.1	Maximum-Likelihood Diversity Reception	52
4.2.2	Optimum Diversity Reception	55
4.3	Results and Discussions	56
5	Cochannel Interference Mitigation Using Whitening Receiver Designs in Bandlimited Microcellular Wireless Systems	62
5.1	Signal Model	64
5.2	Interference Whitening Filter	67
5.2.1	Asynchronous CCI	67
5.2.2	Synchronous CCI	70
5.2.3	Discussion	71
5.3	Derivation of the SINR-Maximizing Filter	72
5.3.1	IIR Realization	72
5.3.2	FIR Realization	74
5.4	SINR Evaluation	75
5.4.1	WMF Receiver	76
5.4.1.1	Asynchronous Channel	76
5.4.1.2	Synchronous channel	77
5.4.2	SINR-Maximizing Filter	78

5.5	Numerical Results	79
6	ISI-free Transmitter-Receiver Designs for Bandlimited Microcellular Wireless Systems	90
6.1	Optimal 100% Excess Bandwidth Signaling in Cochannel Interference . .	90
6.1.1	Signal Model	91
6.1.2	Filter Design	92
6.1.3	Numerical Results	94
6.2	ISI-Free Cochannel Interference Whitening for Bandlimited Systems . .	96
6.2.1	Signal Model and Whitening Filter	97
6.2.2	ISI-Free Transmitter-Receiver Design	98
6.2.3	ISI-Free SINR-Maximizing Receiver	100
6.2.4	Optimum Transmitter Filter Design	102
6.2.5	SINR Analysis	104
6.2.5.1	SINR Comparison	105
6.2.5.2	SINR Evaluation for the RC and BTD Pulses	106
6.2.6	Numerical Results	107
7	Conclusion and Future Work	116
7.1	Concluding Remarks	116
7.2	Suggestions for Future Work	118
	References	120
	Appendix A Proof of Fact 1	128
A.1	$\theta \in [\frac{\pi}{2}, \pi)$	128
A.2	$\theta \in [\pi, \frac{3\pi}{2})$	129
A.3	$\theta \in [\frac{3\pi}{2}, 2\pi)$	129
	Appendix B Evaluating \hat{E}_g	131
	Appendix C Evaluating the SINR of the SINRMF Receiver	133
	Vitae	135

List of Figures

2.1	The block diagram of the baseband cochannel interference communication system with $(K + 1)$ synchronous users.	8
3.1	The received signal constellation and decision boundaries for a BPSK signal with one identical cochannel interferer for $0 \leq \theta < \pi/2$	23
3.2	The BEP of the jointly optimal receiver as a function of SIR for SNR = 15 dB and various values of θ	26
3.3	The performance of the jointly optimal receiver as a function of the SIR for various values of SNR.	27
3.4	The worst case SIR as a function of SNR.	28
3.5	The performance of the jointly optimal receiver as a function of the SIR for some fixed values of INR.	29
3.6	A typical received signal constellation and the decision boundary for a BPSK signal with one similar cochannel interferer for $\rho > 0$	32
3.7	A typical received signal constellation and the decision boundary for a BPSK signal with one similar cochannel interferer for $\rho < 0$	33
3.8	The average probability of error of the IOR and JOR for $A_0 = A_1$ and $\rho = 0.99, 0.9, .5$ and 0 and $\rho = \cos \theta$ where θ is uniformly distributed over $[0, 2\pi)$	37
3.9	The multiuser efficiencies of the IOR and JOR as a function of A_1/A_0 for $\rho = \cos \theta$ where θ is uniformly distributed over $[0, 2\pi)$ and SNR = 4, 8 and 12 dB.	38

3.10	A typical received signal constellation and the corresponding decision boundaries for a BPSK signal and one identical cochannel interferer in the presence of carrier phase error for $\hat{\rho} > 0$	42
3.11	A typical received signal constellation and the corresponding decision boundaries for a BPSK signal and one identical cochannel interferer in the presence of carrier phase error for $\hat{\rho} < 0$	43
3.12	The worst case SIR as a function of $ \rho $ for different SNR values.	44
3.13	The JOD receiver's BER as a function of SIR for various values of $\hat{\theta}_0$ and $\hat{\theta}_1$, SNR = 12 dB, $\theta = 45^\circ$ and $\mu = 1$	45
3.14	The receiver's BER as a function of $\hat{\theta}_0$ for SNR = 12 dB, $\theta = 45^\circ$, $\mu = 1$ and SIR = -10 dB.	46
3.15	The receiver's BER as a function of $\hat{\theta}_0$ for SNR = 12 dB, $\theta = 45^\circ$, $\mu = 1$ and SIR = 10 dB.	47
4.1	The system model of the baseband received signal at the m th element of the antenna array.	50
4.2	The block diagram of the ML diversity receiver with $(K + 1)$ users and M receiver antennas.	54
4.3	The SNR loss of the MRC, OC, ML and optimum diversity receivers relative to the SU receiver as a function of the SIR in a two-user channel with Rayleigh fading, $M = 4$, $\bar{\gamma}_c = 4$ dB and $\rho_{0,1} = 0.25$ and 1.	57
4.4	The effect of the number of receiver antennas on the SNR loss of the ML and OC receivers with respect to the SU receiver in a two-user channel with Rayleigh fading and $\rho_{0,1} = 1$	59
4.5	The average BER of the MRC, OC, ML and optimum receivers as a function of the SIR in a two-user channel with Rayleigh fading, $\rho_{0,1} = 0.25$ and $M = 2, 4$ and 6.	60
4.6	The average BER of the OC, MRC and ML receivers as a function of the SIR in Rayleigh fading with $K = 8$, $\{\rho_{k,j}\}_{k \neq j} = 0.1$ and $M = 2, 4$ and 6.	61
5.1	The block diagram of the cochannel interference communication system with $(K + 1)$ asynchronous users.	65

5.2	The SINR gain achieved by the WMF over the CMF for the RC and BTB pulses, $\beta = 1$, $\psi = 0$ dB for a synchronous channel.	80
5.3	The SINR gain achieved by the WMF over the CMF for the RC and BTB pulses, $\beta = 1$, $\psi = 0$ dB for an asynchronous channel.	81
5.4	The WMF receiver's SINR gain over the CMF receiver for RC and BTB pulses in synchronous and asynchronous CCI for Nakagami- m fading ($m = 2$), with $\beta = 0.35$ and $\psi = 0$ dB. Markers denote simulation results.	82
5.5	The effect of roll-off factor on the SINR gain of the WMF receiver over the CMF receiver for RC and BTB pulses in asynchronous CCI and Nakagami- m fading, for SNR = 15 dB and $\psi = 0$ dB. Markers denote simulation results.	83
5.6	The effect of SIR on the SINR gain of the WMF receiver over the CMF receiver for RC and BTB pulses in asynchronous CCI and Nakagami- m fading ($m = 0.5$), for SNR = 15 dB and $\beta = 0.35$. Markers denote simulation results.	84
5.7	Performance of the whitening and the conventional MF receivers in Nakagami- m fading ($m = 8$) with synchronous CCI and AWGN for SIR = 10 dB and BTB and RC pulses with 100% excess bandwidth.	85
5.8	Performance of the CMF, WMF and SINRMF receivers in Nakagami- m fading ($m = 8$) with asynchronous CCI and AWGN for SIR = 10 dB and BTB and RC pulses with 100% excess bandwidth.	86
5.9	The ASINR of the SINRMF, WMF and CMF receivers versus β in Nakagami- m fading ($m = 0.5$) for RC and BTB pulses, with $\psi = 0$ dB.	87
5.10	The SINR gain over the CMF receiver versus SNR in Nakagami- m fading ($m = 0.5$) and asynchronous CCI, with $\psi = 10$ dB, $\mathcal{M} = 12$, $\beta = 0.35$ and $\beta = 1$ for an SINRMF receiver.	88
5.11	The SINR gain over the CMF receiver versus SNR in Nakagami- m fading ($m = 0.5$) and asynchronous CCI, with $\psi = 10$ dB, $\mathcal{M} = 12$, $\beta = 0.35$ and $\beta = 1$ for an ISI-impaired WMF receiver (markers denote simulation results).	89

6.1	The block diagram of the baseband cochannel interference communication system with $(K + 1)$ asynchronous users.	91
6.2	The SINR gain of the optimal T-R filter design over the conventional RC design as a function of γ_b and ψ	95
6.3	The BER versus SNR of the optimal T-R filter design and the conventional root RC design as a function of γ_b for perfect and imperfect timing recovery, SIR = 8 dB and $K = 8$	96
6.4	The effect of SIR on the SINR gain over the CMF receiver for RC and BTM pulses in asynchronous CCI and Nakagami- m fading, for SNR = 10 dB and $\beta = 0.35$	108
6.5	The SINR gain over the CMF receiver as a function of SNR for RC and BTM pulses in asynchronous CCI and Nakagami- m fading, with $\beta = 0.35$ and SIR = 0 dB.	109
6.6	The effect of roll-off factor on the SINR gain over the CMF receiver for RC and BTM pulses in asynchronous CCI and Nakagami- m fading, for SNR = 10 dB and SIR = 0 dB.	110
6.7	The ASINR gain of the ISI-free WMF, SINRMF and proposed receivers over the CMF receiver for RC and BTM pulses in asynchronous CCI and Nakagami- m fading ($m = 0.5$), for SIR = 0 dB.	111
6.8	The SINR gain achieved by the proposed receiver with an optimum transmitter filter over the CMF receiver with a root RC filter for Nakagami- m fading ($m = 0.5$), asynchronous CCI and $\beta = 0.35$	112
6.9	The SINR gain achieved by the SINRMF receiver with an optimum transmitter filter over the SINRMF receiver with a root RC filter for Nakagami- m fading ($m = 0.5$), asynchronous CCI and $\beta = 1$	113
6.10	The SINR gain achieved by the proposed receiver with an optimum transmitter filter over the proposed receiver with a root RC filter for Nakagami- m fading ($m = 0.5$), asynchronous CCI and SNR = 10 dB.	114

6.11	The SINR gain achieved by the SINRMF receiver with an optimum transmitter filter over the proposed receiver with its corresponding optimum transmitter filter for Nakagami- m fading ($m = 0.5$), asynchronous CCI and $\beta = 0.35$	115
A.1	The received signal constellation points and decision boundaries for $\pi/2 \leq \theta < \pi$	129
A.2	The received signal constellation points and decision boundaries for $\pi \leq \theta < 3\pi/2$	130
A.3	The received signal constellation points and decision boundaries for $3\pi/2 \leq \theta < 2\pi$	130

List of Abbreviations

AWGN	Additive white Gaussian noise
AME	Asymptotic multiuser efficiency
ASINR	Asymptotic signal-to-interference-plus-noise ratio
ACF	Autocorrelation function
BTD	Beaulieu-Tan-Damen
BTOC	Better than optimum combining
BPSK	Binary phase-shift keying
BEP	Bit error probability
BER	Bit error rate
CCI	Cochannel interference
CDMA	Code-division multiple access
CMF	Conventional matched filter
DS-CDMA	Direct-sequence code-division multiple access
FIR	Finite impulse response
FDMA	Frequency-division multiple access
i.i.d.	Independent and identically distributed
IOD	Individually optimum detector
IOR	Individually optimum receiver
IIR	Infinite impulse response

INR	Interference-to-noise ratio
ISI	Intersymbol interference
JOD	Jointly optimum detector
JOR	Jointly optimum receiver
LRT	Likelihood ratio test
MF	Matched filter
MRC	Maximal ratio combining
ML	Maximum-likelihood
MMSE	Minimum mean-square error
MAI	Multiple access interference
MUD	Multiuser detector
OC	Optimum combining
PIC	Parallel interference cancellation
PE	Polynomial expansion
PSD	Power spectral density
PDF	Probability density function
RC	Raised-cosine
RV	Random variable
SIR	Signal-to-interference ratio
SINR	Signal-to-interference-plus-noise ratio
SINRMF	Signal-to-interference-plus-noise ratio maximizing filter
SNR	Signal-to-noise ratio
SU	Single-user
SIC	Successive interference cancellation
TDMA	Time-division multiple access

T-R	Transmitter-receiver
UWB	Ultra-wideband
WMF	Whitening matched filter
WSS	Wide-sense stationary
ZF-DF	Zero-forcing decision-feedback

List of Symbols

$(\cdot)!$	Factorial
A_k	k th user's amplitude
$E\{\cdot\}$	Ensemble average
E_g	$g_d(\ell)$'s energy
$G_{R,k}(\omega)$	k th user's receiver filter in frequency domain
$G_{T,k}(\omega)$	k th user's transmitter filter in frequency domain
K	Number of interferers
$Q(\cdot)$	The Gaussian Q -function
$R_\chi(t, t + \eta)$	Autocorrelation function of the random process $\chi(t)$
$R_{xy}(\tau)$	Cross-correlation function between $x(t)$ and $y(t)$ defined in (4.3)
$S_{\mathcal{I}}(\omega)$	PSD of the overall cochannel interference
T	Symbol interval
$X_{\text{BTD}}(\omega)$	Beaulieu-Tan-Damen frequency-domain characteristics
$X_{\text{RC}}(\omega)$	Raised-cosine frequency-domain characteristics
$[\cdot]^*$	Conjugate of a complex number
$[\cdot]^H$	Conjugate transpose of a matrix
$[\cdot]^T$	Transpose of a matrix
\mathcal{E}_0	Desired user's energy
$E_{\mathcal{I}}$	Total interference energy

\hat{E}_g	$E_g - g_d(0)^2$
$\Gamma(\cdot)$	Gamma function defined in (5.3)
Γ	SINR
P_I	Total interference power
P_e	Error probability
$\Re\{\cdot\}$	Real part of a complex number
Υ	Asymptotic SINR defined in (5.51)
α_k	k th user's channel gain
$\arg \max$	Argument of the maximum
β	Excess bandwidth of the pulse-shaping filter
$\binom{n}{k}$	Binomial coefficient
$\delta(\cdot)$	Kronecker delta function
η_k	k th user's asymptotic multiuser efficiency
$\frac{N_0}{2}$	Power spectral density of the white noise process
γ_b	SNR per bit
$\bar{\gamma}_c$	Average SNR per channel
$\mathcal{L}\{\cdot\}$	Likelihood function
$\log(\cdot)$	Natural logarithm
$\log_n(\cdot)$	Base n logarithm
\mathbf{I}	Identity matrix
\mathbf{M}_k	k th column of the matrix \mathbf{M}
\mathbf{M}_{kk}^+	kk th element of the matrix \mathbf{M}^{-1}
$\mathcal{F}\{\cdot\}$	Fourier transform
$\mathcal{I}(t)$	Overall cochannel interference term
$\mathcal{I}_k(t)$	k th interfering signal

\mathcal{J}	Intersymbol interference term
ω_c	Carrier frequency
$\phi_0(t), \phi_1(t)$	Orthogonal basis functions
ψ	SIR
ρ_{kl}	Cross-correlation between $s_k(t)$ and $s_l(t)$
$\text{sgn}(\cdot)$	Signum function
$\sigma_{\mathcal{I}}^2$	Variance of the overall cochannel interference
τ_k	k th user's delay
θ_k	k th user's carrier phase
b_k	k th user's information bit
$b_{k,i}$	k th user's information bit in the i th bit interval
$c_{k,m}$	Complex channel gain between the k th user's transmitter and the m th receive antenna
$g_R(t)$	Receiver filter impulse response
$g_T(t)$	Transmitter filter impulse response
$g_d(\ell)$	Sampled $g(t)$, at ℓT (ℓ integer)
$n(t)$	Gaussian noise process
n_ℓ	Projection of $n(t)$ along $s_\ell(t)$
$r(t)$	Received signal
r_ℓ	Sampled received signal at the output of the ℓ th matched filter
$s_k(t)$	k th user's deterministic signal

Chapter 1

Introduction

1.1 Background

The use of wireless communications systems has been growing rapidly in the past decade. Today, in some societies, the number of subscribed cell phone users exceeds the population of those societies. In addition to cell phones, there is a large variety of other wireless applications such as wireless local access networks, digital video broadcasting, digital audio broadcasting, local multi-point distribution services and mobile ad hoc networks that use part of the frequency spectrum. Thus, one of the most fundamental problems in wireless communications systems is “how can multiple users transmit efficiently and reliably over a limited available radio frequency spectrum?” To overcome the bandwidth and connectivity limitations in wireless communication systems, several novel technologies have been developed over the past decades. Multiuser communication systems such as code-division multiple access (CDMA), frequency-division multiple access (FDMA), time-division multiple access (TDMA) and space-division multiple access systems are all designed to improve radio spectral efficiency through accommodating several users on a common channel.

Among the above systems, CDMA has received much attention because of its capability of providing *soft capacity*. That is, a new user can always be added to a CDMA channel at the expense of inflicting more interference on the other users. However, increasing the number of users in TDMA or FDMA systems can be practically prohibitive.

For example, an inherent difficulty with TDMA systems is that by increasing the number of users, the transmitters have to transmit the same amount of energy over a shorter time interval. Thus, the instantaneous transmitter power for each user becomes large. Moreover, in FDMA systems the larger the number of users the wider the signal in the time domain will be. Thus, the coherence time of the channel will be comparable to the symbol interval and so the channel has stronger deleterious effects on the transmitted signal. However, in CDMA systems if users are selected to have different rates, the overall rate can exceed that of the FDMA or TDMA [1].

In an ideal CDMA system, if the signature waveforms are orthogonal and the channel is synchronous, i.e., all users have the same time offset which is known at the receiver, the sum of rates of all users can be increased by increasing the number of users. Unfortunately, the orthogonality between the transmitted signals can not be maintained in these systems and, thus, CDMA systems suffer from multiple access interference (MAI). On the other hand, practical TDMA and FDMA systems employ frequency reuse plans to achieve higher spectral efficiencies, i.e., users in different cells concurrently use an identical carrier frequency [2]. As a consequence, TDMA and FDMA systems suffer from cochannel interference (CCI). Therefore, practical multiuser communication systems are mostly *interference-limited* rather than noise-limited as the received signal always has some amount of MAI. In many interference-limited multiuser systems the output of the matched filter (MF) is used as the decision statistic to detect the information bits. The MF used in these systems is either a conventional matched filter (CMF) [1], [3] or an interference-plus-noise whitening matched filter (WMF) [4]. As implied by its name, the latter receiver whitens the interference-plus-noise term prior to filtering the received signal using a MF. In these systems, employing a CMF or WMF receiver may lead to serious performance degradation if the open-eye condition does not hold.¹

In order to achieve a better performance than the MF receiver in interference-limited systems, more sophisticated detectors, referred to as multiuser detectors (MUDs), have been proposed. In these detectors, the amplitudes and signature waveforms as well as timing and carrier phase of all users are concurrently used to detect the information

¹The open-eye condition holds if, in the absence of background noise, the desired signal's component is greater than the maximum destructive MAI component [3].

symbols. MUDs make use of the output of the MF bank for all users and obtain the decision statistic for each user by applying a transformation to the sampled outputs of the MF bank. Depending on the type of their transformation, MUDs can be either linear or nonlinear. The structure and performance analysis of several well-known linear and nonlinear MUDs are presented in Chapter 2. Minimum mean-square error (MMSE) [5], decorrelating [6], and polynomial expansion (PE) detectors [7] are well-known examples of linear MUDs. The optimum MUD [8], [9] and almost all decision-driven detectors are nonlinear MUDs. A very well-known nonlinear MUD is the jointly optimum detector (JOD). This detector, also known as maximum-likelihood (ML) detector, chooses the information sequence that maximizes the joint *a posteriori* probability [3]. An inherent difficulty with the JOD (as with other ML sequence detectors) is that its complexity grows exponentially in the number of users that share the channel. Hence, a large body of research in multiuser detection has been focused on suboptimal detectors that have lower complexity than the JOD, yet perform very close to the optimum MUD. An important group of suboptimal MUDs are decision-driven MUDs [3].² In these detectors, the entire or part of the MAI is subtracted out from the output of the desired user's MF output to obtain a possibly less interference-limited decision statistic for the user of interest. Successive interference cancellation (SIC) [11]–[13] and parallel interference cancellation (PIC) [14] are two examples of subtractive MUDs.

1.2 Thesis Outline and Contributions

As mentioned earlier, optimum MUD is not desirable for practical implementation due to its prohibitive computational complexity. Nevertheless, the bit error probability (BEP) performance of this receiver has received considerable attention as it can serve as a baseline of comparison for the suboptimal MUD receivers [3]. In other words, the BEP of the optimal MUD is a means to determine how close the suboptimal MUDs can perform to the optimal MUD. Motivated by this fact, in Chapters 3 and 4 we mainly focus on jointly and individually optimum MUDs.

In Chapter 3, we first derive an exact expression for the BEP of a two-user jointly

²Decision-driven MUDs are also known as subtractive interference cancelers [10].

optimum receiver for the case when the carrier phase recovery is perfect, the channel is synchronous and the users employ rectangular pulse-shaping filters. The expression is insightful as it decomposes into the BEP of a single-user MF receiver plus a term due to the CCI. In Section 3.2, we derive the error probability of a two-user individually optimum detector (IOD) [15] in a synchronous additive white Gaussian noise (AWGN) channel and show that the error probability of the JOD can be considered as a special limiting case of the IOD when the signal-to-noise ratio (SNR) is large. We show that the receiver structures do not perform the same for small SNR values, particularly when the desired and interfering signals are highly correlated. We conclude this chapter by obtaining the error probability of the two-user JOD for the case where carrier phase recovery is imperfect and nonrectangular pulse-shaping is employed. This model represents a general case of the model considered in Section 3.1 of this chapter. We show that in this case the JOD is very sensitive to carrier phase recovery errors. In particular, we show that the JOD is not robust to the carrier phase recovery errors when the signal-to-interference ratio (SIR) is small.

In Chapter 4, the problem of optimum signal detection in CCI, multipath fading and AWGN is considered. The desired and interfering signals are assumed to be like-modulated and Rayleigh-faded. We raise the question of whether there are reception strategies that can outperform optimum combining (OC) in the sense of minimizing the error probability. Then, we address this question by deriving two better than OC multiuser combining receiver diversity structures. The first receiver concurrently minimizes the error probability for all users and is composed of a bank of maximal ratio combining (MRC) modules followed by a ML detector. The ML detector used in this receiver is similar to the JOD used in multiuser communication systems. In the second receiver, the error probability is minimized only for the desired user. It is shown that the receiver comprises a MRC module followed by a likelihood ratio test (LRT) that picks the globally best hypothesis. The latter block is identical to the IOD in the multiuser detection context. Simulation results illustrate the superiority of the proposed detection strategies over a receiver which makes use of OC, especially for small values of SIR.

The WMF receiver does not require any information about the MAI other than its total power [4]. Thus, in the environments where a MUD can not be used due to lack of

information about the interfering signals, a WMF receiver may be employed instead of a CMF. In the absence of intersymbol interference (ISI), the WMF receiver is superior to the CMF receiver in having larger signal-to-interference-plus-noise ratio (SINR) [4]. Thus, the transmitter requires less energy to achieve a specific BEP when the system makes use of a WMF rather than a CMF receiver. Another attractive feature of the WMF is that it can coexist in conjunction with a MMSE-like MUD when some of the interferers are tracked, i.e., their information is available at the receiver [16]. Motivated by these facts we focus on the WMF receiver in Chapters 5 and 6.

In Chapter 5, the problem of CCI suppression using a noise-plus-interference WMF receiver is studied. It is assumed that all signals are like-modulated and transmitted over a multipath fading channel in a bandlimited microcellular wireless system. We analyze the WMF receiver both in synchronous and asynchronous channels and show that the SINR of the WMF can not exceed that of the CMF receiver in synchronous CCI. This corrects some results reported in previous works on WMF receivers. In asynchronous channels, we show that CCI whitening can be used to improve the receiver's performance provided that the transmission is free of ISI. However, we show that in the presence of ISI, the WMF receiver is no longer SINR-maximizing and can degrade both the SINR and the error probability performance of the system relative to the case where a CMF receiver is employed. In this case, we derive the signal-to-interference-plus-noise ratio maximizing filter (SINRMF) in an asynchronous channel and show that it is composed of a WMF followed by a discrete time filter which combats the ISI. The SINRs of the ISI-free WMF and SINRMF receivers are analytically evaluated and compared for a standard raised-cosine (RC) and a Beaulieu-Tan-Damen (BTD) pulse. The SINR of the ISI-impaired system is also evaluated and the conditions under which this system can achieve close to ISI-free SINR are studied. It is shown that the SINRMF receiver can restore much of the SINR loss incurred due to ISI introduced by the WMF.

Chapter 6 consists of two sections. In the first section, the problem of transmitter-receiver (T-R) filter design for detection of a binary phase-shift keying (BPSK) signal in asynchronous cochannel interference and Gaussian noise is considered. It is shown that maximum signal-to-interference-plus-noise ratio (SINR) can be achieved only if the T-R filters have a flat spectrum with 100% excess bandwidth. The BEP performance

of a system with the proposed filters is compared to that of a system with conventional root RC filters both for perfect and imperfect timing recovery cases. It is shown that the proposed T-R filter design is superior to the conventional root RC filters both in having larger SINR and smaller BEP. In the second section, a more general form of the foregoing problem is considered in which the transmitter and the receiver filters do not necessarily have 100% excess bandwidth. We propose two T-R filter design methodologies to maximize the SINR without introducing ISI. In the first methodology, the transmitter and receiver filters are designed to maximize the SINR while their overall spectrum maintains a given Nyquist spectrum to avoid ISI. In the second method, however, the transmitter filter is assumed to be fixed and only the receiver filter is designed to achieve our goals. The SINR of the ISI-free SINR-maximizing filter is then analytically compared with that of the ISI-free WMF, SINRMF and CMF receivers. We also evaluate the SINR of the proposed receiver for the cases where root RC and root BTB pulses are used at the transmitter.

In Chapter 7, we present a summary of the results reported in this thesis. We conclude this chapter by providing some suggestions for future work.

Chapter 2

Overview of Multiuser Detection

In this chapter, we first present a basic signal model for a $(K + 1)$ -user communication system to be used in the sequel. Then, several well-known linear and nonlinear multiuser detectors are introduced.

2.1 Signal Model

The system model of the baseband received signal is shown in Fig. 2.1. We assume $(K + 1)$ users are sharing an asynchronous AWGN channel. Denoting the k th user's deterministic signal by $s_k(t)$, the baseband received signal is given by [3]

$$r(t) = \sum_{i=-\infty}^{\infty} \sum_{k=0}^K A_k b_{k,i} s_k(t - iT - \tau_k) + n(t) \quad (2.1)$$

where

- A_k and τ_k are the k th user's amplitude and propagation delay, respectively. $b_{k,i}$ is the k th user's information bit in the i th symbol interval and can take value either -1 or 1 .
- The $s_k(t)$'s are chosen such that they have unit energy and there is neither single-user nor cross-user ISI between them when the τ_k 's are zero, i.e.,

$$\int_{-\infty}^{\infty} s_k(t) s_l(t - iT) dt = \begin{cases} \delta(i), & k = l \\ \rho_{kl} \delta(i), & k \neq l \end{cases} \quad (2.2a)$$

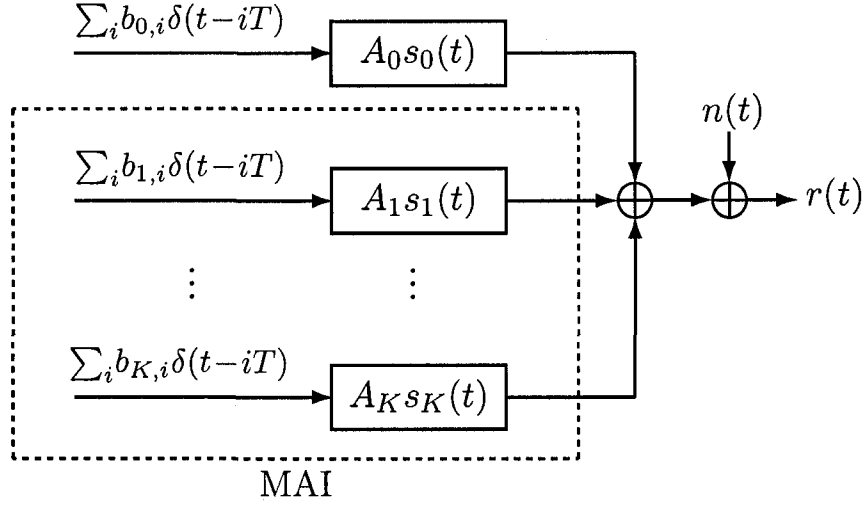


Figure 2.1. The block diagram of the baseband cochannel interference communication system with $(K + 1)$ synchronous users.

where

$$\rho_{kl} = \int_{-\infty}^{\infty} s_k(t) s_l(t) dt \quad (2.2b)$$

and $\delta(\cdot)$ is the Kronecker delta function defined as

$$\delta(k) = \begin{cases} 1, & k = 0 \\ 0, & k \neq 0 \end{cases} \quad (2.3)$$

- $n(t)$ is the AWGN with mean zero and power spectral density (PSD) $N_0/2$.

When the channel is synchronous, we can drop the time index in (2.1) and express the received signal as

$$r(t) = \sum_{k=0}^K A_k b_k s_k(t) + n(t). \quad (2.4)$$

At the receiver, the received signal is passed through a bank of filters matched to $\{s_k(t)\}_{k=0}^K$ and sampled at $t = 0$. The sampled received signal at the output of the ℓ th MF is then given by

$$r_\ell = A_\ell b_\ell + \sum_{\substack{k=0 \\ k \neq \ell}}^K A_k b_k \rho_{k\ell} + n_\ell, \quad \ell = 0, \dots, K \quad (2.5)$$

where n_ℓ is the projection of $n(t)$ along $s_\ell(t)$ and has a Gaussian distribution with mean zero and variance

$$E\{n_k n_\ell\} = \begin{cases} \frac{N_0}{2}, & k = \ell \\ \frac{N_0}{2} \rho_{k\ell}, & k \neq \ell. \end{cases} \quad (2.6)$$

Eq. (2.5) can be written in matrix form as

$$\mathbf{r} = \mathbf{R} \mathbf{A} \mathbf{b} + \mathbf{n} \quad (2.7a)$$

where

$$\mathbf{r} \triangleq [r_0, r_1, \dots, r_K]^T \quad (2.7b)$$

$$\mathbf{b} \triangleq [b_0, b_1, \dots, b_K]^T \quad (2.7c)$$

$$\mathbf{n} \triangleq [n_0, n_1, \dots, n_K]^T \quad (2.7d)$$

$$\mathbf{A} \triangleq \begin{bmatrix} A_0 & 0 & 0 & \dots & 0 \\ 0 & A_1 & 0 & \dots & 0 \\ \vdots & \vdots & \vdots & \ddots & \vdots \\ 0 & 0 & 0 & \dots & A_K \end{bmatrix} \quad (2.7e)$$

$[\cdot]^T$ denotes the matrix transpose and \mathbf{R} is the covariance matrix whose ij th element is ρ_{ij} . Note that \mathbf{n} is a zero-mean Gaussian vector with covariance matrix $E\{\mathbf{n}\mathbf{n}^T\} = (N_0/2)\mathbf{R}$.

2.2 Matched Filter Receiver

The MF receiver simply detects the k th information bit as $\hat{b}_k = \text{sgn}(r_k)$ where r_k is the output of the k th matched filter and $\text{sgn}(\cdot)$ denotes the signum function. The receiver filter can be either a CMF or an interference-plus-noise WMF.

2.2.1 Conventional Matched Filter Receiver

In a CMF receiver, the k th user's receiver filter impulse response is defined as $s_k(-t)$.¹ Assuming that $\{s_k(t)\}_{k=0}^K$ satisfy the Nyquist criterion for zero ISI [1] and the transmitted bits are equiprobable, the error probability of the CMF receiver is given by [3]

$$P_e = E \left\{ Q \left(\frac{A_0 - \sum_{k=1}^K A_k b_k \rho_{k0}}{\sqrt{N_0/2}} \right) \right\} \quad (2.8)$$

¹We assume the $s_k(t)$'s are real.

where

$$Q(x) = \frac{1}{\sqrt{2\pi}} \int_x^\infty e^{-\frac{t^2}{2}} dt \quad (2.9)$$

and the expectation in (2.8) should be taken over all 2^K possible values of $\{b_k\}_{k=1}^K$. For example for $K = 1$, (2.8) becomes [3, 3.75]

$$P_e = \frac{1}{2} \left[Q\left(\frac{A_0 - \rho A_1}{\sqrt{N_0/2}}\right) + Q\left(\frac{A_0 + \rho A_1}{\sqrt{N_0/2}}\right) \right] \quad (2.10)$$

where for simplicity we have dropped the index of ρ_{01} .

The exact error probability of the MF receiver in slow Rayleigh fading channel with asynchronous users is given by [17] using the characteristic function of the interfering signals. For the synchronous case and independent complex-valued Rayleigh fading channels the bit error probability for the desired user is given by [3, eq. 3.135]

$$P_e = \frac{1}{2} \left[1 - \frac{A_0}{\sqrt{N_0 + A_0^2 + \sum_{k=1}^K A_k^2 \rho_{k0}^2}} \right]. \quad (2.11)$$

2.2.2 Interference-Plus-Noise Whitening Matched Filter Receiver

The interference-plus-noise WMF receiver was first proposed in [4]. This receiver first whitens the colored noise term composed of the CCI and AWGN and then passes the resulting signal through a filter matched to the desired user's deterministic signal. Assume that $s_k(t)$ in (2.4) equals $g_T(t) \cos \theta_k$ where θ_k is a random phase uniformly distributed over $[0, 2\pi)$ and $\theta_0 = 0$. Then, provided that the desired user (i.e., the 0th user) has infinite observation time and the ISI is negligible, the WMF receiver is defined as [4]

$$g_R(t) = \mathcal{F}^{-1} \left[\frac{G_T(\omega)}{\frac{N_0}{2} + \frac{1}{2T} \sum_{k=1}^K A_k^2 |G_T(\omega)|^2} \right] \quad (2.12)$$

where \mathcal{F}^{-1} denotes the inverse Fourier transform and $G_T(\omega)$ is the Fourier transform of the transmitter filter, $g_T(t)$. Note that the only information that the WMF receiver needs about the CCI is its total power. More importantly, the interference-plus-noise whitening filter maximizes the output SINR [18], i.e.,

$$\text{SINR} = \frac{A_0^2}{2\pi} \int_{-\infty}^{\infty} \frac{|G_T(\omega)|^2}{\frac{N_0}{2} + \frac{1}{2T} \sum_{k=1}^K A_k^2 |G_T(\omega)|^2} d\omega. \quad (2.13)$$

When the observation time is limited to one symbol interval, $g_R(t)$ for the desired user is obtained by solving the integral equation [4]

$$s_0(t) = \int_0^T R(t-u) g_R(u) du \quad (2.14)$$

where $R(\eta)$ is the autocorrelation function of the noise-plus-interference term given by

$$R(\eta) = \frac{N_0}{2} \delta(\eta) + \frac{1}{2T} \sum_{k=1}^K A_k^2 \int_{-\infty}^{\infty} g_T(t) g_T(t+\eta) dt. \quad (2.15)$$

In this case the output SINR equals [4]

$$\text{SINR} = A_0^2 \int_0^T s_0(t) g_T(t) dt. \quad (2.16)$$

2.3 Multiuser Detection

The conventional MF receiver only uses the output of the desired user's MF. Therefore, the receiver's structure does not depend on number of users and is fixed for any number of interfering signals. Despite this advantage, the performance of this receiver becomes very poor when the interference power increases. Moreover, the conventional receiver suffers from the *near-far problem*. This problem occurs when the desired user is farther to the basestation than some or all of the interfering users. In this situation, the SIR of the desired user is so small that the error probability for this user approaches 0.5 even for vanishing small background noise.

A MUD uses the sampled received signals at the outputs of all the MFs to generate a decision statistic for the user of interest. The MUD usually outperforms a conventional MF receiver. However, this is at the expense of higher complexity than the conventional receiver. In general, MUDs can be either linear or nonlinear. In next two subsections, we will review several important linear and nonlinear MUD designs.

2.3.1 Linear MUD

In a linear MUD, a linear transformation is applied to the sampled output vector of the MF bank to obtain a decision statistic for each user. Denoting the transformation

matrix by \mathbf{M} , the detected information bits at the output of the linear MUD are given by

$$\hat{\mathbf{b}} = \text{sgn}(\mathbf{M} \mathbf{r}) \quad (2.17)$$

where \mathbf{M} is a $(K + 1) \times (K + 1)$ matrix whose k th row is denoted by \mathbf{M}_k^T . Note that, the receiver does not need to know the whole matrix \mathbf{M} as it can detect the k th symbol using $\hat{b}_k = \text{sgn}(\mathbf{M}_k^T r_k)$. The bit error probability and asymptotic multiuser efficiency (AME)² of this receiver, η_0 , for the desired user are [19], [20]

$$P_e = E \left\{ Q \left(\frac{A_0 \mathbf{M}_0^T \mathbf{R}_0 + \sum_{k=1}^K A_k b_k \mathbf{M}_0 \mathbf{R}_k}{\sqrt{\frac{N_0}{2} \mathbf{M}_0^T \mathbf{R} \mathbf{M}_0}} \right) \right\} \quad (2.18)$$

$$\eta_0 = \frac{1}{\mathbf{M}_0^T \mathbf{R} \mathbf{M}_0} \left[\max \left\{ 0, \mathbf{M}_0^T \mathbf{R}_0 - \sum_{k=1}^K \frac{A_k}{A_0} |\mathbf{M}_0^T \mathbf{R}_k| \right\} \right]^2 \quad (2.19)$$

respectively, where \mathbf{R}_k is the k th column of \mathbf{R} , and the expectation in (2.18) is with respect to $\{b_k\}_{k=1}^K$. Decorrelating and MMSE detectors are the most well-known linear MUDs.

2.3.1.1 Decorrelating detector

In a decorrelating detector $\mathbf{M} = \mathbf{R}^{-1}$ and each resulting decision statistic constitutes the desired signal plus an AWGN component. An important advantage of the decorrelating detector is that it does not need to estimate the received amplitudes. Furthermore, it can decorrelate the transmitted bits separately. It has been shown that the decorrelating detector is optimum when the received amplitudes are unknown [19]. The bit error probability and the AME of this detector for the k th user are given by

$$P_e = Q \left(\frac{A_k}{\sqrt{N_0 \mathbf{R}_{kk}^+ / 2}} \right) \quad (2.20)$$

$$\eta_k = \frac{1}{\mathbf{R}_{kk}^+} \quad (2.21)$$

²The effective energy of the k th user in a multiuser system, E_k , is defined as the energy that the k th user requires to achieve its multiuser error probability in a single-user AWGN channel with the same level of background noise. The multiuser efficiency is the ratio between the actual and effective energies, i.e., A_k^2/E_k . The asymptotic multiuser efficiency defined in [3, eq. (3.111)] is the limit of the multiuser efficiency as $N_0 \rightarrow 0$.

respectively, where \mathbf{R}_{kk}^+ is the kk th element of \mathbf{R}^{-1} . Obviously, neither P_e nor the AME depend on the interfering users' energies. It has been shown that when $\{A_k\}_{k=0}^K$ are unknown the joint maximum likelihood estimation of the b_k and A_k are given by

$$\hat{A}_k = |\mathbf{e}_k| \quad (2.22)$$

$$\hat{b}_k = \text{sgn}(\mathbf{e}_k) \quad (2.23)$$

where $\mathbf{e} = \mathbf{R}^{-1}\mathbf{r}$ and \mathbf{e}_k is the k th element of \mathbf{e} [19].

2.3.1.2 MMSE Detector

The MMSE detector [5] minimizes the mean-square error between the vector of information bits and the soft output of the detector, i.e.,

$$E\{\|\mathbf{b} - \mathbf{M}\mathbf{r}\|^2\}. \quad (2.24)$$

The matrix \mathbf{M} that minimizes (2.24) has been shown to be [5]

$$\mathbf{M} = \left[\mathbf{R} + \frac{N_0}{2} \mathbf{A}^{-2} \right]^{-1}. \quad (2.25)$$

Clearly, in this case \mathbf{M} depends on both the noise variance and the received signal amplitudes. Moreover, as $N_0 \rightarrow 0$ the MMSE detector approaches the decorrelating detector while for large values of N_0 the MMSE receiver performs almost the same as the conventional MF detector. Indeed, when N_0 increases, the matrix \mathbf{M} tends to become a diagonal matrix and $\mathbf{M} \cdot \mathbf{r}$ elements have the same sign as \mathbf{r} . The MMSE detector is the optimal linear detector in the sense of maximizing the output SIR. The error probability of the MMSE receiver for the desired user is given by [21]

$$P_e = E \left\{ Q \left(\frac{A_0}{\sqrt{N_0/2}} \frac{(\mathbf{M}\mathbf{R})_{00}}{\sqrt{(\mathbf{M}\mathbf{R}\mathbf{M})_{00}}} \left[1 + \sum_{k=1}^K \beta_k b_k \right] \right) \right\} \quad (2.26)$$

where $\beta_k = B_k/B_0$, $B_k = A_k(\mathbf{M}\mathbf{R})_{0k}$, \mathbf{M} is given by (2.25), $(\mathbf{M})_{mn}$ denotes the mn th element of the matrix \mathbf{M} and the average in (2.26) is taken over all possible values of $\{b_k\}_{k=1}^K$. Because the MMSE detector converges to decorrelating detector as $N_0 \rightarrow 0$, its AME is the same as that of the decorrelating detector.

2.3.1.3 Polynomial expansion detector

An approximate realization of either the decorrelating or MMSE detectors can be accomplished using a PE detector [7], [22]. The PE detector approximates the matrix \mathbf{M} in either of the above detectors by a polynomial in \mathbf{R} . The PE detector has some attractive properties like simplicity and low computational complexity. Moreover, this detector does not need to estimate the received amplitudes.

2.3.2 Nonlinear MUD

In a nonlinear MUD, the decision statistics are obtained by applying a nonlinear transformation to the sampled outputs of the MF bank. The optimum MUD as well as successive interference cancellation receivers are well-known nonlinear MUDs.

2.3.2.1 Optimum MUD

There are two types of optimum MUD receivers, IOD [15] and JOD [9]. The IOD chooses b_0 that maximizes the *a posteriori* probability, i.e., [3], [15]

$$\text{Prob}\{b_0|r(t), t \in \mathcal{T}\} \quad (2.27)$$

where \mathcal{T} is the observation interval. The JOD, however, chooses $\{b_k\}_{k=0}^K$ that maximizes the joint *a posteriori* probability, i.e., [8], [9]

$$\text{Prob}\{(b_0, b_1, \dots, b_K)|r(t), t \in \mathcal{T}\}. \quad (2.28)$$

It can be shown that (2.27) is equivalent to finding b_0 that maximizes

$$E \left\{ \exp \left[-\frac{1}{N_0} \int_{\mathcal{T}} \left(r(t) - A_0 b_0 s_0(t) - \sum_{k=1}^K A_k b_k s_k(t) \right)^2 dt \right] \right\} \quad (2.29)$$

where the expectation in (2.29) should be taken over all 2^K possible $\{b_1, b_2, \dots, b_K\}$ sets. The IOD usually has a very complicated structure and involves hyperbolic and exponential functions. For the two-user case the desired bit estimate can be expressed as [3]

$$\hat{b}_0 = \text{sgn} \left[r_0 - \frac{N_0}{4A_0} \log \left(\cosh \left[\frac{2A_1 r_1 + 2A_0 A_1 \rho}{N_0} \right] / \cosh \left[\frac{2A_1 r_1 - 2A_0 A_1 \rho}{N_0} \right] \right) \right] \quad (2.30)$$

where $\log(\cdot)$ denotes the natural logarithm function. The decision rule of the JOD is simpler than that of the IOD and can alternatively be expressed as

$$\arg \max_{\{b_0, b_1, \dots, b_K\}} \left\{ \exp \left[-\frac{1}{N_0} \int_{\mathcal{T}} \left(r(t) - \sum_{k=0}^K A_k b_k s_k(t) \right)^2 dt \right] \right\}. \quad (2.31)$$

Again, for the two-user case, the desired bit is estimated as

$$\hat{b}_0 = \text{sgn} \left[A_0 r_0 + \frac{A_1}{2} (|r_1 - A_0 \rho| - |r_1 + A_0 \rho|) \right] \quad (2.32)$$

which is much simpler than (2.30) and does not depend on N_0 . In general, the jointly optimal decision rule for a system with $K + 1$ users can be expressed as [3]

$$\arg \max_{\mathbf{b}} \{ 2\mathbf{b}^T \mathbf{A} \mathbf{r} - \mathbf{b}^T \mathbf{A} \mathbf{R} \mathbf{A} \mathbf{b} \}. \quad (2.33)$$

Obviously, the complexity of this receiver grows exponentially with the number of users. Therefore, for a system with a large number of users, using a JOD is practically prohibited, even though it has a remarkable superiority over the conventional receiver.

An upper and lower bound analysis of the JOD was first given by [9] based on indecomposable error sequences. Assume that \mathbf{b} and $\hat{\mathbf{b}}$ are the transmitted and the detected vectors of information bits, respectively. Also assume that

- $\boldsymbol{\epsilon} = [\epsilon_0, \epsilon_0, \dots, \epsilon_K]^T$ is an error vector.
- $E_k = \{ \boldsymbol{\epsilon} \in \{-1, 0, 1\}^{K+1}, \epsilon_k \neq 0 \}$ is the set of the error vectors that affect the k th user.
- $E = \bigcup_{k=0}^K E_k$ is the set of all error vectors.
- $A(\mathbf{b}) = \{ \boldsymbol{\epsilon} \in E, 2\boldsymbol{\epsilon} - \mathbf{b} \in \{-1, 1\}^{K+1} \}$ is the admissible set of error vectors for \mathbf{b} .
- $w(\boldsymbol{\epsilon}) = \sum_{k=0}^K |\epsilon_k|$ is the weight of the error vector $\boldsymbol{\epsilon}$.
- $\boldsymbol{\epsilon}$ is decomposable into $\boldsymbol{\epsilon}'$ and $\boldsymbol{\epsilon}''$ if
 1. $\boldsymbol{\epsilon} = \boldsymbol{\epsilon}' + \boldsymbol{\epsilon}''$
 2. If $\epsilon_k = 0$, then $\epsilon'_k = 0$ and $\epsilon''_k = 0$
 3. $\boldsymbol{\epsilon}'^T \mathbf{A} \mathbf{R} \mathbf{A} \boldsymbol{\epsilon}'' \geq 0$

If we denote the subset of indecomposable error vectors in E_k by F_k , it has been shown that the error probability of the JOD can be upper and lower bounded as [9]

$$2^{1-w(\epsilon^*)}Q\left(\frac{d_{k,\min}}{\sqrt{N_0/2}}\right) \leq P_e < \sum_{\epsilon \in F_k} 2^{-w(\epsilon)}Q\left(\sqrt{\frac{2\epsilon^T \mathbf{A} \mathbf{R} \mathbf{A} \epsilon}{N_0}}\right) \quad (2.34)$$

where $d_{k,\min} = \min_{\epsilon \in F_k} \epsilon^T \mathbf{A} \mathbf{R} \mathbf{A} \epsilon$ and $\epsilon^* = \arg \min_{\epsilon \in F_k} \epsilon^T \mathbf{A} \mathbf{R} \mathbf{A} \epsilon$. Note that for single-path fading channels, the upper and lower bound analysis has been done in [23]. These bounds have been further improved in [24], [25] using a new method for identifying decomposable error sequences.

2.3.2.2 Decision-Driven MUD

The idea of decision-driven MUD³ is similar to that of decision feedback equalizers used to remove ISI [1]. In these detectors, the symbols which have been detected in the previous stage are used to remove the CCI. The most important decision-driven MUDs are SICs and PICs.

The SIC is a nonlinear MUD that uses the previously detected bits to reproduce the entire or part of the interference (depending on the number of interfering symbols that have been detected in the previous stage) and subtract it out from the received signal [11]–[13]. In SIC, the order in which the users are demodulated is important and directly affects the receiver's performance. One approach is to demodulate users in the order of decreasing received powers. Another approach which seems to be more efficient, orders users according to the mean-square of their MF output [3], i.e.,

$$E \left\{ \left(\int_{\mathcal{T}} r(t) s_k(t) dt \right)^2 \right\} = \frac{N_0}{2} + A_k^2 + \sum_{\substack{j=0 \\ j \neq k}}^K A_j^2 \rho_{jk}^2. \quad (2.35)$$

Since this approach accounts for the cross-correlation between users, it is expected to be more efficient than the previous approach. Assuming that the $k+1, k+2, \dots, K$ th symbols have been already detected, the k th user's bit can be estimated as

$$\hat{b}_k = \text{sgn} \left[r_k - \sum_{j=k+1}^K A_j \rho_{jk} \hat{b}_j \right]. \quad (2.36)$$

³Also known as subtractive interference cancellation MUD.

Note that the SIC requires advance knowledge of the received amplitudes. Moreover, it has an inherent demodulation delay which increases linearly with the number of users. The SIC's performance can be improved by partially canceling the interference, i.e., weak interfering signals that are very unlikely to be detected reliably should not be canceled. This is because incorrectly canceling a weak interfering signal may double its amplitude and increase the overall interference power.

PIC is very similar to the SIC except that it attempts to cancel the entire CCI for each user at once [11], [12], [26]. Assuming that all detected symbols are available, the k th symbol estimate will be

$$\hat{b}_k = \text{sgn} \left[r_k - \sum_{\substack{j=0 \\ j \neq k}}^K A_j \rho_{jk} \hat{b}_j \right]. \quad (2.37)$$

At the first stage, the PIC can use either a CMF receiver [14] or a decorrelating receiver [27].

We finally note that successive interference cancellation can also be accomplished using a zero-forcing decision-feedback (ZF-DF) detector [28], [29]. The ZF-DF detector has two stages:

1. A linear transformation which partially decorrelates the received samples.
2. An SIC that subtracts out the remaining interference from the previous stage.

The ZF-DF detector uses the fact that the matrix \mathbf{R} is a positive definite matrix that can be decomposed as $\mathbf{R} = \mathbf{F}^T \mathbf{F}$ where \mathbf{F} is a lower triangular matrix, i.e., Cholesky decomposition. By multiplying both sides of (2.7a) by $(\mathbf{F}^T)^{-1}$ on the right one obtains

$$\tilde{\mathbf{r}} = \mathbf{F} \mathbf{A} \mathbf{b} + \tilde{\mathbf{n}} \quad (2.38)$$

where $\tilde{\mathbf{n}}$ is a white Gaussian noise vector with mean zero and covariance matrix $(N_0/2) \mathbf{I}$ and \mathbf{I} is the identity matrix with appropriate dimensions. The k th bit can then be detected as

$$\hat{b}_k = \tilde{r}_k - \sum_{j=0}^{k-1} F_{kj} A_j \hat{b}_j \quad (2.39)$$

where \tilde{r}_k and F_{kj} are the k th and kj th elements of $\tilde{\mathbf{r}}$ and \mathbf{F} , respectively. Similar to the MMSE detector, the ZF-DF detector requires knowledge of the received amplitudes, i.e.,

A_0, A_1, \dots, A_K . If the received amplitudes are estimated using a decorrelating detector, the ZF-DF detector performs the same as the decorrelating detector. It performs, however, better than the decorrelating detector if the estimates are more reliable than those produced by the decorrelating detector and worse if less reliable [10].

Chapter 3

Performance Analysis of Jointly and Individually Optimum Receivers

In this chapter, we analyze the performance of the jointly and individually optimum detectors derived in Subsection 2.3.2.1, in a two-user synchronous Gaussian channel. In the first two sections, we derive the error probability of the JOD and the IOD when the carrier phase is perfectly known at the receiver. In the third section, we consider a more practical scenario in which the carrier phase recovery is imperfect and the desired and interfering signals are bandlimited, i.e., a nonrectangular pulse-shaping filter is used.

Note that the BEP performance analyses given in this chapter are valid for a two-user synchronous channel. This is because many interference-limited multiuser communication systems are dominated by only one interferer and the contribution of other interferers is negligible (see [30] and references [18], [19] therein). Furthermore, in some multiuser systems only two users concurrently share the available radio spectrum. For example, in a nonorthogonal cooperative diversity system the source and the relay transmit simultaneously over the same subspace [31]. Thus, in nonorthogonal cooperative systems each user experiences only one interferer at each time interval and the performance analyses given in this chapter are applicable to these systems.

3.1 Error Probability of a Two-User Synchronous JOD in AWGN

The BEP of a synchronous optimal receiver [3] in the presence of a similar cochannel interferer and AWGN has been considered in [3], [32]–[35]. In [32], extensive computer simulation was used to evaluate the BEP of the receiver. Although, this method is a straightforward method for obtaining the BEP, it can be very time consuming and even impractical for large values of SNR, i.e., small values of the probability of error. When the users employ a BPSK modulation scheme, the jointly optimal receiver has only two decision regions in the two-dimensional received signal space [3], [33], [35]. In [35], the decision region is divided into three distinct regions for each desired user constellation point (six regions in total), and an extension of Craig’s method [36] is used to evaluate the probability of the error of the receiver. The result, though exact, is somewhat complex, as it involves five numerical integrations whose integrands and limits of integration change for high, moderate and small values of SIR. In [3], upper and lower bounds to the exact probability of error were derived. However these bounds, though simple, are not tight for small SNR values. In [37], a union bound for the BER of a two-user JOD which makes use of diversity arrays is derived. The resulting bound is identical to that given in [38] but is obtained using a different approach. Also presented in [37] is an exact expression for the bit error probability of the two-user JOD. The final result, however, depends on four distinct events whose occurrence probabilities are not given in the paper.

In this section, we derive a new, exact expression for the BEP of the receiver that is both simple and intuitive. We divide the decision region into two subregions and then, calculate the probability that noise components move the desired constellation point to each of these subregions, i.e., an error happens. The result involves a single definite integral and has the form of the BEP of BPSK in an AWGN channel plus an interference term. The latter has the same form for all values of SIR (in contrast to the solution in [33], [35]) and approaches zero when either the interference power or the correlation between desired and interferer signals tends to zero.

3.1.1 Signal Model

Following [32]–[35], we assume that a desired BPSK signal, $b_0 A_0 \sqrt{2/T} \cos(\omega t)$, is transmitted over an AWGN channel in the presence of an interfering like-modulated signal, $b_1 A_1 \sqrt{2/T} \cos(\omega t + \theta)$. Furthermore, we assume that the desired and interfering users use a rectangular pulse whose duration is the same as their bit interval. Then, the received signal in the interval $[0, T]$ is given by

$$r(t) = b_0 A_0 \sqrt{\frac{2}{T}} \cos(\omega t) + b_1 A_1 \sqrt{\frac{2}{T}} \cos(\omega t + \theta) + n(t) \quad (3.1)$$

where b_i , A_i and $n(t)$ are defined in Subsection 2.1, θ is the phase difference between desired and interferer unmodulated carriers and ω is the carrier frequency. Moreover, we define the SNR and SIR of the system as A_0^2/N_0 and A_0^2/A_1^2 , respectively. Eq. (3.1) can be rewritten as

$$\begin{aligned} r(t) &= (b_0 A_0 + b_1 A_1 \cos \theta) \sqrt{\frac{2}{T}} \cos(\omega t) - b_1 A_1 \sin \theta \sqrt{\frac{2}{T}} \sin(\omega t) + n(t) \\ &= (b_0 A_0 + b_1 A_1 \cos \theta) \phi_0(t) + b_1 A_1 \sin \theta \phi_1(t) + n(t) \end{aligned} \quad (3.2)$$

where

$$\phi_0(t) \triangleq \sqrt{\frac{2}{T}} \cos(\omega t) \quad (3.3)$$

$$\phi_1(t) \triangleq -\sqrt{\frac{2}{T}} \sin(\omega t). \quad (3.4)$$

Clearly, $\phi_0(t)$ and $\phi_1(t)$ are orthogonal and have unit energy. Let the received signal components along $\phi_0(t)$ and $\phi_1(t)$ be denoted r_0 and r_1 , respectively, defined as

$$\begin{aligned} r_0 &\triangleq \int_0^T r(t) \phi_0(t) dt \\ &= b_0 A_0 + b_1 A_1 \cos \theta + n_0 \end{aligned} \quad (3.5)$$

$$\begin{aligned} r_1 &\triangleq \int_0^T r(t) \phi_1(t) dt \\ &= b_1 A_1 \sin \theta + n_1 \end{aligned} \quad (3.6)$$

where n_0 and n_1 are independent and identically distributed (i.i.d) Gaussian random variables (RVs) with zero mean, variance $N_0/2$ and common probability density function

(PDF), $f(\cdot)$. Assume that the unmodulated carriers of the two users are known at the receiver following the method explained in [39]. Then, the jointly optimum decisions for bits b_0 and b_1 are given by [3]

$$\hat{b}_0 = \text{sgn} \left[A_0 r_0 + \frac{1}{2} A_1 \left\{ |r_1 \sin \theta + (r_0 - A_0) \cos \theta| - |r_1 \sin \theta + (r_0 + A_0) \cos \theta| \right\} \right] \quad (3.7)$$

$$\hat{b}_1 = \text{sgn} \left[A_1 (r_0 \cos \theta + r_1 \sin \theta) + \frac{1}{2} A_0 \left\{ |r_0 - A_1 \cos \theta| - |r_0 + A_1 \cos \theta| \right\} \right]. \quad (3.8)$$

3.1.2 BEP Derivation

Based on the values of b_0 and b_1 , there are four distinct points (called C_0 , C_1 , C_2 and C_3) in the received signal space as shown in Fig. 3.1. The coordinates of these points are given by

$$C_0 : (-A_0 - A_1 \cos \theta, -A_1 \sin \theta) \quad (3.9a)$$

$$C_1 : (-A_0 + A_1 \cos \theta, A_1 \sin \theta) \quad (3.9b)$$

$$C_2 : (A_0 - A_1 \cos \theta, -A_1 \sin \theta) \quad (3.9c)$$

$$C_3 : (A_0 + A_1 \cos \theta, A_1 \sin \theta). \quad (3.9d)$$

Furthermore, the intersection points of the decision boundaries are P_i and P_j with coordinates given by [33], [35]

$$P_i : \left(A_1 \cos \theta, \frac{A_0 - A_1 \cos \theta}{\tan \theta} \right) \quad (3.10)$$

$$P_j : \left(-A_1 \cos \theta, -\frac{A_0 - A_1 \cos \theta}{\tan \theta} \right). \quad (3.11)$$

Before going further, we establish the following fact which is used in the sequel (the proof is given in Appendix A.)

Fact 1. *The receiver's BEP for all values of θ , can be evaluated using the BEP expression given for $\theta \in [0, \pi/2)$.*

In the remainder of this section, θ is assumed to be in the interval $[0, \pi/2)$. Assume that the desired bits are transmitted with equal probability. Then, because of symmetry, it is enough to consider the BEP of the receiver when the desired bit is equal to -1 .

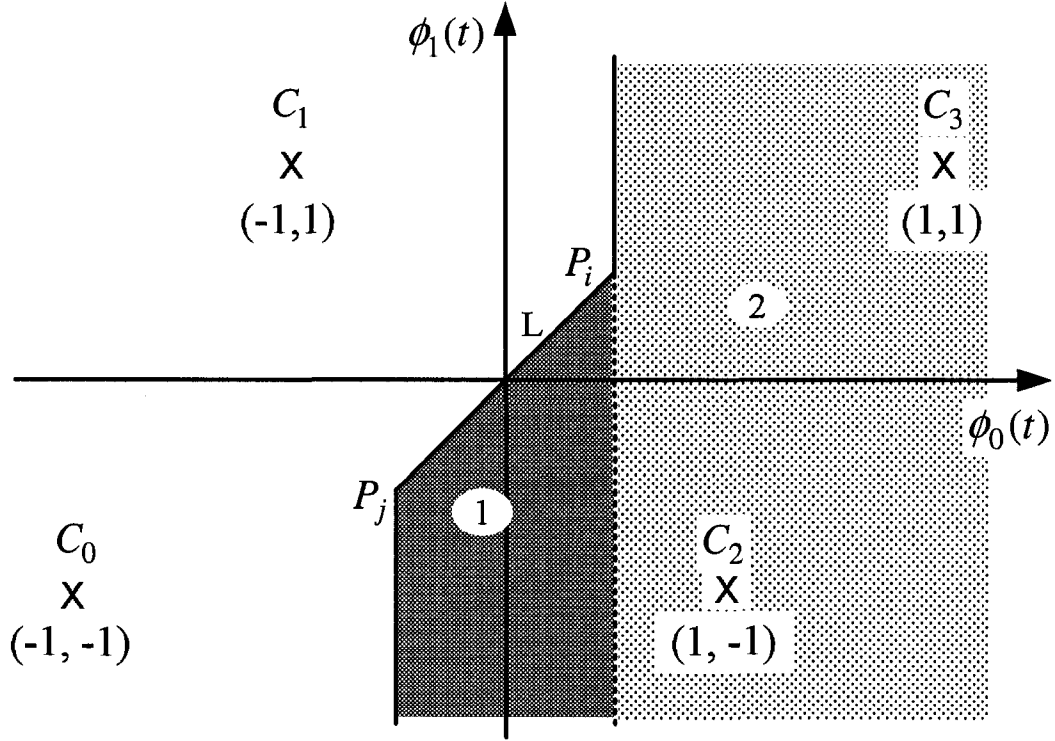


Figure 3.1. The received signal constellation and decision boundaries for a BPSK signal with one identical cochannel interferer for $0 \leq \theta < \pi/2$.

Assume that the origin is shifted to point C_0 in Fig. 3.1. Then the new coordinates of the points P_i and P_j and the equation defining the diagonal line L , are given by

$$P_i : \left(A_0 + 2A_1 \cos \theta, \frac{A_0 \cos \theta - A_1 \cos(2\theta)}{\sin \theta} \right) \quad (3.12)$$

$$P_j : \left(A_0, \frac{A_1 - A_0 \cos \theta}{\sin \theta} \right) \quad (3.13)$$

$$L : n_1 = mn_0 + \alpha \quad (3.14a)$$

where

$$m \triangleq \frac{A_0 - A_1 \cos \theta}{A_1 \sin \theta} \quad (3.14b)$$

$$\alpha \triangleq \frac{A_1^2 - A_0^2}{A_1 \sin \theta}. \quad (3.14c)$$

Since we assumed $b_0 = -1$, depending on the value of b_1 , the desired constellation point would be C_0 or C_1 . The probability of error in this case is the probability that the noise

components along $\phi_0(t)$ and $\phi_1(t)$ move the desired constellation point to the shaded area in Fig. 3.1. This probability is the integral of the joint PDF of n_0 and n_1 over the shaded area. For calculating the integral, one can split the shaded area into two sub-areas 1 and 2 as shown in Fig. 3.1. Then, integrate the joint PDF over each sub-area separately. This yields

$$p_0 = \int_{A_0}^{A_0+2A_1 \cos \theta} \int_{-\infty}^{mn_0+\alpha} f(n_1)dn_1 f(n_0)dn_0 + \int_{A_0+2A_1 \cos \theta}^{\infty} \int_{-\infty}^{\infty} f(n_1)dn_1 f(n_0)dn_0. \quad (3.15)$$

Similarly, if the origin is shifted to point C_1 in Fig. 3.1, the coordinates of the points P_i and P_j and the equation defining the diagonal line L , will be changed to

$$P_i : \left(A_0, \frac{A_0 \cos \theta - A_1}{\sin \theta} \right) \quad (3.16)$$

$$P_j : \left(A_0 - 2A_1 \cos \theta, \frac{A_1 \cos(2\theta) - A_0 \cos \theta}{\sin \theta} \right) \quad (3.17)$$

$$L : n_1 = mn_0 + \beta \quad (3.18a)$$

where

$$\beta \triangleq \frac{2A_0A_1 \cos \theta - A_0^2 - A_1^2}{A_1 \sin \theta}. \quad (3.18b)$$

Again the probability of error can be determined by integrating the joint PDF of n_0 and n_1 over the subregions 1 and 2 in Fig. 3.1 which results in

$$p_1 = \int_{A_0-2A_1 \cos \theta}^{A_0} \int_{-\infty}^{mn_0+\beta} f(n_1)dn_1 f(n_0)dn_0 + \int_{A_0}^{\infty} \int_{-\infty}^{\infty} f(n_1)dn_1 f(n_0)dn_0. \quad (3.19)$$

Using eqs. (3.15) and (3.19), the overall probability of error becomes

$$\begin{aligned} P_e(\theta) &= \frac{1}{2}p_0 + \frac{1}{2}p_1 \\ &= \frac{1}{2} \left\{ Q\left(\frac{A_0}{\sqrt{N_0/2}}\right) - \int_{A_0}^{A_0+2A_1 \cos \theta} Q\left(\frac{mn_0 + \alpha}{\sqrt{N_0/2}}\right) f(n_0)dn_0 \right. \\ &\quad \left. + Q\left(\frac{A_0 - 2A_1 \cos \theta}{\sqrt{N_0/2}}\right) - \int_{A_0-2A_1 \cos \theta}^{A_0} Q\left(\frac{mn_0 + \beta}{\sqrt{N_0/2}}\right) f(n_0)dn_0 \right\}. \quad (3.20) \end{aligned}$$

By changing the variable n_0 to $x + A_0$ in the first integral and n_0 to $-x + A_0$ in the second integral in (3.20), we obtain

$$P_e(\theta) = \frac{1}{2} \left\{ Q\left(\frac{A_0}{\sqrt{N_0/2}}\right) + Q\left(\frac{A_0 - 2A_1 \cos \theta}{\sqrt{N_0/2}}\right) - \int_0^{2A_1 \cos \theta} [Q(\alpha(x))f(x + A_0) + Q(-\alpha(x))f(x - A_0)] dx \right\} \quad (3.21)$$

where

$$\alpha(x) = -\frac{(\cos \theta - \frac{A_0}{A_1})x + A_0 \cos \theta - A_1}{\sqrt{N_0/2} \sin \theta}. \quad (3.22)$$

Denoting the integral term in (3.21) as \mathcal{I} and replacing $Q(-\alpha(x))$ with $1 - Q(\alpha(x))$ one can obtain

$$\mathcal{I} = Q\left(\frac{A_0 - 2A_1 \cos \theta}{\sqrt{N_0/2}}\right) - Q\left(\frac{A_0}{\sqrt{N_0/2}}\right) + \int_0^{2A_1 \cos \theta} Q(\alpha(x))[f(x + A_0) - f(x - A_0)] dx. \quad (3.23)$$

Now, we replace the integral term in (3.21) by the expression given for \mathcal{I} in (3.23) to obtain the error probability as

$$P_e(\theta) = Q\left(\frac{A_0}{\sqrt{N_0/2}}\right) + \frac{A_1}{2\sqrt{\pi N_0}} \int_0^{2 \cos \theta} \left[\exp\left(-\frac{(A_1 x - A_0)^2}{N_0}\right) - \exp\left(-\frac{(A_1 x + A_0)^2}{N_0}\right) \right] \times Q\left(\frac{(A_0 - A_1 \cos \theta)x + A_1 - A_0 \cos \theta}{\sqrt{N_0/2} \sin \theta}\right) dx \quad (3.24)$$

which can be simplified to

$$P_e(\theta) = Q\left(\frac{A_0}{\sqrt{N_0/2}}\right) + \frac{A_1}{\sqrt{\pi N_0}} \int_0^{2 \cos \theta} \sinh\left(\frac{2A_0 A_1 x}{N_0}\right) \exp\left(-\frac{(A_1 x)^2 + A_0^2}{N_0}\right) \times Q\left(\frac{(A_0 - A_1 \cos \theta)x + A_1 - A_0 \cos \theta}{\sqrt{N_0/2} \sin \theta}\right) dx. \quad (3.25)$$

Note that eq. (3.25) is valid for $\theta \in [0, \pi/2)$. For other values of θ , $\cos \theta$ and $\sin \theta$ in (3.25) must be replaced by $|\cos \theta|$ and $|\sin \theta|$, respectively (see Appendix A for a proof).

3.1.3 Results and Discussion

The probability of the error of the receiver can be easily calculated from (3.25), for arbitrary values of SIR and θ . In Fig. 3.2 we have evaluated the BEP of the receiver for

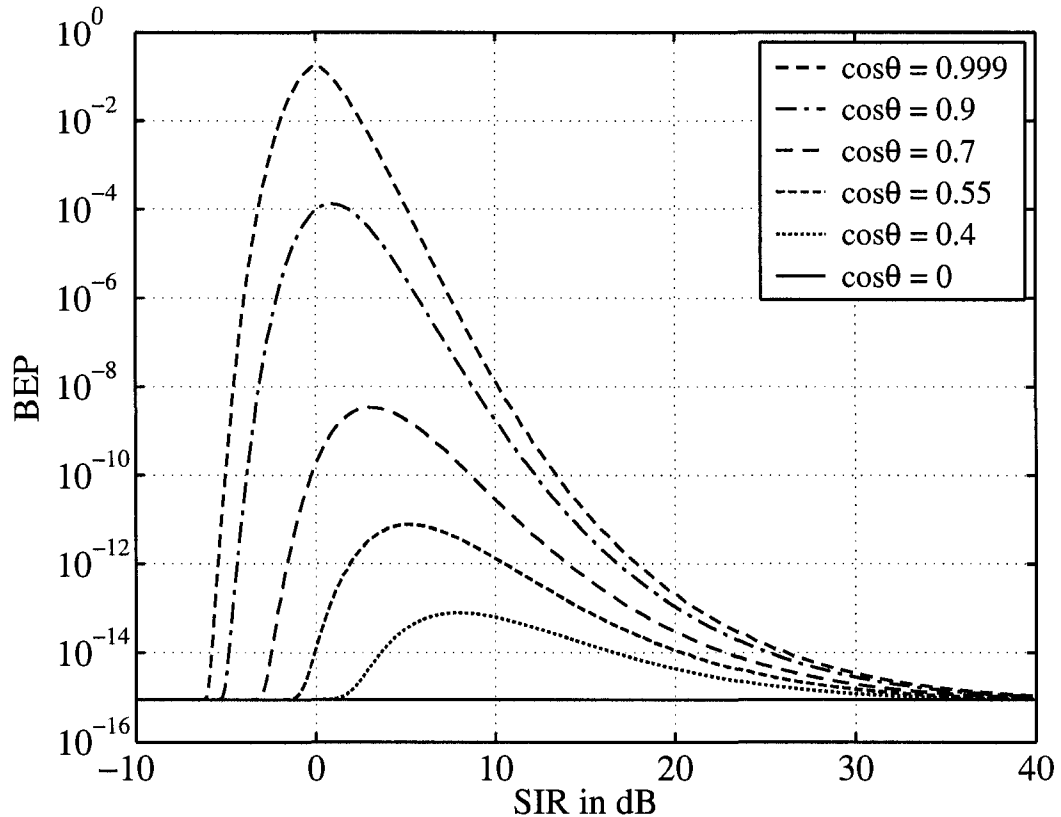


Figure 3.2. The BEP of the jointly optimal receiver as a function of SIR for SNR = 15 dB and various values of θ .

SNR = 15 dB and some θ values. From this figure we can see that the performance of the receiver is poorer for larger values of $\cos \theta$. This is because the correlation between the desired and interfering signals increases as $\cos \theta$ increases. Thus, the receiver is less likely to correctly detect the desired information bit. Note that by decreasing the value of $\cos \theta$ the worst case SIR, i.e., the SIR at which the BEP is maximum, is increased. This happens because for a two-user synchronous jointly optimal receiver, the asymptotic multiuser efficiency is minimum at $A_1/A_0 = |\rho|$ (or equivalently, $\text{SIR} = \rho^{-2}$) where ρ is the correlation between desired and interfering signals [19]. Thus, by decreasing the value of $\cos \theta$ the worst case SIR becomes larger.

Fig. 3.3 shows the BEP performance of the jointly optimal receiver, averaged over θ , i.e.,

$$P_e = \frac{1}{2\pi} \int_0^{2\pi} P_e(\theta) d\theta, \quad (3.26)$$

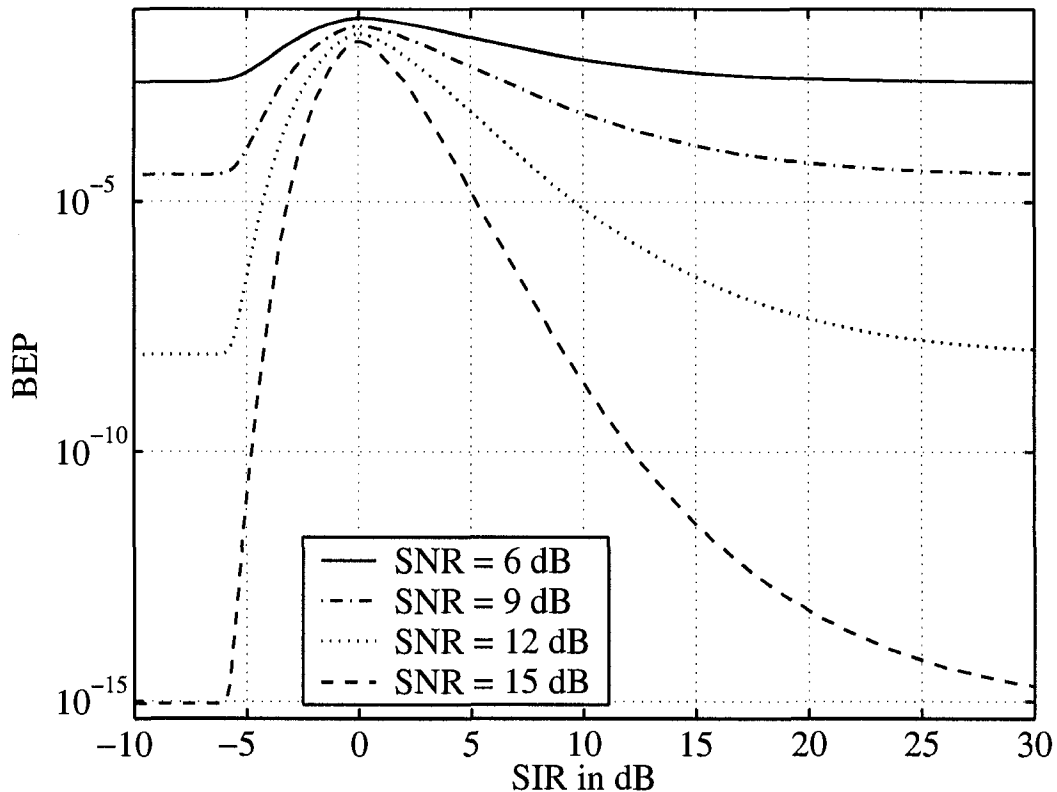


Figure 3.3. The performance of the jointly optimal receiver as a function of the SIR for various values of SNR.

as a function of SIR, obtained for different values of SNR. Note that, (3.25) has the interesting and intuitive form of the BEP of BPSK in AWGN (the first term) plus an additional error rate (the second term) due to interference. When $A_1 = 0$ there is no interference and the second term disappears, so the BEP of the receiver becomes that of BPSK in AWGN. Also, one can show using (3.25) that as $A_0/A_1 \rightarrow \infty$ or $A_1/A_0 \rightarrow \infty$, corresponding to a very large and very small SIR condition, $P_e \rightarrow Q(A_0/\sqrt{N_0/2})$. This is clearly seen in Fig. 3.3. In contrast to previous results [32]–[35], (3.25) highlights the dependence of P_e on θ . For example, when $\theta = \pi/2$ and $3\pi/2$, the second term in (3.25) is zero and P_e is the same as BPSK in AWGN. This is because the interference is orthogonal to the desired signal and the component of the interference affecting the detection of the desired signal is zero.

References [33], [35], have questioned the location of the maximum, i.e., worst case,

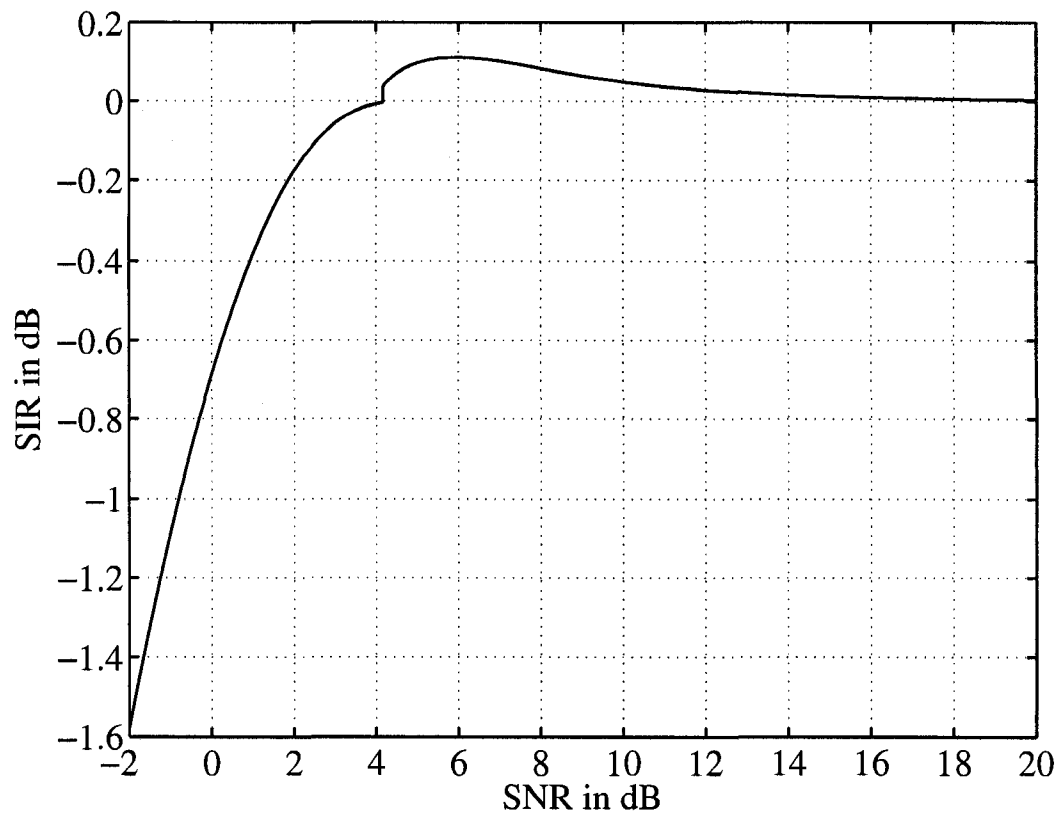


Figure 3.4. The worst case SIR as a function of SNR.

BEP as a function of the SIR for various SNR values. Using (3.25) we have obtained the SIR values at which the BEP is maximum, for different values of SNR shown in Fig. 3.4. Clearly, the maximum BEP does not always occur at $\text{SIR} = 0$ dB as conjectured in [33], [35]. For example, when the SNR is less than 4.17 dB, the worst case BEP occurs at some negative value of SIR as shown in Fig. 3.4. Moreover, the worst case SIR is not monotonically increasing for all values of SNR. Interestingly, the worst case SIR curve has a jump at $\text{SNR} = 4.17$ dB, and then asymptotically approaches 0 dB for $\text{SNR} \geq 4.17$ dB. This jump occurs because the BEP versus SIR curve has two local maxima on different sides of $\text{SIR} = 0$ dB (these maxima are very close to $\text{SIR} = 0$ dB and can not be seen in Fig. 3.3.) As the SNR increases from below 4.17 dB to greater than 4.17 dB, the global maximum jumps from the local maximum below $\text{SIR} = 0$ dB to the local maximum above $\text{SIR} = 0$ dB which causes a jump in the worst case SIR versus SNR curve.

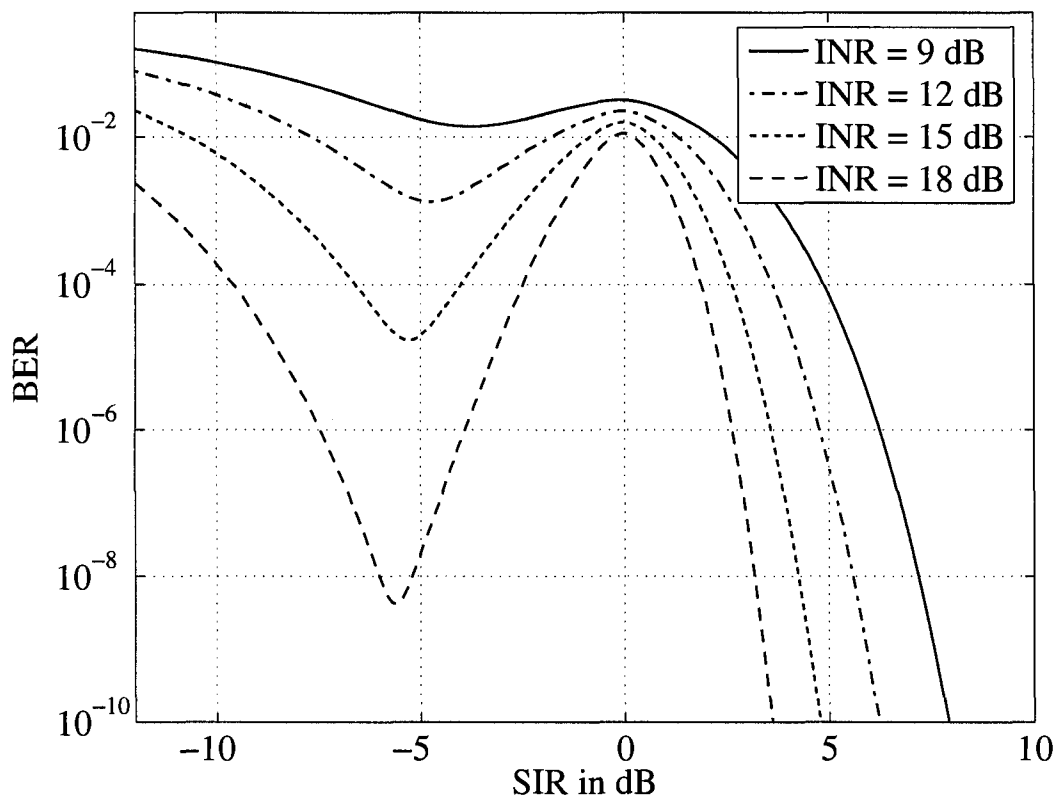


Figure 3.5. The performance of the jointly optimal receiver as a function of the SIR for some fixed values of INR.

Fig. 3.5 shows the error probability of the JOD as a function of SIR when the interference-to-noise ratio (INR), i.e., A_1^2/N_0 is fixed. Since $SIR = A_0^2/A_1^2$, one can readily find the SNR in dB as INR in dB plus SIR in dB. Interestingly, the BEP in this case is not a monotonically decreasing function of the SIR (or SNR) and has a local minimum around $SIR = -6$ dB. In other words, for some SIR range, increasing the desired user's power, just increases the BEP. For example, when $INR = 18$ dB and $SIR = -6$ dB increasing the SIR from -6 to 3 dB (or equivalently increasing the SNR from 12 to 21 dB) just degrades the receiver's performance. Thus, an efficient power control is one that attempts to keep the desired user's amplitude half of the amplitude of the interfering signal.

3.2 BER of a Two-User Synchronous IOD in AWGN

As mentioned earlier, the IOD maximizes the *a posteriori* probability for the desired user's information bit and outperforms JOD. The structure of the IOD was first derived in [15] for a two-user synchronous Gaussian channel. In [32], the error probability of the IOD was compared to that of the conventional MF receiver for the case when users employ pure cosine waves with different phases which are time-limited to a symbol interval, or effectively, rectangular pulse-shaping is used. While the performance of the jointly optimum receiver (JOR) is well-studied in the literature (see [3, Chapter 4] and references therein), to the best of our knowledge there are no exact analytical results on the bit error probability of the individually optimum receiver (IOR). Using the results of [40], in this section we derive an exact expression for the error probability of an IOR used to detect a BPSK signal corrupted by a similar cochannel interferer and AWGN. We will show that both detectors perform almost the same for large values of SNR and use this fact to specialize the resulting bit error rate (BER) expression to give the error probability of a two-user synchronous JOD in AWGN.

3.2.1 Signal Model and Receiver Structure

Assume that the received signal is given by

$$r(t) = A_0 b_0 s_0(t) + A_1 b_1 s_1(t) + n(t) \quad (3.27)$$

where $s_k(t)$ ($k = 0, 1$) is the k th user's signal waveform which has unit energy and is zero outside the interval $[0, T]$. The sampled output of the receiver filters matched to $s_0(t)$ and $s_1(t)$ are given by

$$r_0 = A_0 b_0 + A_1 b_1 \rho + n_0 \quad (3.28)$$

$$r_1 = A_0 b_0 \rho + A_1 b_1 + n_1 \quad (3.29)$$

respectively, where $\rho \triangleq \int_0^T s_0(t)s_1(t)dt$ is the cross-correlation between $s_0(t)$ and $s_1(t)$ and $n_k \triangleq \int_0^T n(t)s_k(t)dt$ is the noise component along $s_k(t)$ which is a Gaussian RV with mean zero and variance $N_0/2$. Moreover, n_0 and n_1 have covariance $\rho N_0/2$. Assume now that $\rho \neq 0$ (i.e., $s_0(t)$ and $s_1(t)$ are correlated) and $|\rho| < 1$. Then one can use the

Gram-Schmidt orthonormalization procedure [1] to obtain two orthogonal basis functions as

$$\phi_0(t) = s_0(t) \quad (3.30)$$

$$\phi_1(t) = \frac{s_1(t) - \rho s_0(t)}{\sqrt{1 - \rho^2}}. \quad (3.31)$$

Clearly, the projection of $r(t)$ onto $\phi_1(t)$ is

$$\begin{aligned} r_{\phi_1} &= A_1 b_1 \sqrt{1 - \rho^2} + n_{\phi_1} \\ &= \frac{1}{\sqrt{1 - \rho^2}} (r_1 - r_0 \rho) \end{aligned} \quad (3.32)$$

where n_{ϕ_1} is the component of $n(t)$ along $\phi_1(t)$ and is a zero-mean Gaussian RV with variance $N_0/2$. Eq. (3.32) can be rewritten as

$$r_1 = r_{\phi_1} \sqrt{1 - \rho^2} + r_0 \rho. \quad (3.33)$$

Note that the components of $n(t)$ along $\phi_0(t)$ and $\phi_1(t)$, i.e., n_{ϕ_0} and n_{ϕ_1} , are i.i.d. with common PDF, $f(\cdot)$.

3.2.2 BER Derivation

Some typical constellation points and the corresponding decision boundary of an IOR are shown in Figs. 3.6 and 3.7. The constellation points and the decision boundary are different depending on the sign of ρ . Thus, we obtain the probability of error for $\rho > 0$ and $\rho < 0$, separately. Furthermore, it will be seen that for BER evaluation we need to find an equation defining the curve \mathcal{B} in Figs. 3.6 and 3.7. To this end, one can obtain the equation of the decision boundary, \mathcal{B} , from (2.30) by equating the argument of the signum function to zero, i.e.,

$$r_0 = \frac{N_0}{4A_0} \log \left(\frac{\cosh \left[\frac{2A_1 r_1 + 2A_0 A_1 \rho}{N_0} \right]}{\cosh \left[\frac{2A_1 r_1 - 2A_0 A_1 \rho}{N_0} \right]} \right). \quad (3.34)$$

After some algebraic manipulations, one can obtain

$$e^{-\frac{2A_0 r_0}{N_0}} \cosh \left[\frac{2A_1 r_1 - 2A_0 A_1 \rho}{N_0} \right] = e^{\frac{2A_0 r_0}{N_0}} \cosh \left[\frac{2A_1 r_1 + 2A_0 A_1 \rho}{N_0} \right]. \quad (3.35)$$

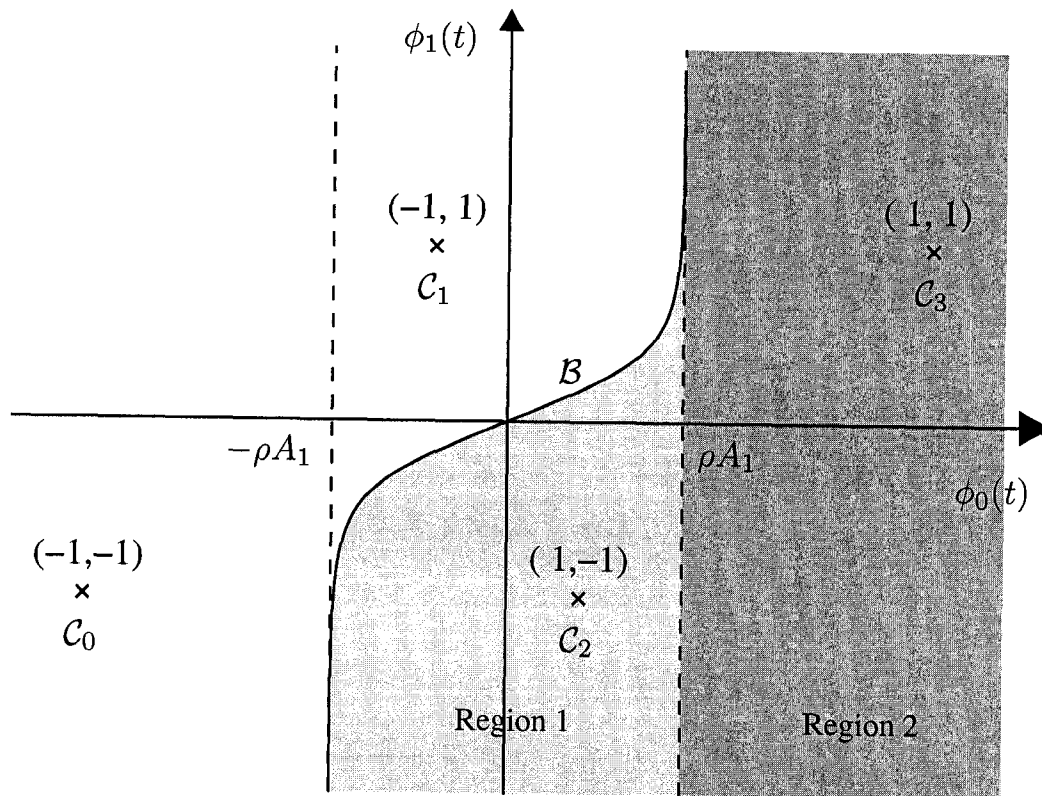


Figure 3.6. A typical received signal constellation and the decision boundary for a BPSK signal with one similar cochannel interferer for $\rho > 0$.

Now, we separate the terms which include $\exp[\frac{2A_1 r_1}{N_0}]$ from those which include $\exp[-\frac{2A_1 r_1}{N_0}]$ to obtain

$$-e^{-\frac{2A_1 r_1}{N_0}} \sinh\left[\frac{2A_0 r_0 + 2A_0 A_1 \rho}{N_0}\right] = e^{-\frac{2A_1 r_1}{N_0}} \sinh\left[\frac{2A_0 r_0 - 2A_0 A_1 \rho}{N_0}\right]. \quad (3.36)$$

The last equation is equivalent to

$$r_1 = \frac{N_0}{4A_1} \log\left(-\frac{\sinh\left[\frac{2A_0 r_0 + 2A_0 A_1 \rho}{N_0}\right]}{\sinh\left[\frac{2A_0 r_0 - 2A_0 A_1 \rho}{N_0}\right]}\right). \quad (3.37)$$

Now we replace r_1 in (3.37) with the expression on the right in (3.33) and rearrange to obtain

$$r_{\phi_1} = g(r_0) = -\frac{r_0 \rho}{\sqrt{1 - \rho^2}} + \frac{N_0}{4A_1 \sqrt{1 - \rho^2}} \log\left(-\frac{\sinh\left[\frac{2A_0 r_0 + 2A_0 A_1 \rho}{N_0}\right]}{\sinh\left[\frac{2A_0 r_0 - 2A_0 A_1 \rho}{N_0}\right]}\right). \quad (3.38)$$

Eq. (3.38) is an end result that defines the decision boundary in the ϕ_0 - ϕ_1 plane and will be used to determine the BER. It can be shown that $g(\cdot)$ is an odd function, i.e.,

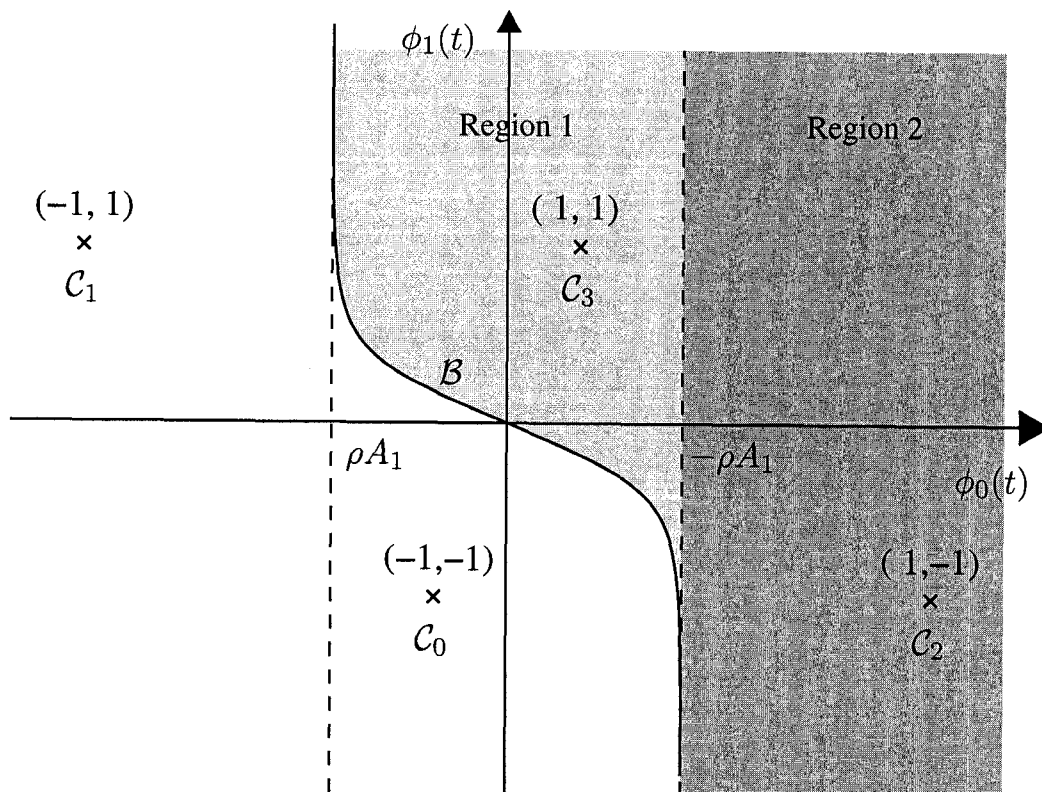


Figure 3.7. A typical received signal constellation and the decision boundary for a BPSK signal with one similar cochannel interferer for $\rho < 0$.

$g(x) = -g(-x)$. Moreover, $g(x)$ has two asymptotes at $x = A_1\rho$ and $x = -A_1\rho$. That is, $g(x) \rightarrow \infty$ when $x \rightarrow A_1\rho$ and $g(x) \rightarrow -\infty$ when $x \rightarrow -A_1\rho$ as seen in Figs. 3.6 and 3.7. When ρ is positive, an error will occur if n_{ϕ_0} and n_{ϕ_1} move the desired constellation point (C_0 or C_1) into the shaded area in Fig. 3.6. In order to calculate the probability of this event, we shift the origin to the point C_0 in Fig. 3.6. Then, the new equation defining the decision boundary, B , in terms of n_{ϕ_0} and n_{ϕ_1} will be

$$B: \quad n_{\phi_1} = g(n_{\phi_0} - A_0 - A_1\rho) + A_1\sqrt{1 - \rho^2} \quad (3.39)$$

where $g(\cdot)$ is given by (3.38). In order to find the BEP, we split the shaded area in Fig. 3.6 into two regions and integrate the joint PDF of n_{ϕ_0} and n_{ϕ_1} over these regions. This

leads to

$$p_0 = \int_{A_0}^{A_0+2A_1\rho} \int_{-\infty}^{g(n_{\phi_0}-A_0-A_1\rho)+A_1\sqrt{1-\rho^2}} f(n_{\phi_1}) dn_{\phi_1} f(n_{\phi_0}) dn_{\phi_0} \\ + \int_{A_0+2A_1\rho}^{\infty} \int_{-\infty}^{\infty} f(n_{\phi_1}) dn_{\phi_1} f(n_{\phi_0}) dn_{\phi_0}. \quad (3.40)$$

Similarly, if we shift the origin to point \mathcal{C}_1 , the new equation of \mathcal{B} and the error probability will be

$$\mathcal{B}: \quad n_{\phi_1} = g(n_{\phi_0} - A_0 + A_1\rho) - A_1\sqrt{1-\rho^2} \quad (3.41)$$

$$p_1 = \int_{A_0-2A_1\rho}^{A_0} \int_{-\infty}^{g(n_{\phi_0}-A_0+A_1\rho)-A_1\sqrt{1-\rho^2}} f(n_{\phi_1}) dn_{\phi_1} f(n_{\phi_0}) dn_{\phi_0} \\ + \int_{A_0}^{\infty} \int_{-\infty}^{\infty} f(n_{\phi_1}) dn_{\phi_1} f(n_{\phi_0}) dn_{\phi_0} \quad (3.42)$$

respectively. By comparing Figs. 3.6 and 3.7, one can see that the constellation points and the decision boundary for the case when $\rho < 0$ are the reflection in the ϕ_0 -axis of those of the case when $\rho > 0$. In particular, \mathcal{C}_0 and \mathcal{C}_1 in Fig. 3.7 are the reflection in the ϕ_0 -axis of \mathcal{C}_1 and \mathcal{C}_0 in Fig. 3.6, respectively. In other words, when $\rho < 0$, the probability that the noise components move the constellation points \mathcal{C}_0 and \mathcal{C}_1 to the shaded area in Fig. 3.7 are p_1 and p_0 , respectively, where p_0 and p_1 are given by (3.40) and (3.42). Since the overall probability of error, P_e , equals $\frac{1}{2}(p_0 + p_1)$, it can be seen that P_e is identical for the two cases provided that ρ is replaced with $|\rho|$ in (3.40) and (3.42).

Using (3.40) and (3.42), one can obtain the probability of error as

$$P_e = \frac{1}{2} \left\{ Q\left(\frac{A_0}{\sqrt{N_0/2}}\right) + Q\left(\frac{A_0 - 2A_1|\rho|}{\sqrt{N_0/2}}\right) - \int_0^{2A_1|\rho|} \left[Q\left(\frac{g(x - A_1|\rho|) + A_1\sqrt{1-\rho^2}}{\sqrt{N_0/2}}\right) \right. \right. \\ \left. \left. \times f(x + A_0) + Q\left(\frac{g(-x + A_1|\rho|) - A_1\sqrt{1-\rho^2}}{\sqrt{N_0/2}}\right) f(x - A_0) \right] dx \right\}. \quad (3.43)$$

Since $g(\cdot)$ is an odd function, the argument of the first Q -function in the integrand in (3.43) is the negative of the argument of the second Q -function in the integrand. Using this fact and replacing $Q(-\alpha)$ with $1 - Q(\alpha)$ in (3.43), one can obtain after some

manipulations,

$$P_e = Q\left(\frac{A_0}{\sqrt{N_0/2}}\right) + \frac{A_1}{\sqrt{\pi N_0}} \int_0^{2|\rho|} \exp\left(-\frac{(A_1 x)^2 + A_0^2}{N_0}\right) \sinh\left(\frac{2A_0 A_1 x}{N_0}\right) \\ \times Q\left(\frac{A_1(1-|\rho|x)}{\sqrt{N_0(1-\rho^2)}/2} + \frac{\sqrt{N_0/2}}{2A_1\sqrt{1-\rho^2}} \log\left[-\frac{\sinh\left[\frac{2A_0 A_1 x}{N_0}\right]}{\sinh\left[\frac{2A_0 A_1(x-2|\rho|)}{N_0}\right]}\right]\right) dx. \quad (3.44)$$

Eq. (3.44) is a general expression for the BER and is valid for all values of ρ , $|\rho| \neq 1$.

3.2.3 Results

When the SNR is large, i.e., N_0 is very small, the logarithm term in (3.44) quickly approaches $4A_0 A_1(x + |\rho|)/N_0$. Thus, the second term in the argument of the Q -function in the integrand in (3.44) approaches $A_0(x + |\rho|)/\sqrt{N_0(1-\rho^2)}/2$. Interestingly, if we replace the second term in the argument of the second Q -function in (3.44) by $A_0(x + |\rho|)/\sqrt{N_0(1-\rho^2)}/2$, we obtain

$$P_e = Q\left(\frac{A_0}{\sqrt{N_0/2}}\right) + \frac{A_1}{\sqrt{\pi N_0}} \int_0^{2|\rho|} \exp\left(-\frac{(A_1 x)^2 + A_0^2}{N_0}\right) \sinh\left(\frac{2A_0 A_1 x}{N_0}\right) \\ \times Q\left(\frac{(A_0 - A_1|\rho|x) + A_1 - A_0|\rho|}{\sqrt{N_0(1-\rho^2)}/2}\right) dx. \quad (3.45)$$

Eq. (3.45) is equivalent to the expression for the probability of error of a JOR in the presence of AWGN and a similar cochannel interferer derived in [40]. Correspondingly, when $N_0 \rightarrow 0$ and $\rho > 0$ the logarithm term in (3.38) approaches $4A_0 r_0/N_0$. Thus, (3.38) becomes

$$r_{\phi_1} = \frac{A_0 - A_1\rho}{A_1\sqrt{1-\rho^2}} r_0 \quad (3.46)$$

which is the equation defining the diagonal line in the decision boundary of a JOR in a two-user BPSK channel when $\rho > 0$. Note that when $|\rho| \rightarrow 1$, the Q -function in the integrand of (3.45) takes one of the values 0, 1 or $\frac{1}{2}$ corresponding to positive, negative or zero values of $(A_0 - A_1)(x - 1)$. Using this fact, one can obtain the error probability for the case when $|\rho| = 1$ as

$$P_e = \begin{cases} \frac{1}{2} \left[Q\left(\frac{A_0 - A_1}{\sqrt{N_0/2}}\right) + Q\left(\frac{A_0 + A_1}{\sqrt{N_0/2}}\right) \right], & \text{if } A_0 > A_1 \\ \frac{1}{2} \left[Q\left(\frac{A_0}{\sqrt{N_0/2}}\right) + \sum_{k=-2}^2 (-1)^k Q\left(\frac{A_0 + kA_1}{\sqrt{N_0/2}}\right) \right], & \text{if } A_0 < A_1 \\ \frac{1}{4} \left[1 + Q\left(\frac{A_0}{\sqrt{N_0/2}}\right) + Q\left(\frac{3A_0}{\sqrt{N_0/2}}\right) \right], & \text{if } A_0 = A_1. \end{cases} \quad (3.47)$$

The error probability of the CMF receiver in a two-user synchronous AWGN channel is [3]

$$P_e = \frac{1}{2} \left[Q \left(\frac{A_0 - \rho A_1}{\sqrt{N_0/2}} \right) + Q \left(\frac{A_0 + \rho A_1}{\sqrt{N_0/2}} \right) \right]. \quad (3.48)$$

When $|\rho| = 1$, the error probability given by (3.47) is the same as the BER of the jointly optimal receiver for $A_0 > A_1$. In other words, in this special case the JOD does not have any superiority over the conventional MF receiver. Moreover, when $|\rho| = 1$ and $A_0 = A_1$, eq. (3.48) simplifies to

$$P_e = \frac{1}{4} + \frac{1}{2} Q \left(\frac{2A_0}{\sqrt{N_0/2}} \right). \quad (3.49)$$

Observing that $Q(x)$ is concave up for $x > 0$ [3], we can use Jensen's inequality [41] to obtain

$$Q \left(\frac{2A_0}{\sqrt{N_0/2}} \right) \leq \frac{1}{2} Q \left(\frac{A_0}{\sqrt{N_0/2}} \right) + \frac{1}{2} Q \left(\frac{3A_0}{\sqrt{N_0/2}} \right). \quad (3.50)$$

Using (3.50) one can compare (3.49) with the expression given for the BER in (3.47) for $A_0 = A_1$ and conclude that the conventional receiver outperforms the ML receiver that jointly detects b_0 and b_1 . This is because the ML receiver tries to maximize the decision metric for both b_0 and b_1 , not for b_0 individually. In this special case, the individually optimal receiver outperforms the ML receiver and its probability of error equals that of a conventional MF receiver. Note that in this case, both receivers suffer from an irreducible error floor, i.e., the minimum error probability is $\frac{1}{4}$ even when $\text{SNR} \rightarrow \infty$.

We have evaluated the BER of the IOR and JOR as a function of SNR for $A_0 = A_1$ and the following cases:

- i. ρ is deterministic and equals 0.99, 0.9, 0.5 and 0.
- ii. ρ is a random variable defined as $\rho \triangleq \cos \theta$, where θ is a uniform random variable over $[0, 2\pi)$. In this case, the BER is averaged over θ .

The results are shown in Fig. 3.8. When $\rho = \cos \theta$, and the BER is averaged over θ , the IOR achieves slightly better performance than the JOR only when the SNR is small and the BER is impractically large, or bordering on being so. For example, for BER = 0.2 the JOR needs almost 0.31 dB more power to achieve the same performance as the IOR, while at SNR = 3 dB and BER = 0.08, the receivers perform approximately

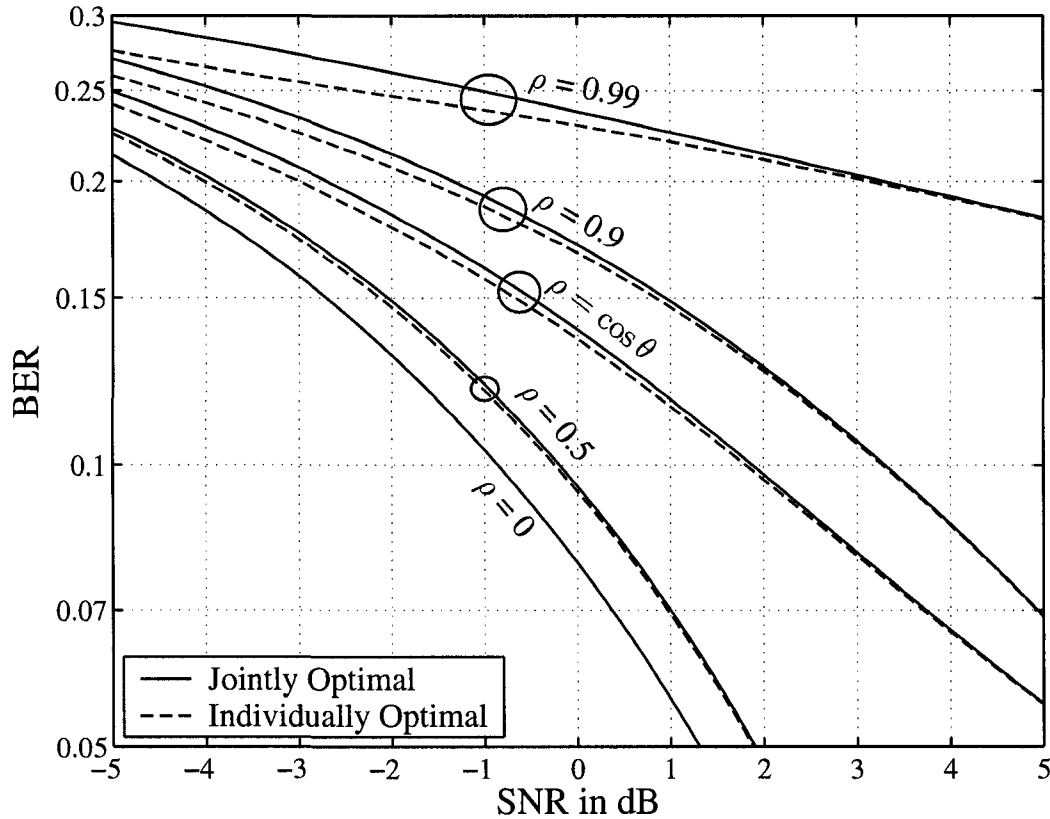


Figure 3.8. The average probability of error of the IOR and JOR for $A_0 = A_1$ and $\rho = 0.99, 0.9, .5$ and 0 and $\rho = \cos \theta$ where θ is uniformly distributed over $[0, 2\pi)$.

the same. Furthermore, Fig. 3.8 shows that the BER of the JOR approaches that of the IOR (even for low SNR values) as ρ approaches zero.

The multiuser efficiency of the IOD and JOD as a function of A_1/A_0 is depicted in Fig. 3.9 for some selected values of SNR and $\rho = \cos \theta$ where θ is uniformly distributed over $[0, 2\pi)$. Clearly, the IOD performs more efficiently than the JOD for all three values of SNR. Furthermore, for low SNR values the IOR has a higher multiuser efficiency than the JOR while for high SNRs the multiuser efficiency of both receivers is approximately the same. This is because for low SNR values the decision boundary of IOR is too *curved* to be approximated with the straight lines that constitute the JOR's decision boundaries [40]. Note that when SNR increases, the dominant source of error for the multiuser detectors (MUD's) is no longer background noise but the CCI. Thus, the multiuser efficiency of the MUD's decreases as SNR increases.

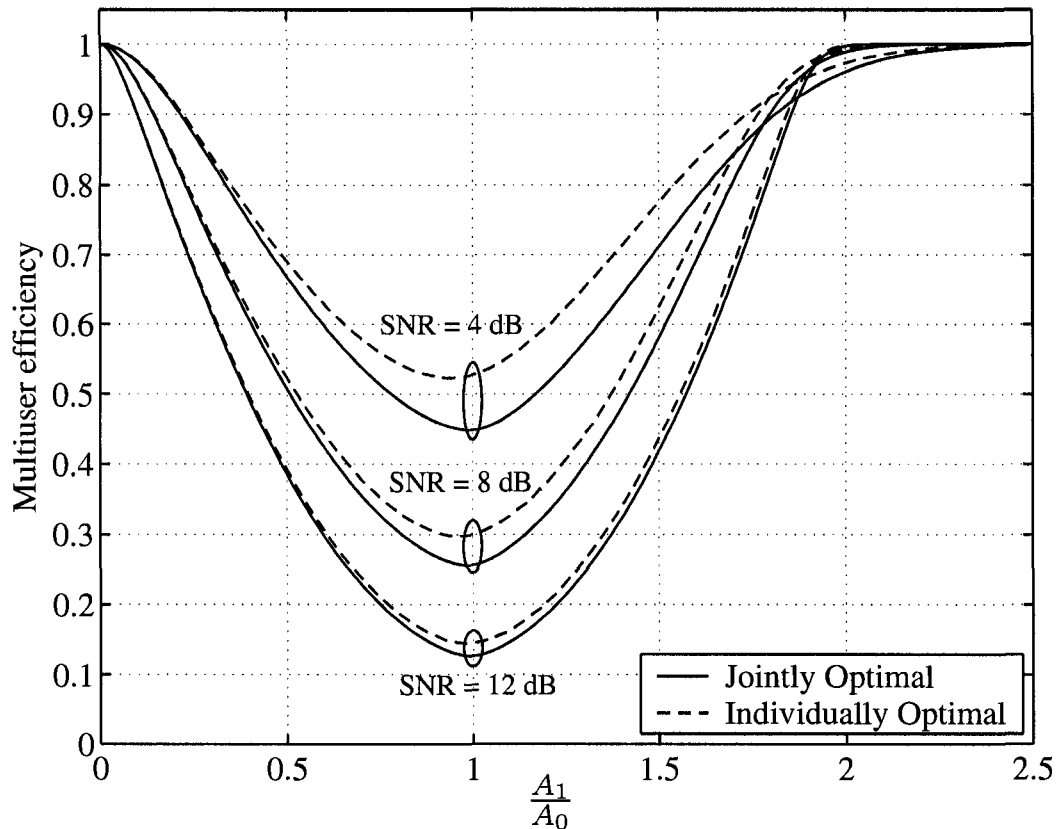


Figure 3.9. The multiuser efficiencies of the IOR and JOR as a function of A_1/A_0 for $\rho = \cos \theta$ where θ is uniformly distributed over $[0, 2\pi)$ and SNR = 4, 8 and 12 dB.

3.3 BER of a Bandlimited Two-User JOD With Carrier Phase Error

Two important limitations regarding the results in [3], [32]–[35], [40] are that in these references the carrier phase recovery is assumed perfect, and that the users are assumed to use a rectangular pulse. Most practical communications systems operating at finite values of SIR will exhibit some carrier phase recovery error mainly due to background noise, interference and instabilities in carrier frequency. Furthermore, in receivers which make use of a phase-locked loop for phase acquisition, severe phase offsets may be caused by hangups, cycle slippings and false locks [42]. On the other hand, using a rectangular pulse is practically prohibited because a practical channel always has a limited bandwidth which distorts the rectangular pulse and causes intersymbol interference (ISI). In this

section, we extend the results in [40] to derive a new, exact BER expression for a ML receiver used to detect two BPSK signals in the presence of AWGN and imperfect carrier phase recovery. Different from the results in [35], [40], the new BER expression is valid for all values of cross-correlation between transmitted signals (not just for positive values) and accounts for both carrier phase recovery error and pulse-shaping. The results show that the BER is quite sensitive to phase errors, particularly for small values of SIR.

3.3.1 System Model

Consider the transmission of two bandlimited BPSK signals over a synchronous, AWGN channel. Then, the received signal is given by

$$r(t) = \sqrt{2} \sum_{n=-\infty}^{\infty} \{A_0 b_{0,n} p_0(t - nT) \cos \omega t + A_1 b_{1,n} p_1(t - nT) \cos(\omega t + \theta)\} + n(t) \quad (3.51)$$

where $b_{k,n} \in \{-1, 1\}$ and $p_k(t)$ are the information bit in the n th symbol interval and the transmitter pulse-shaping filter's impulse response of the k th user, respectively; T is the symbol interval and θ and $n(t)$ are as defined in Subsection 3.3.1. Assume that $p_k(t)$ has unit energy and satisfies Nyquist's first criterion [1], i.e., $R_{p_k p_k}(nT) = \delta(n)$ and $R_{p_k p_l}(t)$ is defined as

$$R_{p_k p_l}(t) \triangleq \int_{-\infty}^{\infty} p_k(\tau) p_l(\tau - t) d\tau, \quad k, l = 0, 1. \quad (3.52)$$

Also assume that there is no cochannel interference from the symbols transmitted before or after the n th symbol, i.e., $R_{p_0 p_1}(nT) = \mu \delta(n)$ where $|\mu| \leq 1$. Defining $s_0(t) \triangleq \sqrt{2} p_0(t) \cos \omega t$ and $s_1(t) \triangleq \sqrt{2} p_1(t) \cos(\omega t + \theta)$, it can be readily seen that

$$\rho = \int_{-\infty}^{\infty} s_0(t) s_1(t) dt = \mu \cos \theta \quad (3.53)$$

provided that $\omega T \gg 1$. At the receiver, $r(t)$ is passed through two filters matched to $\phi_0(t)$ and $\phi_1(t)$ defined by (3.30) and (3.31), and sampled at $t = lT$. Using the assumption $\omega T \gg 1$ and the fact that $R_{p_k p_l}(nT)$ is nonzero only if n equals zero, the sampled received signal at the output of the matched filters will be

$$r_0(lT) = \sum_{n=-\infty}^{\infty} \{A_0 b_0 \cos \omega lT + A_1 b_1 \mu \cos(\omega lT + \theta)\} \delta(l - n) + n_0(lT) \quad (3.54)$$

$$r_1(lT) = \frac{1}{\sqrt{1-\rho^2}} \sum_{n=-\infty}^{\infty} \{A_0 b_0 [\mu \cos(\omega lT + \theta) - \rho \cos \omega lT] \\ + A_1 b_1 [\cos \omega lT - \rho \mu \cos(\omega lT + \theta)]\} \delta(l-n) + n_1(lT) \quad (3.55)$$

where $n_k(lT) \triangleq \int_{-\infty}^{\infty} n(\tau) \phi_k(\tau - lT) d\tau$ and $n_0(lT)$ and $n_1(lT)$ are two independent Gaussian random variables with mean zero, variance $N_0/2$ and common PDF $f(\cdot)$. Assuming that ωT is an integer multiple of 2π , eqs. (3.54) and (3.55) can be simplified to

$$r_0 = b_0 A_0 + b_1 A_1 \rho + n_0 \quad (3.56)$$

$$r_1 = b_1 A_1 \sqrt{1-\rho^2} + n_1 \quad (3.57)$$

where for simplicity of notation we have dropped the arguments of $r_k(lT)$ and $n_k(lT)$. The maximum likelihood decision rule for bits b_0 and b_1 (jointly optimal detection) is given by [3]

$$\arg \max_{\hat{b}_0, \hat{b}_1} \left\{ \hat{b}_0 A_0 r_0 + \hat{b}_1 A_1 \left(\rho r_0 + \sqrt{1-\rho^2} r_1 \right) - \hat{b}_0 \hat{b}_1 A_0 A_1 \rho \right\} \quad (3.58)$$

where \hat{b}_0 and \hat{b}_1 are the estimated bits corresponding to the desired and interfering users, respectively.

3.3.2 BER Derivation

Assume that the carrier phases of the desired and interfering users are not perfectly known at the receiver and denote the estimated phase of the desired and interfering carriers as $\hat{\theta}_0$ and $\hat{\theta}_1$, respectively. Then, the k th user's signal is given by

$$\hat{s}_k(t) \triangleq \sqrt{2} p_k(t) \cos(\omega t + \hat{\theta}_k) \quad k = 0, 1. \quad (3.59)$$

Furthermore, the cross-correlation between $\hat{s}_0(t)$ and $\hat{s}_1(t)$ becomes $\hat{\rho} = \mu \cos(\hat{\theta}_1 - \hat{\theta}_0)$. Using the Gram-Schmidt orthonormalization procedure one can get two basis functions $\hat{\phi}_0(t)$ and $\hat{\phi}_1(t)$ defined by (3.30) and (3.31) with ρ , $s_0(t)$ and $s_1(t)$ replaced by $\hat{\rho}$, $\hat{s}_0(t)$ and $\hat{s}_1(t)$, respectively. The sampled received signal at the output of the filters matched to the new basis functions are

$$\hat{r}_0 = b_0 c_0 + b_1 c_1 + \hat{n}_0 \quad (3.60a)$$

$$\hat{r}_1 = b_0 d_0 + b_1 d_1 + \hat{n}_1 \quad (3.60b)$$

where

$$c_0 \triangleq A_0 \cos \hat{\theta}_0 \quad (3.60c)$$

$$c_1 \triangleq A_1 \mu \cos(\theta - \hat{\theta}_0) \quad (3.60d)$$

$$d_0 \triangleq A_0 \left[\frac{\mu \cos \hat{\theta}_1 - \hat{\rho} \cos \hat{\theta}_0}{\sqrt{1 - \hat{\rho}^2}} \right] \quad (3.60e)$$

$$d_1 \triangleq A_1 \left[\frac{\cos(\theta - \hat{\theta}_1) - \mu \hat{\rho} \cos(\theta - \hat{\theta}_0)}{\sqrt{1 - \hat{\rho}^2}} \right] \quad (3.60f)$$

and \hat{n}_0 and \hat{n}_1 are the components of $n(t)$ along $\hat{\phi}_0(t)$ and $\hat{\phi}_1(t)$, which are independent Gaussian random variables with the same mean, variance and PDF as n_0 and n_1 . In this case, the ML decision rule is again given by (3.58) with ρ , r_0 and r_1 replaced by $\hat{\rho}$, \hat{r}_0 and \hat{r}_1 , respectively. This decision rule for bit b_0 can be alternatively expressed as [3]

$$\hat{b}_0 = \text{sgn} \left\{ A_0 \hat{r}_0 + \frac{1}{2} A_1 \left| \hat{\rho} \hat{r}_0 + \sqrt{1 - \hat{\rho}^2} \hat{r}_1 - A_0 \hat{\rho} \right| - \frac{1}{2} A_1 \left| \hat{\rho} \hat{r}_0 + \sqrt{1 - \hat{\rho}^2} \hat{r}_1 + A_0 \hat{\rho} \right| \right\} \quad (3.61)$$

The constellation points and the corresponding decision boundaries for $\hat{\rho} > 0$ and $\hat{\rho} < 0$ are shown in Figs. 3.10 and 3.11, respectively. In order to obtain the equation defining the line L in the $\hat{\phi}_0 - \hat{\phi}_1$ plane, one should equate the argument of the signum function in (3.61) to zero, to get

$$L : \hat{r}_1 = \frac{A_0 \text{sgn}(\hat{\rho}) - \hat{\rho} A_1}{A_1 \sqrt{1 - \hat{\rho}^2}} \hat{r}_0. \quad (3.62)$$

Furthermore, it can be shown that the coordinates of the points P_i and P_j are given by

$$P_i : \left(A_1 \hat{\rho}, \frac{A_0 - A_1 |\hat{\rho}|}{\sqrt{1 - \hat{\rho}^2}} |\hat{\rho}| \right) \quad (3.63)$$

$$P_j : \left(-A_1 \hat{\rho}, -\frac{A_0 - A_1 |\hat{\rho}|}{\sqrt{1 - \hat{\rho}^2}} |\hat{\rho}| \right). \quad (3.64)$$

From Figs. 3.10 and 3.11 one can readily see that the constellation points are not symmetric about the decision boundaries. In other words, the receiver whose boundaries are shown in Figs. 3.10 and 3.11 is no longer *minimum distance*. It is important to note that if the carrier phase estimates, i.e., $\hat{\theta}_0$ and $\hat{\theta}_1$ are such that $c_0 + c_1 < \hat{\rho} A_1$, then \mathcal{C}_0 and \mathcal{C}_3 will move to the $b_0 = 1$ and $b_0 = -1$ decision regions, respectively. Hence,

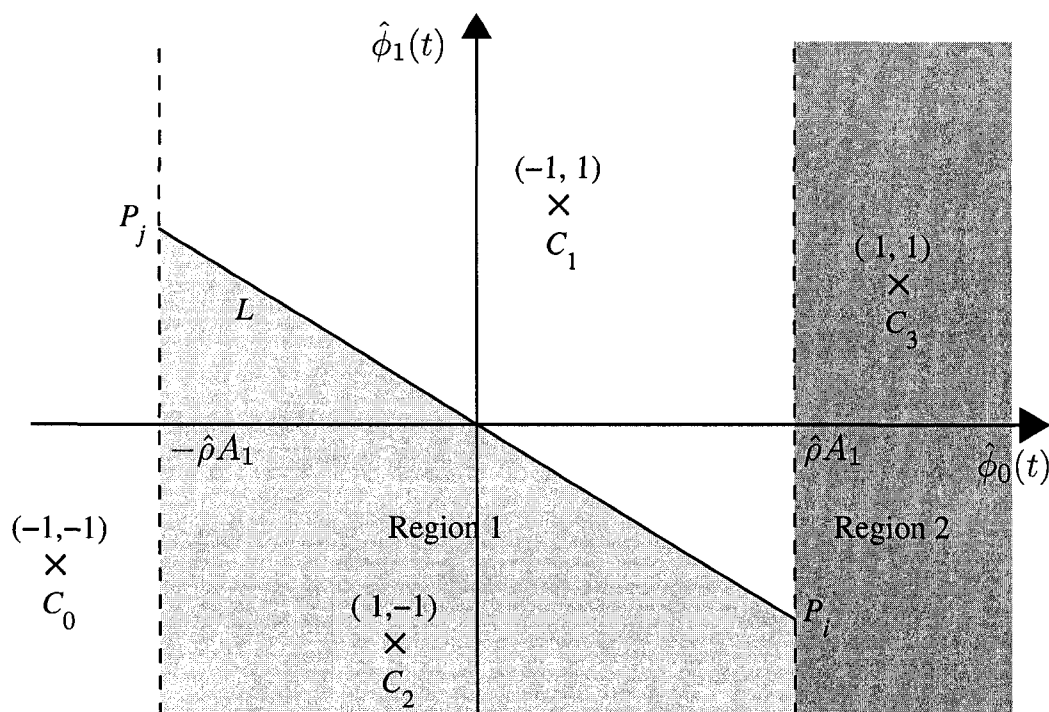


Figure 3.10. A typical received signal constellation and the corresponding decision boundaries for a BPSK signal and one identical cochannel interferer in the presence of carrier phase error for $\hat{\rho} > 0$.

when $b_0 = b_1$, i.e., the desired constellation point is either C_0 or C_3 , and the background noise is negligible, the receiver is likely to detect b_0 in error. Since b_0 equals b_1 in 50% of the cases (provided the transmitted bits are equiprobable), we expect the receiver's error probability to be approximately equal to 0.5.¹ Similarly, if $-c_0 + c_1 > \hat{\rho}A_1$ and $b_0 = -b_1$ the receiver is likely to detect b_0 in error in approximately 50% of the cases even for vanishing small background noise. When $c_0 + c_1 < \hat{\rho}A_1 < -c_0 + c_1$ and the background noise is negligible, the receiver always detects b_0 in error. In this case the background noise can improve the receiver's performance by moving the constellation points to their designated decision regions.

Assume that the information bits are equiprobable. Then, because of symmetry, the probability of error is the same for $b_0 = -1$ and $b_0 = 1$. Thus, it is sufficient to derive

¹When $\hat{\rho} > 0$ and $-\hat{\rho}A_1 < c_0 + c_1 < \hat{\rho}A_1$ an error floor occurs only if C_0 is below, and C_3 is above, the diagonal line L .

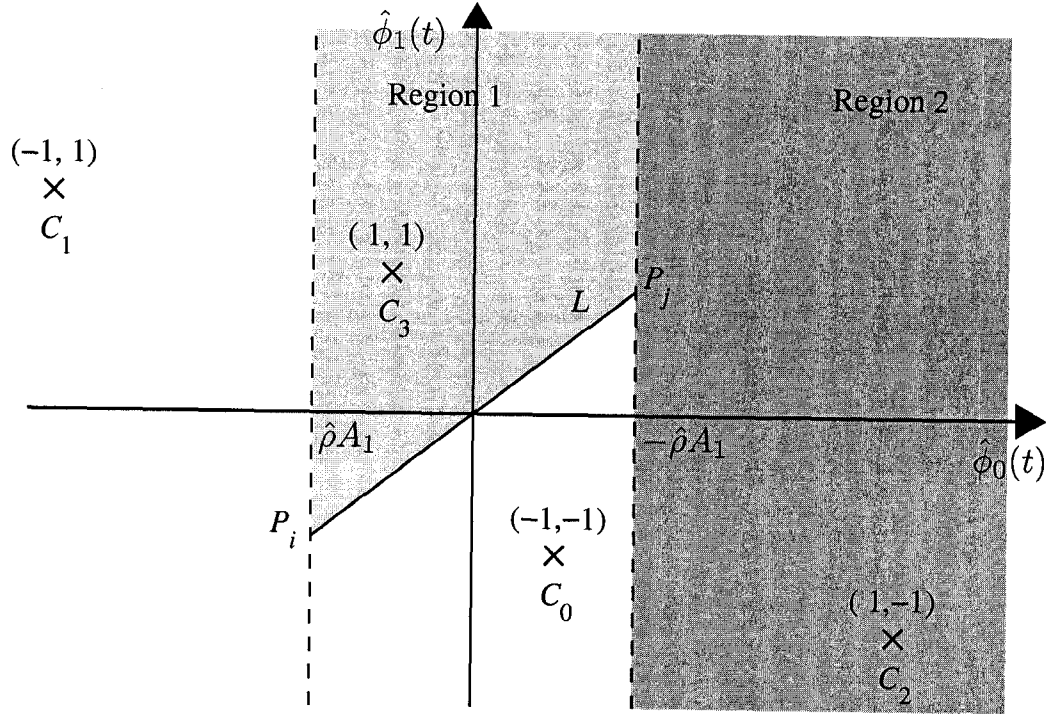


Figure 3.11. A typical received signal constellation and the corresponding decision boundaries for a BPSK signal and one identical cochannel interferer in the presence of carrier phase error for $\hat{\rho} < 0$.

the probability of error for $b_0 = -1$. Using this fact along with the procedure described in [40], one can obtain the receiver's bit error probability as

$$\begin{aligned}
 P_e = \frac{1}{2} \sum_{i=0}^1 \left\{ Q \left(\frac{-A_1 \hat{\rho} + c_0 + (-1)^i c_1}{\sqrt{N_0/2}} \right) \right. \\
 \left. - A_1 \int_0^{2\hat{\rho}} Q \left(\frac{(A_0 - |\hat{\rho}|A_1)(x - \hat{\rho})}{\sqrt{(1 - \hat{\rho}^2)N_0/2}} + \frac{d_0 + (-1)^i d_1}{\sqrt{N_0/2}} \right) \right. \\
 \left. \times f(A_1 \operatorname{sgn}(\hat{\rho})(x - \hat{\rho}) + c_0 + (-1)^i c_1) \right\} dx. \quad (3.65)
 \end{aligned}$$

Eq. (3.65) is a general expression for the receiver's error probability in the presence of carrier phase recovery error. By replacing $\hat{\theta}_0$ with 0 and $\hat{\theta}_1$ with θ in (3.65) (through (3.60)), one can obtain the receiver's error probability in the case of perfect carrier phase recovery for all values of $\rho \in (-1, 1)$ as obtained in (3.45).

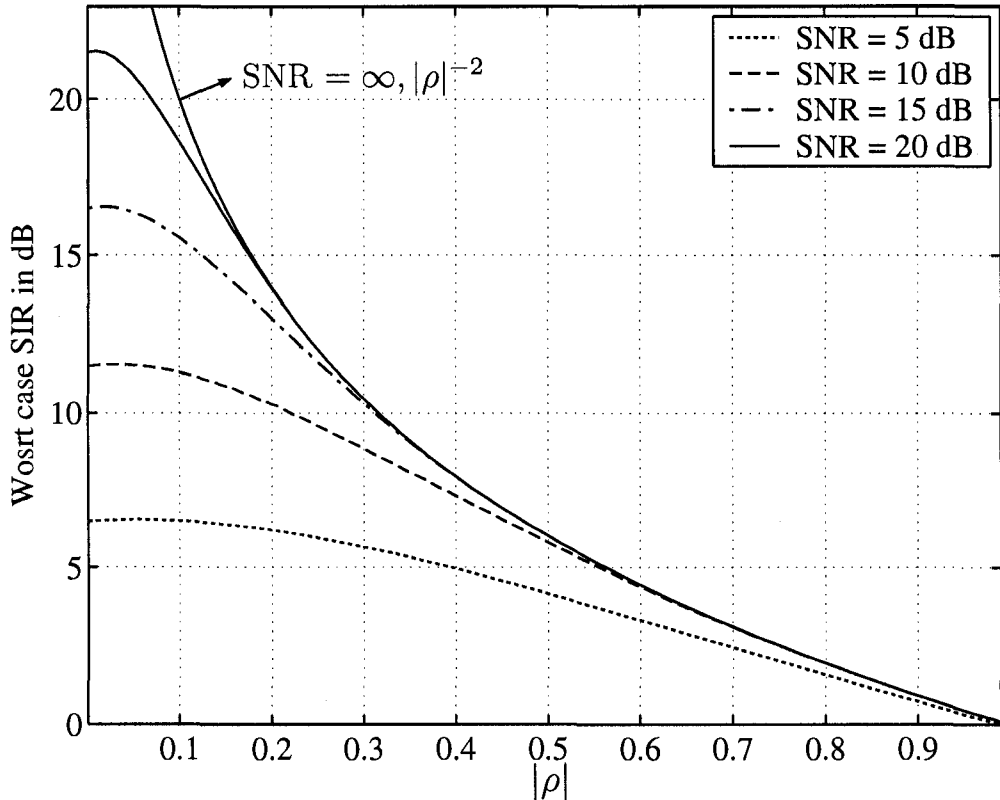


Figure 3.12. The worst case SIR as a function of $|\rho|$ for different SNR values.

3.3.3 Results and Discussion

For a two-user JOR and vanishing background noise (i.e., $N_0 \rightarrow 0$), the maximum BER occurs at $\text{SIR} = |\rho|^{-2}$ [3]. To confirm this fact, and to see how sensitive the BER is to the value of $|\rho|$, we have evaluated the worst case SIR, i.e., the SIR at which the BER is maximum, as a function of $|\rho|$ for some SNR values which are shown in Fig. 3.12. From this figure one can see that for large SNR values, by increasing the value of $|\rho|$, the worst case SIR curve rapidly approaches that of vanishing noise. For example, the worst case SIR for SNR = 20 dB and SNR $\rightarrow \infty$ is graphically the same when $|\rho|$ is greater than 0.17. This happens for SNR = 15 and 10 dB when $|\rho|$ is greater than 0.35 and 0.6, respectively.

The receiver's error probability as a function of SIR for $\theta = 45^\circ$ and various values of $\hat{\theta}_0$ and $\hat{\theta}_1$ is depicted in Fig. 3.13. When the estimated interferer carrier phase is different

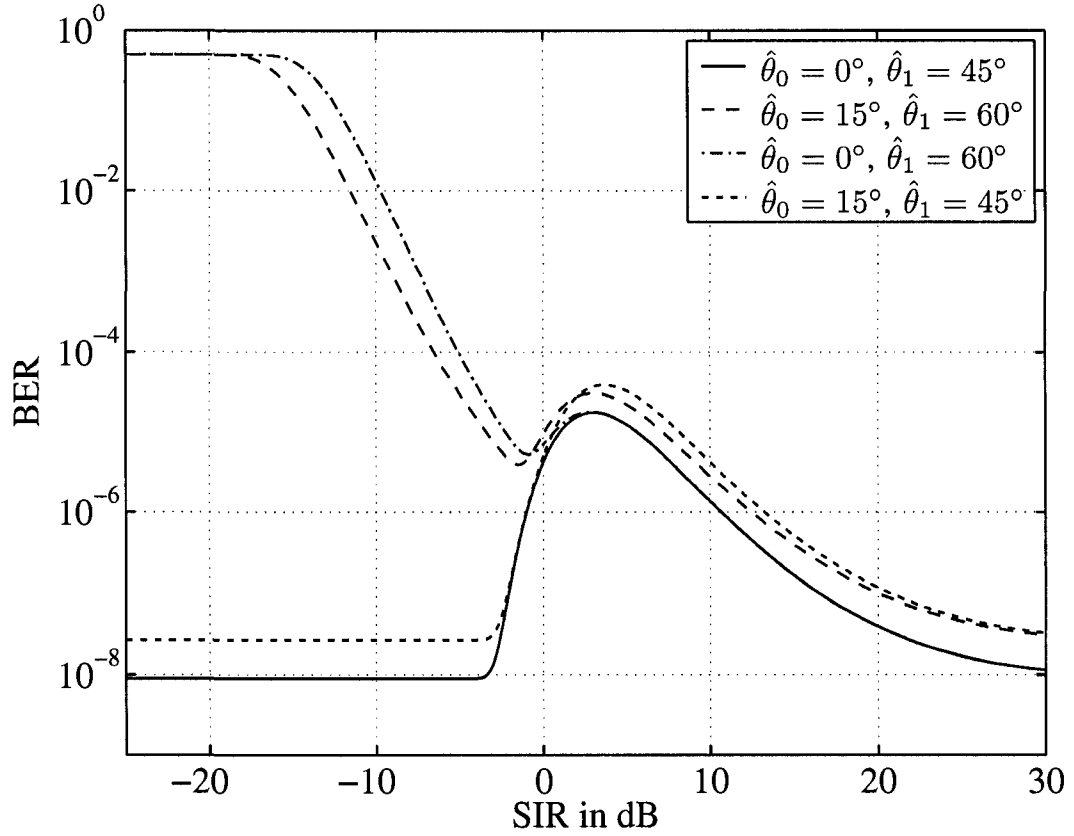


Figure 3.13. The JOD receiver's BER as a function of SIR for various values of $\hat{\theta}_0$ and $\hat{\theta}_1$, SNR = 12 dB, $\theta = 45^\circ$ and $\mu = 1$.

from its actual value, i.e., $\hat{\theta}_1 \neq \theta$, the error probability approaches 0.5 for $\text{SIR} \leq -20$ dB for both $\hat{\theta}_0 = 15^\circ$ and $\hat{\theta}_0 = 0^\circ$. In other words, when the interferer's carrier phase is not exactly recovered ($\hat{\theta}_1 \neq \theta$) and $\text{SIR} \rightarrow -\infty$ dB, the optimum receiver becomes ineffective even if the desired user's carrier phase is perfectly estimated, i.e., $\hat{\theta}_0 = 0^\circ$. Nonetheless, in the latter case, increasing the SIR improves the receiver's performance and for $\text{SIR} > 5$ dB the receiver performs effectively. Note that from (3.65), it can be readily seen that when $\text{SIR} \rightarrow \infty$ the second term on the right approaches zero. Therefore, the receiver's error probability approaches $Q(A_0 \cos \hat{\theta}_0 / \sqrt{N_0/2})$ for large SIR values. Hence, when $\text{SIR} \rightarrow \infty$, the receiver has the same $20 \log_{10} \cos \hat{\theta}_0$ dB SNR loss compared to the case of perfect phase recovery as does a single-user BPSK receiver in AWGN with the same phase error.

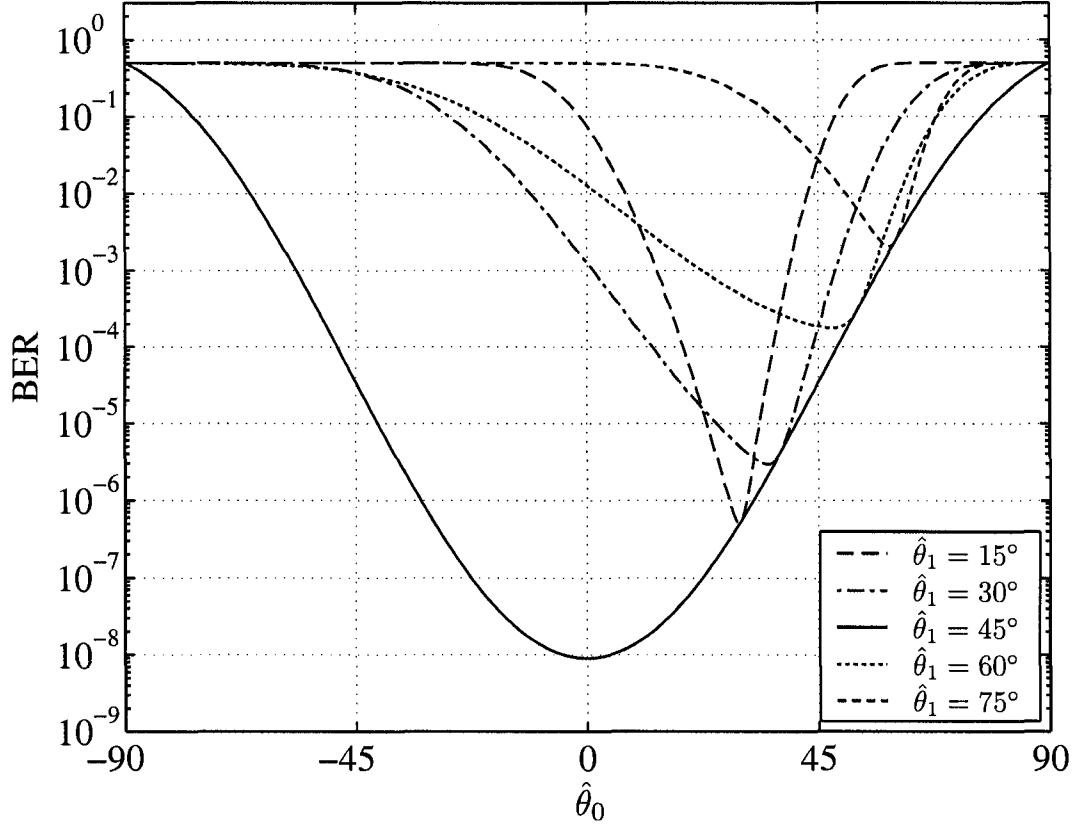


Figure 3.14. The receiver's BER as a function of $\hat{\theta}_0$ for SNR = 12 dB, $\theta = 45^\circ$, $\mu = 1$ and SIR = -10 dB.

Figs. 3.14 and 3.15 show the receiver's BER as a function of $\hat{\theta}_0$ for various values of $\hat{\theta}_1$ and for fixed SIRs of -10 and 10 dB. When SIR = -10 dB and $\hat{\theta}_0$ is fixed, the receiver with $\hat{\theta}_1 = 45^\circ$ outperforms those with an erroneous $\hat{\theta}_1$ as shown in Fig. 3.15. Furthermore, the larger the value $|\theta - \hat{\theta}_1|$, the wider is the $\hat{\theta}_0$ interval for which the receiver becomes ineffective, i.e., BER = 0.5. When SIR = 10 dB, the minimum achievable error probability can be reached by the receiver at or around the exact value of $\hat{\theta}_0$ even for erroneous $\hat{\theta}_1$ values, as shown in Fig. 3.15. Note that when $\hat{\theta}_1 = 75^\circ$, the minimum achievable BER can be reached for a wider $\hat{\theta}_0$ interval compared to the case when $\hat{\theta}_1 \neq 75^\circ$. This can be explained as follows. As the SIR increases the decision boundary in $\hat{\phi}_0 - \hat{\phi}_1$ plane becomes narrower and in limit, i.e., SIR $\rightarrow \infty$, the decision boundary simply is the $\hat{\phi}_1$ axis. Thus, the ML receiver will be the same as the conventional matched filter receiver. In this case, changing $\hat{\theta}_0$ moves the constellation points mostly

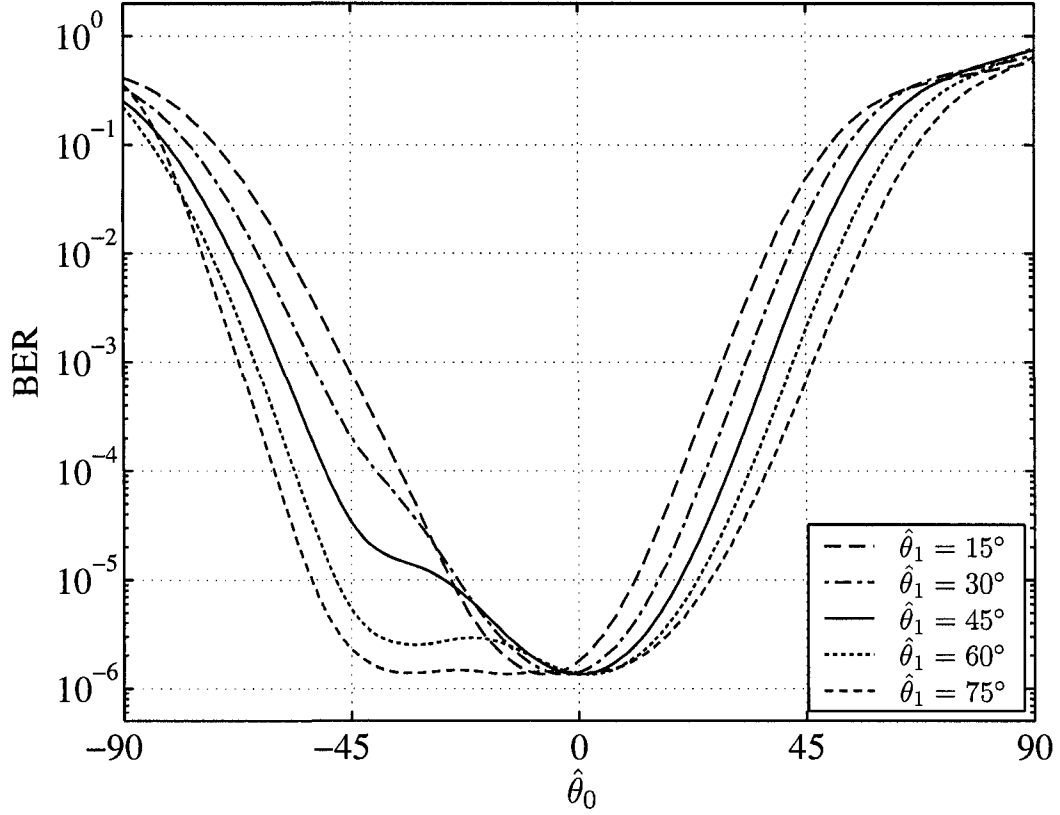


Figure 3.15. The receiver's BER as a function of $\hat{\theta}_0$ for SNR = 12 dB, $\theta = 45^\circ$, $\mu = 1$ and SIR = 10 dB.

along the $\hat{\phi}_1$ axis rather than along the $\hat{\phi}_0$ axis. For the particular case of $\hat{\theta}_1 = 75^\circ$, the constellation points are moving from below the $\hat{\phi}_0$ axis to above it while their distances from the $\hat{\phi}_1$ axis are approximately constant. Hence, we expect the receiver to be more robust to $\hat{\theta}_0$ errors in this case.

Chapter 4

Two Multiuser Combining Receiver Diversity Structures

CCI and multipath fading are two major sources of distortion in multiuser radio communication systems. Receiver antenna diversity has been shown to be an effective means to simultaneously mitigate the fading and CCI [43]. In [43], it is shown that the optimum combining scheme is the best combining strategy in the sense of maximizing the output SINR for the desired user. For this reason, OC is also referred to as MMSE linear combining [44]. A large body of research has been reported that studies the performance of OC in multipath fading environments and compares its performance with that of other combining schemes such as MRC [45]. Many of the existing works have derived the BEP or symbol error probability as a performance indicator of the OC in multipath fading environments (see [46], [47] and references therein). The output SINR and the outage probability are also well-studied in the literature as performance measures of OC [48]–[51].

Although OC can diminish the effects of CCI and fading through maximizing the output SINR, we raise the question of whether there are detection strategies for wireless diversity reception that can outperform OC in the sense of minimizing the error probability, i.e., whether we can find a better than optimum combining (BTOC) receiver. Our strategy for achieving this is to treat the interfering signals as multiusers in a multiuser wireless system and derive ML and optimal digital diversity receivers to detect

the information symbols [3]. Reference [3] only considers MF and decorrelating space diversity receivers and the ML and optimum diversity receivers not examined in this reference are examined here. We note that a similar idea was previously reported in [52] where a ML detector for a multiuser system with receiver antenna diversity in Rayleigh fading and CCI was derived. In this reference, the channel gains are assumed to be unknown but Gaussian distributed with known mean and covariance matrix. However, the final result involves calculating a quadrature form for each hypothesis data sequence that requires inverting a large matrix. Furthermore, comparing the performance of the receiver proposed in [52] with that of the OC would not be a fair comparison as in the latter case the channel gains are assumed to be known.

Motivated by the fact that a MMSE equalizer used to suppress ISI or CCI is inferior to a ML equalizer in terms of BEP [1], in this chapter we address the aforementioned question by deriving a ML as well as an optimum detector¹ for diversity reception of BPSK in CCI and AWGN. The transmitted signals are assumed to be like-modulated and Rayleigh-faded. We show that the channel gains of the interfering users along with their deterministic transmitted waveforms must be exploited in a better way than the OC detection strategy to ensure minimum achievable error probability. In our treatment, we consider both ML [9] and optimum [15] diversity receivers, referred to as the jointly and individually optimal detectors in the context of MUD [3], respectively. We show that the BTOC receiver is composed of a bank of MRC combiners (one for each MF) followed by either a ML detector or a LRT that chooses the hypothesis with maximum *a posteriori* probability. Computer simulations will be used to compare the BER performance of the proposed BTOC receivers with that of the OC and MRC receivers in Rayleigh fading with CCI and AWGN.

4.1 Signal Model and Optimum Combining

The system model of the baseband signal received at the m th receiver antenna is shown in Fig. 4.1. The baseband received signal at the output of the m th antenna ($m =$

¹The optimum diversity detector minimizes the BEP for a specific user only whereas the ML detector minimizes the BEP for all users at the same time.

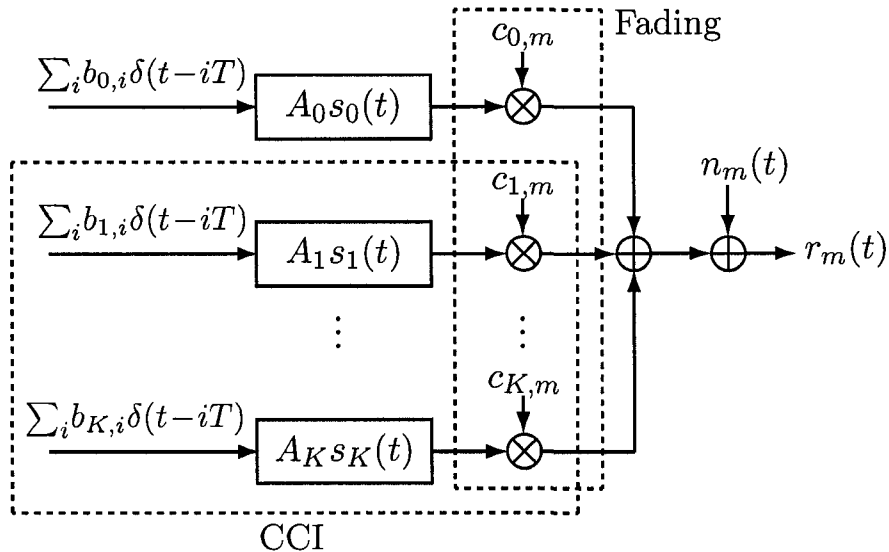


Figure 4.1. The system model of the baseband received signal at the m th element of the antenna array.

$1, 2, \dots, M$) is given by

$$r_m(t) = \sum_{i=-\infty}^{\infty} \sum_{k=0}^K A_k c_{k,m} b_{k,i} s_k(t - iT) + n_m(t) \quad (4.1)$$

where A_k and $b_{k,i} \in \{-1, 1\}$ are the k th user's amplitude and information bit in the i th interval, respectively and $c_{k,m}$ is the complex channel gain between the k th user's transmitter and the m th antenna. We assume that $c_{k,m}$'s are zero-mean complex Gaussian random variables with unit variance and the $b_{k,i}$'s are equiprobable. It is assumed, as usual, that all transmission delays have been compensated. Also in (4.1), M is the number of receiver antennas, K is the number of interfering signals, T is the symbol interval, $s_k(t)$ is the k th user's transmitted waveform and $n_m(t)$ is a complex additive Gaussian noise process whose real and imaginary components are independent and zero-mean with unit PSD. All the random variables are assumed to be mutually independent. Furthermore, we assume that the $s_k(t)$'s have unit energy and the transmission is ISI-free, i.e.,

$$R_{s_k, s_j}(nT) = \begin{cases} \rho_{k,j} \delta(n), & k \neq j \\ \delta(n), & k = j \end{cases} \quad (4.2)$$

where

$$R_{x,y}(\tau) \triangleq \int_{-\infty}^{\infty} x(t)y(t-\tau) dt \quad (4.3)$$

$\rho_{k,j}$ is the cross-correlation between $s_k(t)$ and $s_j(t)$, and $\delta(n)$ denotes the Kronecker delta function. The average SNR per channel and the average SIR at the input of the receiver are

$$\bar{\gamma}_c \triangleq \frac{A_0^2}{2} \quad (4.4)$$

$$\text{SIR} \triangleq \frac{A_0^2/T}{P_I} \quad (4.5)$$

respectively, where $P_I \triangleq \sum_{k=1}^K A_k^2/T$ is the total interference power.

The received signals are passed through a bank of filters matched to $\{s_j(t)\}_{j=0}^K$ and sampled at $t = \ell T$ to obtain

$$\mathbf{r}_j = \sum_{k=0}^K A_k \rho_{k,j} b_{k,\ell} \mathbf{c}_k + \mathbf{n}_j, \quad j = 0, 1, \dots, K \quad (4.6a)$$

where

$$\mathbf{r}_j \triangleq [r_{1,j}, r_{2,j}, \dots, r_{M,j}]^T \quad (4.6b)$$

$$\mathbf{c}_k \triangleq [c_{k,1}, c_{k,2}, \dots, c_{k,M}]^T \quad (4.6c)$$

$$\mathbf{n}_j \triangleq [n_{1,j}, n_{2,j}, \dots, n_{M,j}]^T \quad (4.6d)$$

$r_{m,j} = R_{r_{m,s_j}}(\ell T)$ and $n_{m,j} = R_{n_{m,s_j}}(\ell T)$. In the OC scheme, the elements of the 0th received array, \mathbf{r}_0 , are weighted and combined according to [43]

$$\Re \left\{ \mathbf{c}_0^H \left[\mathbf{I} + \sum_{k=1}^K A_k^2 \rho_{0,k}^2 \mathbf{c}_k \mathbf{c}_k^H \right]^{-1} \mathbf{r}_0 \right\} \quad (4.7)$$

to obtain the decision statistic for bit $b_{0,\ell}$, where $\Re\{\cdot\}$ and $[\cdot]^H$ denote the real part and conjugate transpose operators respectively, and \mathbf{I} is the identity matrix with appropriate dimension. In the absence of the CCI, the summation in (4.7) vanishes and the decision statistic of the OC simplifies to that of the MRC diversity receiver, i.e., $\Re\{\mathbf{c}_0^H \mathbf{r}_0\}$.

4.2 Better Than Optimum Combining

In this section we derive two BTOC diversity receivers for the signal model given in (4.6) that minimize the error probability either for all users or for the desired user only. In our

treatment, we assume that the channel gains as well as the deterministic transmitted waveforms of all users are known at the receiver. These assumptions are exactly the same as those made for the OC receiver when an OC scheme is to be used to detect information bits [43] and allow comparison to be made. We first consider the case where all signals have the same propagation delay and derive a ML receiver for this case. Then, we extend the results to the case where propagation delays are different. We also derive the BTOC receiver structure for the case where the detection of the information bit of a specific user is concerned. In this case, the receiver requires the knowledge of the interfering users deterministic waveforms in contrast to the OC receiver. Nevertheless, if all users use the same transmitted waveforms, the required information by the OC and BTOC receivers is again the same.

4.2.1 Maximum-Likelihood Diversity Reception

Assume that $\{A_k\}_{k=0}^K$, $\{s_k(t)\}_{k=0}^K$ and $\{c_k\}_{k=0}^K$ are *a priori* known at the receiver. Then, the ML receiver chooses $\{b_k\}_{k=0}^K$ that maximize [3]²

$$\text{Prob}\left\{\{b_k\}_{k=0}^K \mid \{r_m(t)\}_{m=1}^M, t \in \mathcal{T}\right\} \quad (4.8)$$

where \mathcal{T} is the observation time and is assumed to be long enough to ensure that (4.2) is satisfied. Recalling that $\{n_m(t)\}_{m=1}^M$ are independent random processes and that $\{b_k\}_{k=0}^K$ are equiprobable, it can be shown that maximizing (4.8) is equivalent to maximizing

$$\prod_{m=1}^M \mathcal{L}\left\{r_m(t), t \in \mathcal{T} \mid \{b_k\}_{k=0}^K\right\} \quad (4.9)$$

where

$$\mathcal{L}\left\{r_m(t), t \in \mathcal{T} \mid \{b_k\}_{k=0}^K\right\} = \exp\left(-\frac{1}{2} \int_{\mathcal{T}} \left|r_m(t) - \sum_{k=0}^K A_k c_{k,m} b_k s_k(t)\right|^2 dt\right) \quad (4.10)$$

is the likelihood function of $r_m(t)$ [3]. Eq. (4.9) can be simplified using (4.10) to obtain the ML estimates for the information bits as

$$\arg \min_{\{b_k\}_{k=0}^K} \left[\sum_{m=1}^M \int_{\mathcal{T}} \left|r_m(t) - \sum_{k=0}^K A_k c_{k,m} b_k s_k(t)\right|^2 dt \right] \quad (4.11)$$

²For simplicity of notation, we drop the redundant time index, ℓ , in the sequel.

or analogously

$$\arg \min_{\{b_k\}_{k=0}^K} \left[\sum_{m=1}^M \int_T \left[|r_m(t)|^2 + \sum_{k=0}^K A_k^2 |c_{k,m}|^2 s_k^2(t) - 2\Re \left\{ \sum_{k=0}^K A_k c_{k,m}^* b_k r_m(t) s_k(t) \right\} + \sum_{k=0}^K \sum_{\substack{j=0 \\ j \neq k}}^K A_k A_j c_{k,m}^* c_{j,m} b_k b_j s_k(t) s_j(t) \right] dt \right] \quad (4.12)$$

where $[\cdot]^*$ denotes complex conjugation. Denoting the double summation in the integrand of (4.12) by Ψ and observing that interchanging k and j in the summand of Ψ yields the complex conjugate of its summand, it can be readily seen that

$$\Psi = 2\Re \left\{ \sum_{k=0}^K \sum_{j=k+1}^K A_k A_j c_{k,m}^* c_{j,m} b_k b_j s_k(t) s_j(t) \right\}. \quad (4.13)$$

After eliminating the terms that do not depend on $\{b_k\}_{k=0}^K$, i.e., the first and the second terms in the integrand of (4.12), and rearranging one obtains

$$\arg \max_{\{b_k\}_{k=0}^K} \left[\sum_{k=0}^K A_k b_k \tilde{r}_k - \sum_{k=0}^{K-1} \sum_{j=k+1}^K A_k A_j b_k b_j \tilde{\rho}_{k,j} \right] \quad (4.14a)$$

where

$$\tilde{r}_k = \Re\{\mathbf{c}_k^H \mathbf{r}_k\} \quad (4.14b)$$

$$\tilde{\rho}_{k,j} = \rho_{k,j} \Re\{\mathbf{c}_k^H \mathbf{c}_j\}. \quad (4.14c)$$

Thus, the ML detection procedure can be summarized as:

1. The received samples at the output of the k th MF, $\{r_{k,m}\}_{m=1}^M$, are weighted by $\{c_{k,m}^*\}_{m=1}^M$ and combined using a MRC approach to obtain the \tilde{r}_k 's (eq. (4.14b))
2. The cross-correlations, $\rho_{k,j}$'s, are adjusted using the estimated channel gains to obtain the $\tilde{\rho}_{k,j}$'s (eq. (4.14c))
3. The \tilde{r}_k 's and $\tilde{\rho}_{k,j}$'s are input to a ML detector to obtain the ML estimate of $\{b_k\}_{k=0}^K$ (eq. (4.14a))

A block diagram of the ML diversity receiver for a $(K+1)$ -user Rayleigh fading channel is depicted in Fig. 4.2.

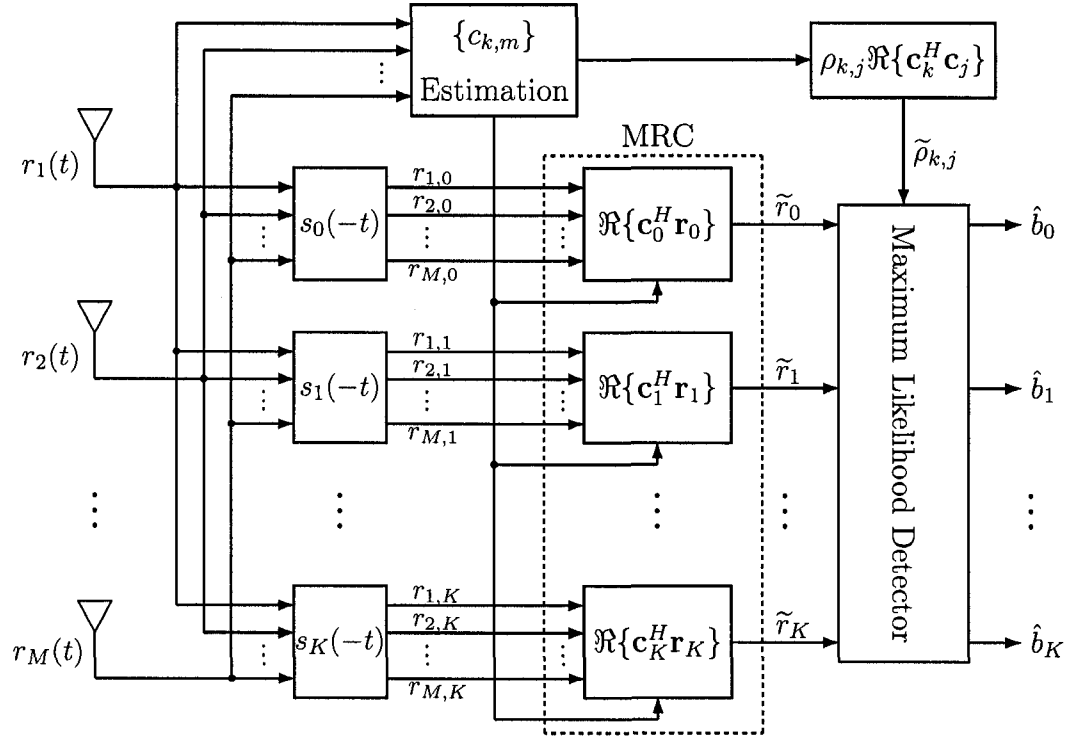


Figure 4.2. The block diagram of the ML diversity receiver with $(K + 1)$ users and M receiver antennas.

Assume now that the interfering signals have different delays than the desired signal. Then, the received signal will be

$$r_m(t) = \sum_{i=-\infty}^{\infty} \sum_{k=0}^K A_k c_{k,m} b_{k,i} s_k(t - iT - \tau_{k,m}) + n_m(t) \quad (4.15)$$

where $\tau_{k,m}$ denotes the delay corresponding to the k th user's signal received at the m th antenna. The main difference between this case and the case where delays are equal is that the information bits overlap each other and the longer the observation interval the better the detection will be. We assume that the receiver detects $(2I + 1)(K + 1)$ information bits labeled as $\{b_{k,i}\}$, $0 \leq k \leq K$, $-I \leq i \leq I$. Similar to the procedure we used for the synchronous case, the ML estimates of the information bits can be shown to be

$$\arg \max_{\{b_{k,i}\}} \left[\sum_{i=-I}^I \sum_{k=0}^K A_k b_{k,i} \left\{ 2\tilde{r}_{k,i} - \sum_{j=-I}^I \sum_{\ell=0}^K A_{\ell} b_{\ell,j} \tilde{\rho}_{k,\ell,i,j} \right\} \right] \quad (4.16a)$$

where

$$\tilde{\rho}_{k,\ell,i,j} \triangleq \sum_{m=1}^M c_{k,m} c_{\ell,m}^* \int_T s_k(t-iT-\tau_{k,m}) s_\ell(t-jT-\tau_{\ell,m}) dt \quad (4.16b)$$

$$\tilde{r}_{k,i} \triangleq \sum_{m=1}^M \Re \left\{ c_{k,m}^* \int_T s_k(t-iT-\tau_{k,m}) r_m(t) dt \right\} \quad (4.16c)$$

Clearly, the ML receiver in this case is very complicated as it must detect all the information bits at the same time. When the $s_k(t)$'s are time-limited (for example, when they are zero outside the $[0, T)$ interval) $\tilde{\rho}_{k,\ell,i,j}$ in (4.16a) will be nonzero only for a limited number of j 's. In this case, a Viterbi decoder [53] whose metric is the summand of the second summation in (4.16a) can be used to detect the information bits [3].

4.2.2 Optimum Diversity Reception

We now turn our attention to the case where optimum detection of a specific user is concerned. Assume that b_0 is the desired information bit to be detected. Then, the optimum receiver should maximize the *a posteriori* probability [3]

$$\text{Prob}\{b_0 \mid \{r_m(t)\}_{m=1}^M, t \in \mathcal{T}\}. \quad (4.17)$$

Recalling that $\{b_k\}_{k=1}^K$ are equiprobable and independent, the *a posteriori* probability in (4.17) can be expressed as

$$\frac{1}{2^K} \sum_{q=1}^{2^K} \text{Prob}\{b_0, \mathfrak{B}^q \mid \{r_m(t)\}_{m=1}^M, t \in \mathcal{T}\} \quad (4.18a)$$

where \mathfrak{B}^q denotes the event that $b_k = \mathfrak{b}_k^q$, $1 \leq k \leq K$, where $\{\mathfrak{b}_k^q\}_{k=1}^K$ are chosen such that

$$q = \sum_{k=1}^K 2^{k-2} (\mathfrak{b}_k^q + 1). \quad (4.18b)$$

Using a procedure similar to that used to derive the ML multiuser receiver in [3], one can show that maximizing (4.18a) is analogous to maximizing

$$\sum_{q=1}^{2^K} \exp \left(-\frac{1}{2} \sum_{m=1}^M \int_T \left| r_m(t) - A_0 c_{0,m} b_0 s_0(t) - \sum_{k=1}^K A_k c_{k,m} \mathfrak{b}_k^q s_k(t) \right|^2 dt \right). \quad (4.19)$$

After some algebraic manipulations, it can be shown that the decision rule for the optimum receiver can be expressed as

$$\sum_{q=1}^{2^K} \exp \left\{ -\frac{1}{2} \left[A_0 \left(\tilde{r}_0 - \sum_{k=1}^K A_k \mathfrak{b}_k^q \tilde{\rho}_{0,k} \right) + A_K \mathfrak{b}_K^q \tilde{r}_K \right. \right. \\ \left. \left. + \sum_{k=1}^{K-1} A_k \mathfrak{b}_k^q \left(\tilde{r}_k - \sum_{j=k+1}^K A_j \mathfrak{b}_j^q \tilde{\rho}_{k,j} \right) \right] \right\} \stackrel{b_0=1}{\underset{b_0=-1}{\geq}} \sum_{q=1}^{2^K} \exp \left\{ \frac{1}{2} \left[A_0 \left(\tilde{r}_0 - \sum_{k=1}^K A_k \mathfrak{b}_k^q \tilde{\rho}_{0,k} \right) \right. \right. \\ \left. \left. - A_K \mathfrak{b}_K^q \tilde{r}_K - \sum_{k=1}^{K-1} A_k \mathfrak{b}_k^q \left(\tilde{r}_k - \sum_{j=k+1}^K A_j \mathfrak{b}_j^q \tilde{\rho}_{k,j} \right) \right] \right\}. \quad (4.20)$$

Note that in this case, the receiver structure is the same as that of the ML diversity receiver (Fig. 4.2) except for the last block, i.e., the ML detector, that should be replaced by an appropriate LRT.

4.3 Results and Discussions

The BER performance of the proposed receivers has been evaluated and compared with that of the OC, MRC and single-user (SU) receivers using computer simulation for different values of M and K . The SU receiver is assumed to use MRC to combine the received signals at the output of the antenna array and its BEP is given by [54]

$$P_{\text{SU}} = \left(\frac{1-\mu}{2} \right)^M \sum_{m=0}^{M-1} \binom{M-1-m}{m} \left(\frac{1+\mu}{2} \right)^m \quad (4.21)$$

where $\mu = \sqrt{\bar{\gamma}_c / (1 + \bar{\gamma}_c)}$, $\binom{n}{k} = n! / ((n-k)! k!)$ and $z!$ denotes the factorial of z . In our treatment, we have considered $M = 2, 4$ and 6 diversity order. For these values of M the average SNR per channel, $\bar{\gamma}_c$, has been assumed to be 7, 4 and 2.2 dB, respectively.

We first assume that there is only one dominant interferer, i.e., $K = 1$. In this case, the ML and the optimum decisions for bit b_0 are shown to be [3]

$$\hat{b}_0^{\text{ML}} = \text{sgn} \left[A_0 \tilde{r}_0 + \frac{A_1}{2} \left(|\tilde{r}_1 - A_0 \tilde{\rho}_{0,1}| - |\tilde{r}_1 + A_0 \tilde{\rho}_{0,1}| \right) \right] \quad (4.22)$$

$$\hat{b}_0^{\text{Optimum}} = \text{sgn} \left[\tilde{r}_0 - \frac{N_0}{4A_0} \log \left(\frac{\cosh(A_1 \tilde{r}_1 + A_0 A_1 \tilde{\rho}_{0,1})}{\cosh(A_1 \tilde{r}_1 - A_0 A_1 \tilde{\rho}_{0,1})} \right) \right] \quad (4.23)$$

respectively, where $\text{sgn}(\cdot)$, $\log(\cdot)$ and $\cosh(\cdot)$ denote the signum, the natural logarithm and the hyperbolic cosine functions, respectively.

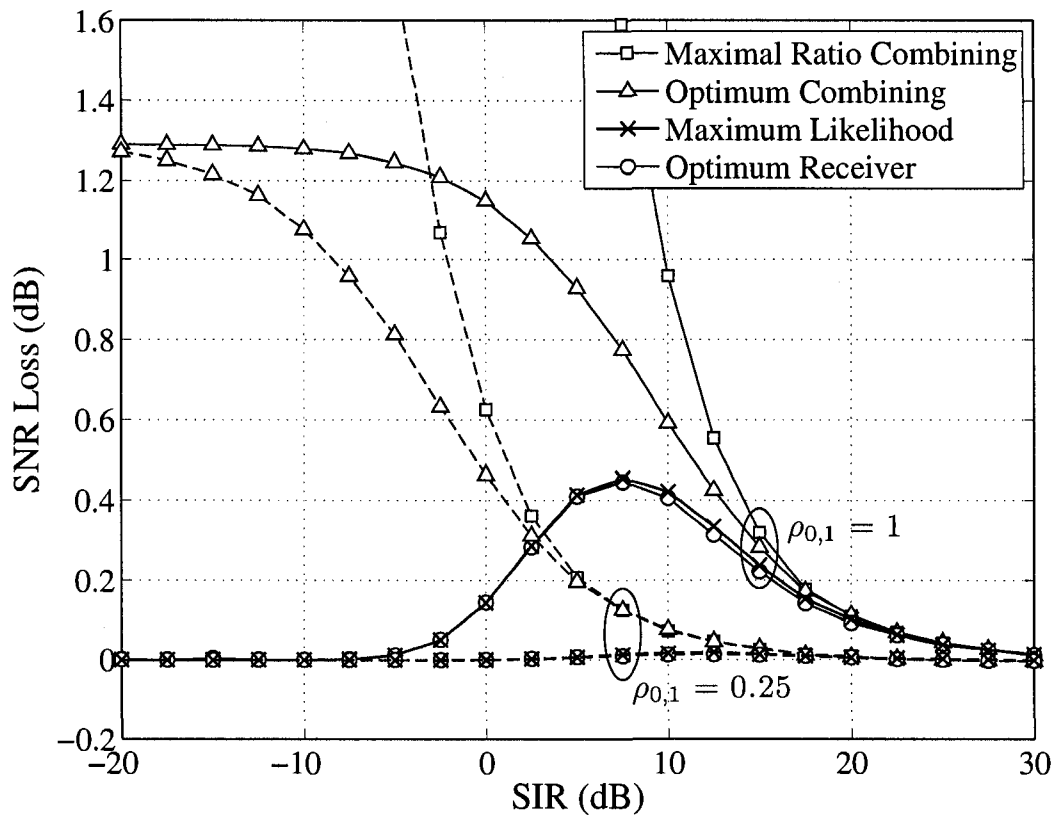


Figure 4.3. The SNR loss of the MRC, OC, ML and optimum diversity receivers relative to the SU receiver as a function of the SIR in a two-user channel with Rayleigh fading, $M = 4$, $\bar{\gamma}_c = 4$ dB and $\rho_{0,1} = 0.25$ and 1.

An insightful performance measure for the receivers in CCI is their SNR loss relative to the SU receiver. This measure indicates the amount of extra SNR required by the receiver to achieve the same error probability as the SU receiver, i.e., a MRC receiver with the same number of receiver antennas and no CCI. We have evaluated the SNR loss of the ML, optimum, MRC and OC receivers for $M = 4$, $\bar{\gamma}_c = 4$ dB and $\rho_{0,1} = 0.25$ and 1. These assumptions lead to a BER of 10^{-3} for the SU receiver. The results are illustrated in Fig. 4.3. When $\rho_{0,1} = 0.25$ neither the ML nor the optimal diversity receivers have significant SNR loss relative to the SU receiver. However, for $\rho_{0,1} = 1$ the maximum loss for both receivers is approximately 0.45 dB for $\text{SIR} = 7.5$ dB. In other words, the optimum receiver can restore most of the SNR loss incurred due to the CCI. Note that the SNR loss of the OC receiver is larger than that of the proposed receivers

for both values of $\rho_{0,1}$ and approaches some constant value when the SIR becomes very small. This is because in a two-user channel with M receiver antennas and very large interference power, an OC receiver performs approximately the same as a MRC receiver with $(M - 1)$ receiver antennas and no interference [43, eq. (23)]. Thus, recalling that the channel gains have unit variance, it can be readily seen that the OC receiver requires $10 \log_{10}(\frac{M}{M-1})$ dB more SNR than the SU receiver to achieve the same BER. For the case where $M = 4$, this SNR loss approximately equals 1.25 dB as shown in Fig. 4.3. Note that the SNR loss of the MRC receiver with respect to the SU receiver, dramatically increases for both values of $\rho_{0,1}$, even when the SIR is not small.

The effect of the number of receiver antennas, M , on the SNR loss of the ML and OC diversity receivers relative to the SU receiver as a function of the SIR is depicted in Fig. 4.4. The number of receiver antennas and their corresponding values of SNR per channel are assumed to be $M = 1, 2, 3$ and 5 and $\bar{\gamma}_c = 10, 7, 5.2$ and 3 dB, respectively. Moreover, both users have the same transmitted waveform, i.e., $s_0(t) = s_1(t)$. The maximum SNR loss of the ML receiver for the case where there is no antenna diversity, i.e., $M = 1$, is approximately equal to 2.15 dB. In this case, the SNR loss of the OC receiver increases as SIR decreases and has a maximum value of 7.34 dB for vanishing small SIR (not shown in the figure). When the number of receiver antennas is increased by one, i.e., $M = 2$, the ML receiver's maximum SNR loss reduces to 1 dB whereas the SNR loss of the OC receiver is close to 3 dB. For $M = 5$, the SNR loss of the ML receiver is less than 0.45 dB for all the examined values of the SIR while the OC incurs a SNR loss of 1 dB, for small SIR values. Observe that the SIR range for which the SNR loss of the ML receiver is nonzero becomes narrower as M increases. For the OC receiver, however, this range is approximately fixed for the examined values of $M > 1$. Note that in this case, the ML receiver achieves the BER of the MF in a SU system even for small SIR values. This is because detecting the desired signal in very small SIR is equivalent to detecting the interfering signal in very large SIR. Thus, for small SIRs the ML receiver effectively mitigates the interference and achieves a performance close to that of the SU system [55]. Expectedly, for each M there is a SIR where the BER of the ML receiver and, thus, the SNR loss is maximum as shown in Fig. 4.4.

The BER performance of the ML, optimum, OC and MRC diversity receivers as

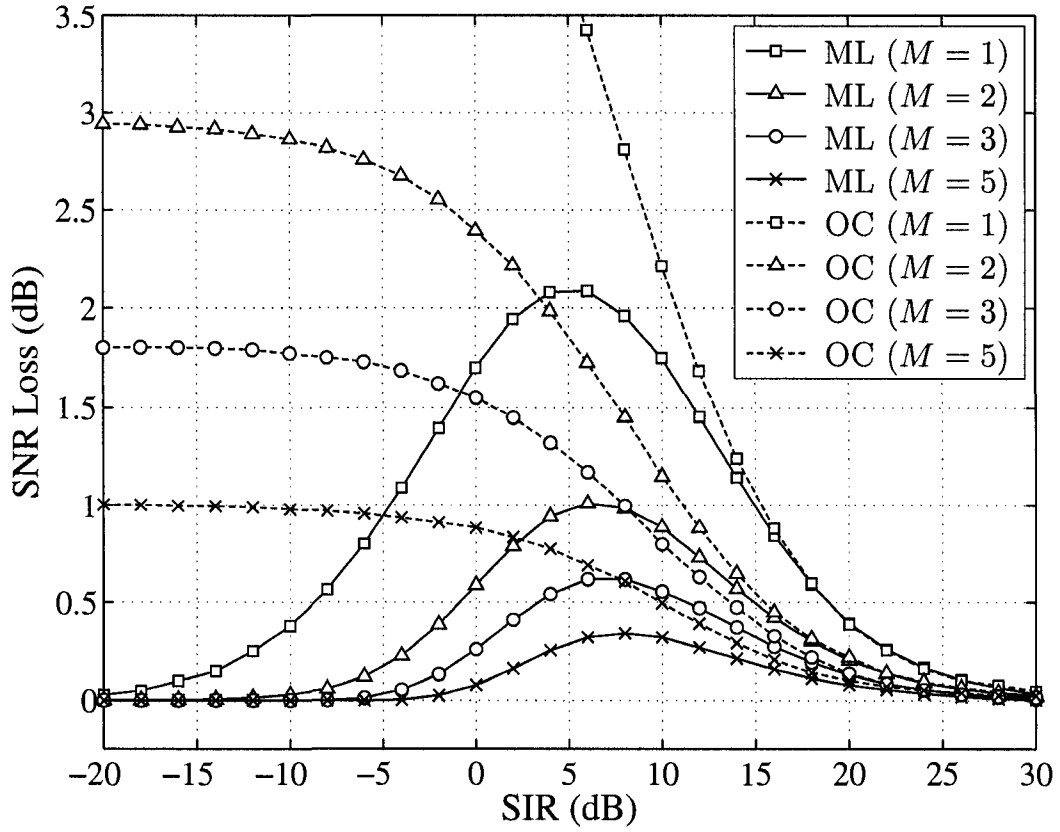


Figure 4.4. The effect of the number of receiver antennas on the SNR loss of the ML and OC receivers with respect to the SU receiver in a two-user channel with Rayleigh fading and $\rho_{0,1} = 1$.

a function of SIR is depicted in Fig. 4.5. The ML and optimum diversity receivers outperform the OC and MRC receivers for all examined values of the SIR and M , even when the number of receiver antennas is as large as 6. The performance improvement of the optimum and ML receivers over the OC and MRC receivers deteriorates when the SIR becomes large and for $\text{SIR} = 6$ dB, i.e., $A_0 = 2A_1$, all receivers perform approximately the same. Note that the proposed receivers have a constant BER for all the examined values of the SIR. To explain this, we recall from Fig. 4.3 that the proposed receivers have negligible SNR loss relative to the SU receiver for $\rho_{0,1} = 0.25$ and, thus, their BER is almost the same as that of the SU receiver.

Fig. 4.6 shows the BER performance of the ML diversity receiver as well as that of the OC and MRC receivers for $K = 8$. In this case, the performance improvement over

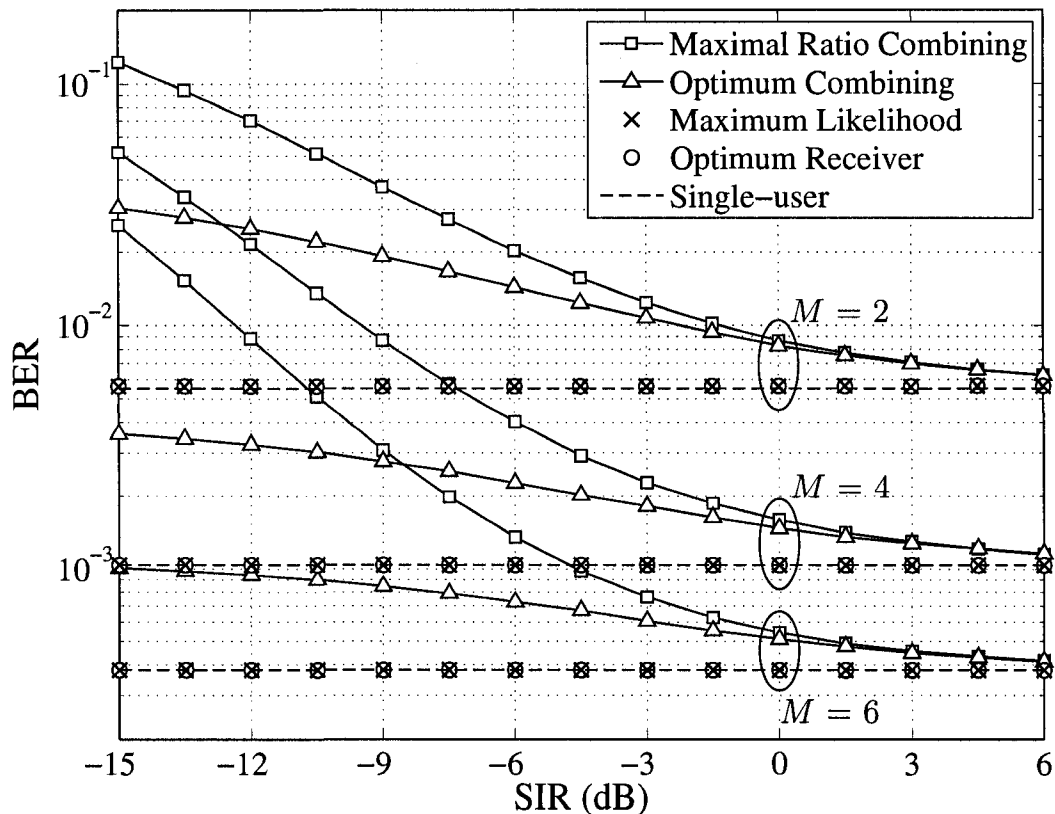


Figure 4.5. The average BER of the MRC, OC, ML and optimum receivers as a function of the SIR in a two-user channel with Rayleigh fading, $\rho_{0,1} = 0.25$ and $M = 2, 4$ and 6 .

the OC achieved by using ML reception is more significant than for the two-user case, particularly when the SIR is very small. In fact, for $M = 2$ and 4 , the OC and MRC receivers in a system with 9 users perform approximately the same and are significantly inferior to the ML receiver whose BER for all the examined SIR's is again nearly constant and very close to that of the SU receiver.

Observe that in Figs. 4.5 and 4.6, the performance improvement achieved by ML detection relative to OC is significant only when the SIR is quite small. One may question whether such SIRs are practically feasible. To answer this question, we recall that the SIR in (4.5) was defined as the ratio of the received signal power to the *total* interference power, i.e., $P_{\mathcal{I}}$. The effective interference power, however, depends on the cross-correlations between the desired and interfering signals and is defined as $P_{\mathcal{I}}^{\text{eff}} \triangleq \frac{1}{T} \sum_{k=1}^K A_k^2 \rho_{0,k}^2$. Thus, it can be much smaller than the total interference power. For

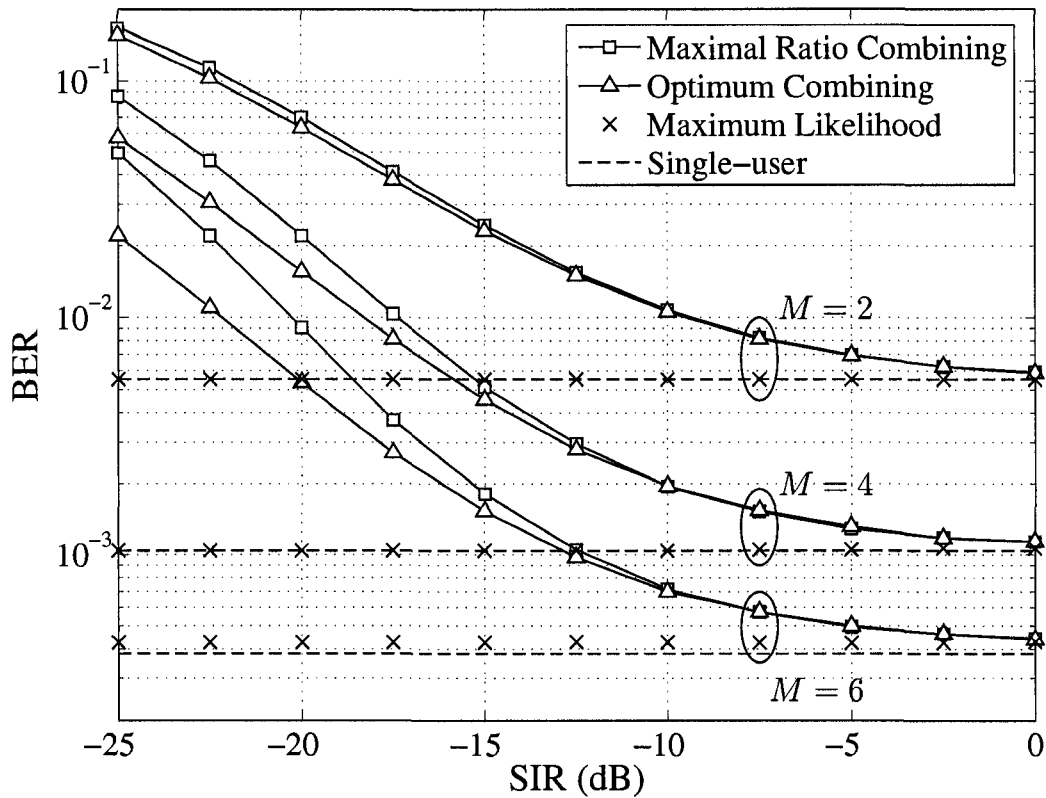


Figure 4.6. The average BER of the OC, MRC and ML receivers as a function of the SIR in Rayleigh fading with $K = 8$, $\{\rho_{k,j}\}_{k \neq j} = 0.1$ and $M = 2, 4$ and 6 .

example, when the $\{\rho_{k,j}\}_{k \neq j} = 0.1$ (as in Fig. 4.6) the effective interference power is only 1% of the total interference power. Consequently, the effective SIR of the system is 20 dB more than the SIR defined by (4.5). Thus, a SIR of as small as -15 dB can be considered feasible for a practical system.

Chapter 5

Cochannel Interference Mitigation Using Whitening Receiver Designs in Bandlimited Microcellular Wireless Systems

Cochannel interference mitigation using an interference WMF in direct-sequence code-division multiple access (DS-SS) systems was first proposed in [4], [56]. The WMF receiver first whitens a colored noise term composed of CCI and AWGN. Then, it maximizes the output SINR by employing a filter matched to the transmitter filter. Under the assumption of identical transmitter pulse-shaping, this receiver has reasonable complexity and does not require any information about the CCI other than its total power [4]. The results in [4] were generalized later in [16] to the case where the received signal observation time is finite and some of the interfering signals are locked, i.e., their chip delays and received powers are known at the receiver. It was shown that the SINR can be further maximized by employing a new filter that can estimate and suppress the contribution of the locked interferers in addition to the unlocked interferers. This receiver is a compromise between the WMF receiver, when there is no locked interferer, and a MMSE multiuser receiver [5], when all interferers are locked.

Little work has been reported that studies whitening filter receiver design for bandlimited microcellular systems. Recently in [57], [58], CCI mitigation using an interference WMF was proposed for fading micro-cellular environments and the effects of the ISI generated by the WMF were studied. In these references, a MMSE equalizer was used to mitigate the ISI caused by the WMF. In this chapter, we examine in detail whether interference whitening can be used with benefit in bandlimited microcellular wireless systems, using realistic system models that account for ISI. Extending and correcting the results in [58], we first consider a WMF receiver in a synchronous fading channel and show that even when the observation time is infinite, the SINR at the output of the WMF receiver is less than that of the CMF receiver. This is due to the fact that in a synchronous channel, the CCI is a cyclostationary rather than a wide-sense stationary (WSS) process and the concept of interference whitening is not applicable to such a system. In consequence, the WMF in a synchronous channel is inferior to the CMF, in contrast to the results reported in [4], [16], [56], [58].

In the asynchronous case, we first consider an ISI-free¹ system and observe that an ISI-free WMF can achieve some SINR gain over the CMF and that the gain depends on the pulse-shaping. We show that the WMF's SINR gain over the CMF is 1.76 dB for a standard RC pulse and 1.07 dB for a BTD [59] pulse. In practice, the desired user transmits more than one information symbol and the cascade of the transmitter and receiver filters does not necessarily satisfy Nyquist's first criterion for zero ISI [1]. Hence, the system is ISI-impaired and the interference WMF is no longer optimum in the sense of maximizing the output SINR. References [4], [16], [56] ignore the effect of the ISI created by the WMF in an asynchronous channel in their treatment; nor do they consider the use of equalization to reduce the ISI introduced by interference whitening as done in [58]. Our analysis for the ISI-impaired systems illustrates that the ISI can dramatically diminish the SINR of the WMF relative to the CMF and make the interference whitening ineffective. Using calculus of variations, we show that the SINRMF in the presence of asynchronous CCI, ISI and AWGN is composed of a continuous-time filter (which turns out to be the WMF receiver) followed by a discrete-

¹An ISI-free system is a system in which the desired user transmits only a single information symbol albeit the interfering users may transmit arbitrarily long information sequences.

time filter which is a MMSE equalizer as proposed in [58]. We then evaluate the SINR of the WMF as well as the SINRMF in an ISI-impaired system and clarify the effects of SIR, pulse-shaping filter excess bandwidth, and the severity of the fading on their SINR gains over the CMF. Our results show that the SINRMF is superior to the ISI-impaired WMF even in the presence of a strong ISI component that makes the WMF inferior to the CMF. The SINR was not considered in [58] when equalization was used. Since multiple access interference is the main source of distortion in multiuser communication systems, we employ the asymptotic SINR as a performance measure to compare the receivers. This performance measure quantifies how well the ISI-free, ISI-impaired and SINRMF receivers can mitigate the interference in a high SNR regime.

5.1 Signal Model

The block diagram of the $(K + 1)$ -user communication system is given in Fig. 5.1. The bandpass received signal at the input of the demodulator is [58]

$$\begin{aligned} \tilde{r}(t) = & \sqrt{2}A_0\alpha_0 \cos(\omega_c t) \sum_{i=-\infty}^{\infty} b_{0,i}g_T(t - iT) \\ & + \sum_{k=1}^K \sqrt{2}A_k\alpha_k \cos(\omega_c t + \theta_k) \sum_{i=-\infty}^{\infty} b_{k,i}g_T(t - \tau_k - iT) + \tilde{n}(t) \end{aligned} \quad (5.1)$$

where A_k , α_k , τ_k , θ_k and $b_{k,i} \in \{-1, 1\}$ are the k th user's amplitude, channel attenuation, timing offset, phase offset and equiprobable information bit in the i th interval, respectively. Also in (5.1), T is the symbol interval, ω_c is the carrier frequency, $\tilde{n}(t)$ is AWGN with mean zero and double-sided PSD $N_0/2$, K denotes the number of interfering signals and $g_T(t)$ is the transmitter pulse-shaping. For simplicity of analysis, we assume $g_T(t)$ is an even function and $G_T^2(\omega)$ satisfies Nyquist's first criterion [1], where $G_T(\omega)$ is the Fourier transform of $g_T(t)$. Assume that θ_k and τ_k are uniformly distributed over $[0, 2\pi)$ and $[0, T)$, respectively.² Also assume that α_0 has a Nakagami- m distribution

²The interfering users are neither synchronous nor coherent with the desired user. Thus, choosing a uniform distribution for θ_k 's and τ_k 's is a reasonable choice as it reflects the fact that the interfering users have minimum information about the timing and carrier phase of the desired user.

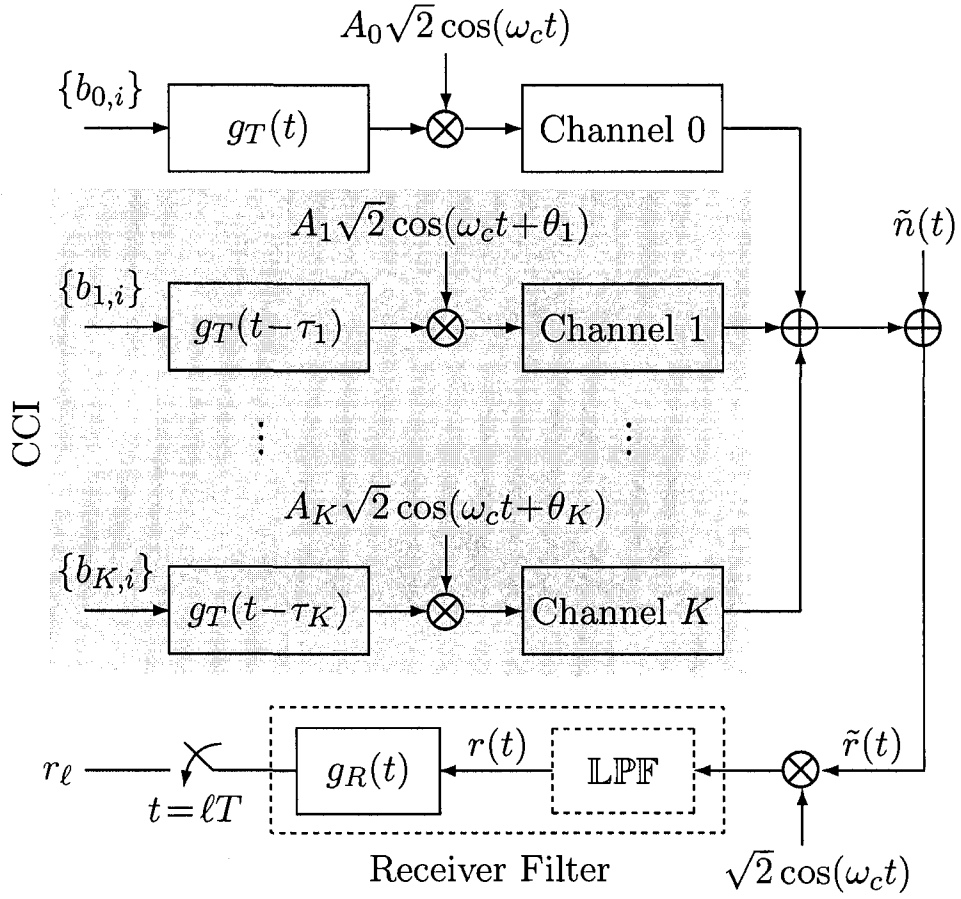


Figure 5.1. The block diagram of the cochannel interference communication system with $(K + 1)$ asynchronous users.

with unit energy [1],

$$f_{\alpha_0}(x) = \frac{2m^m}{\Gamma(m)} x^{2m-1} \exp(-mx^2), \quad m \geq 0.5 \quad (5.2)$$

where $\Gamma(\cdot)$ is the Gamma function defined as [41]

$$\Gamma(m) = \int_0^\infty e^{-t} t^{m-1} dt \quad [\Re\{m\} > 0] \quad (5.3)$$

and the α_k 's ($k \neq 0$) each have a Rayleigh distribution with unit energy [1]

$$f_{\alpha_k}(x) = 2xe^{-x^2}. \quad (5.4)$$

All random variables are assumed to be mutually independent. We can assume, without loss of generality, that the energy of $g_T(t)$ and the noise PSD are equal to unity. The

latter assumption implies that $N_0 = 2$. Thus, the average SNR per bit is

$$\gamma_b = \frac{A_0^2}{2}. \quad (5.5)$$

We also define the average SIR of the system as

$$\psi \triangleq \frac{A_0^2}{\sum_{k=1}^K A_k^2}. \quad (5.6)$$

The received signal is multiplied by $\sqrt{2} \cos(\omega_c t)$ and passed through the receiver filter, $g_R(t)$. For simplicity of analysis we split the receiver filter into an ideal lowpass filter and $g_R(t)$ as shown in Fig. 5.1. The lowpass filter has the same bandwidth as the received signals and passes them without distortion. Then, the received signal at the output of the lowpass filter is

$$r(t) = A_0 \alpha_0 \sum_{i=-\infty}^{\infty} b_{0,i} g_T(t - iT) + \sum_{k=1}^K A_k \alpha_k \cos \theta_k \sum_{i=-\infty}^{\infty} b_{k,i} g_T(t - \tau_k - iT) + n(t) \quad (5.7)$$

where now $n(t)$ is a lowpass zero-mean Gaussian process with unit PSD over the bandwidth of the ideal lowpass filter. The received signal is passed through the receiver filter, $g_R(t)$, and sampled at $t = \ell T$. Then, the resulting decision statistic for the ℓ th bit of the desired user is

$$r_\ell = A_0 \alpha_0 \sum_{i=-\infty}^{\infty} b_{0,i} g((\ell - i)T) + \sum_{k=1}^K A_k \alpha_k \cos \theta_k \sum_{i=-\infty}^{\infty} b_{k,i} g((\ell - i)T - \tau_k) + n_\ell \quad (5.8)$$

where

$$g(t) = \int_{-\infty}^{\infty} g_T(s) g_R(t - s) ds \quad (5.9)$$

and n_ℓ is a zero-mean Gaussian random variable with

$$E\{n_\ell n_k\} = \int_{-\infty}^{\infty} g_R(t) g_R((\ell - k)T - t) dt. \quad (5.10)$$

Since in general $g(t)$ is not a Nyquist pulse, the received sample in (5.8) will have an ISI term in addition to the CCI and noise, defined as

$$\mathcal{J} \triangleq A_0 \alpha_0 \sum_{\substack{i=-\infty \\ i \neq \ell}}^{\infty} b_{0,i} g_d(\ell - i) \quad (5.11)$$

where $g_d(\ell) \equiv g(\ell T)$ and \mathcal{J} is a zero-mean random variable with variance $\sigma_{\mathcal{J}}^2 = \mathcal{E}_0 \dot{E}_g$ where

$$\dot{E}_g \triangleq \sum_{\substack{i=-\infty \\ i \neq 0}}^{\infty} g_d^2(i) \quad (5.12)$$

and $\mathcal{E}_0 \triangleq A_0^2 \alpha_0^2$ is the instantaneous energy of the desired user whose PDF can be expressed as [1, eq. (14.3–14)]

$$f_{\mathcal{E}_0}(\varepsilon) = \left(\frac{m}{A_0^2}\right)^m \frac{\varepsilon^{m-1}}{\Gamma(m)} \exp\left(-\frac{m\varepsilon}{A_0^2}\right), \quad \varepsilon > 0. \quad (5.13)$$

Recalling that the CCI, the ISI and the noise terms in (5.8) are independent random variables, one can obtain the SINR at the output of $g_R(t)$ as

$$\Gamma = \frac{\mathcal{E}_0 g^2(0)}{\sigma_n^2 + \sigma_I^2 + \mathcal{E}_0 \dot{E}_g} \quad (5.14)$$

where σ_I^2 is the variance of the CCI. As we will see in Section 5.2, our analysis depends on the PSD of the CCI which in turn, depends on the type of modulation used in the system [1, Section 4.4]. Thus, our results can be extended to the linear modulation schemes other than BPSK provided that the information symbols are uncorrelated and zero-mean and that the modulation is memoryless.

5.2 Interference Whitening Filter

In this section, we first describe the structure of the interference whitening receiver for asynchronous and synchronous channels. Then, we derive the SINR of the WMF receiver for these channels. In our treatment, we consider both ISI-free and ISI-impaired systems.

5.2.1 Asynchronous CCI

Defining the k th interfering signal, $\mathcal{I}_k(t)$, as

$$\mathcal{I}_k(t) \triangleq A_k \alpha_k \cos \theta_k \sum_{i=-\infty}^{\infty} b_{k,i} g_T(t - \tau_k - iT) \quad (5.15)$$

it can be seen that $\mathcal{I}_k(t)$ is a zero-mean process. When the CCI is asynchronous, the autocorrelation function (ACF) of $\mathcal{I}_k(t)$ can be obtained as

$$\begin{aligned} R_{\mathcal{I}_k}^{\text{ASYNC}}(t, t + \eta) &\triangleq E\{\mathcal{I}_k(t)\mathcal{I}_k(t + \eta)\} \\ &= A_k^2 E_{\alpha_k}\{\alpha_k^2\} E_{\theta_k}\{\cos^2 \theta_k\} \\ &\quad \times \sum_{i=-\infty}^{\infty} \sum_{j=-\infty}^{\infty} E\{b_{k,i}b_{k,j}\} E_{\tau_k}\{g_T(t - \tau_k - iT)g_T(t + \eta - \tau_k - jT)\}. \end{aligned} \quad (5.16)$$

Since $E\{\cos^2 \theta_k\} = 1/2$, the α_k 's have unit energy, τ_k is uniformly distributed over $[0, T]$, and $E\{b_{k,i}b_{k,j}\} = \delta(i - j)$, eq. (5.16) can be simplified to

$$R_{\mathcal{I}_k}^{\text{ASYNC}}(t, t + \eta) = \frac{A_k^2}{2T} \sum_{i=-\infty}^{\infty} \int_0^T g_T(t - \tau_k - iT)g_T(t + \eta - \tau_k - iT) d\tau_k. \quad (5.17)$$

By changing the variable τ_k in (5.17) to $u - iT$ one obtains

$$\begin{aligned} R_{\mathcal{I}_k}^{\text{ASYNC}}(t, t + \eta) &= \frac{A_k^2}{2T} \sum_{i=-\infty}^{\infty} \int_{iT}^{(i+1)T} g_T(t - u)g_T(t + \eta - u) du \\ &= \frac{A_k^2}{2T} \int_{-\infty}^{\infty} g_T(u)g_T(\eta + u) du. \end{aligned} \quad (5.18)$$

Clearly, $R_{\mathcal{I}_k}^{\text{ASYNC}}(t, t + \eta)$ is only a function of η and does not depend on t . Hence, $\mathcal{I}_k(t)$ is a WSS process. Observe that $\{\mathcal{I}_k(t)\}_{k=1}^K$ are independent processes; it follows from (5.18) that the PSD of the overall interference, i.e., $\mathcal{I}(t) \triangleq \sum_{k=1}^K \mathcal{I}_k(t)$, is given by

$$S_{\mathcal{I}}(\omega) = P_{\mathcal{I}}|G_T(\omega)|^2 \quad (5.19)$$

where $P_{\mathcal{I}}$ is the total interference power defined as $P_{\mathcal{I}} \triangleq \sum_{k=1}^K A_k^2/2T$. It is shown in [18] that for a signal distorted by a WSS process whose PSD equals $S_n(\omega)$, the frequency response of the receiver filter that maximizes the SNR is given by $G_R(\omega) = G_T(\omega)/S_n(\omega)$. In our problem, the interference and noise terms in (5.7) are two independent WSS random processes and, thus, their sum is also WSS with PSD, $1 + P_{\mathcal{I}}|G_T(\omega)|^2$. Hence, the WMF and its corresponding SINR are given by [4], [18]

$$G_R(\omega) = \frac{G_T(\omega)}{1 + P_{\mathcal{I}}G_T^2(\omega)} \quad (5.20)$$

$$\begin{aligned}\Gamma_{\text{ISI-free}} &= \frac{\mathcal{E}_0}{2\pi} \int_{-\infty}^{\infty} \frac{G_T^2(\omega)}{1 + P_{\mathcal{I}}G_T^2(\omega)} d\omega \\ &= \mathcal{E}_0 g(0).\end{aligned}\quad (5.21)$$

It can be shown that $\Gamma_{\text{ISI-free}}$ is larger than the SINR of the CMF receiver in an asynchronous channel. To this end, we first use the fact that $G_T^2(\omega)$ satisfies Nyquist's first criterion to obtain the SINR of the CMF as

$$\Gamma_{\text{CMF}} = \frac{\mathcal{E}_0}{1 + \frac{1}{2\pi} \int_{-\infty}^{\infty} P_{\mathcal{I}}G_T^4(\omega) d\omega}.\quad (5.22)$$

Then, we use the Cauchy-Schwarz inequality for integrals [41] to obtain

$$\begin{aligned}1 &= \left(\frac{1}{2\pi} \int_{-\infty}^{\infty} G_T^2(\omega) d\omega \right)^2 \leq \\ &\quad \frac{1}{(2\pi)^2} \int_{-\infty}^{\infty} \frac{G_T^2(\omega)}{1 + P_{\mathcal{I}}G_T^2(\omega)} d\omega \int_{-\infty}^{\infty} [G_T^2(\omega) + P_{\mathcal{I}}G_T^4(\omega)] d\omega\end{aligned}\quad (5.23)$$

where the equality on the left of (5.23) follows from the fact that $g_T(t)$ has unit energy. Multiplying both sides of (5.23) by

$$\frac{2\pi\mathcal{E}_0}{\int_{-\infty}^{\infty} [G_T^2(\omega) + P_{\mathcal{I}}G_T^4(\omega)] d\omega}$$

we obtain

$$\Gamma_{\text{CMF}} \leq \Gamma_{\text{ISI-free}}.\quad (5.24)$$

By comparing (5.21) with (5.14) for the case where $\mathring{E}_g = 0$, one sees that $\sigma_n^2 + \sigma_{\mathcal{I}}^2 = g(0)$. Thus, the SINR in the presence of the ISI is given by

$$\Gamma = \frac{\mathcal{E}_0 g^2(0)}{g(0) + \mathcal{E}_0 \mathring{E}_g}.\quad (5.25)$$

The SINR given by (5.25) depends on α_0^2 through \mathcal{E}_0 and, thus, is random. This dependence can be removed by averaging (5.25) over the distribution of \mathcal{E}_0 to obtain

$$\bar{\Gamma} = \frac{m g^2(0)}{\mathring{E}_g} \exp\left(\frac{m g(0)}{\mathring{E}_g A_0^2}\right) \mathcal{E}_{1+m}\left(\frac{m g(0)}{\mathring{E}_g A_0^2}\right)\quad (5.26a)$$

where

$$\mathcal{E}_\nu(x) \triangleq \int_1^{\infty} \frac{\exp(-xt)}{t^\nu} dt \quad x \geq 0.\quad (5.26b)$$

Obviously, the mean of $\Gamma_{\text{ISI-free}}$ can be evaluated by replacing \mathcal{E}_0 with A_0^2 in (5.21).

5.2.2 Synchronous CCI

When the CCI is synchronous, i.e., $\{\tau_k\}_{k=1}^K = 0$, $\mathcal{I}_k(t)$ is a cyclostationary process with ACF [1, Section 4.4.1]

$$R_{\mathcal{I}_k}^{\text{SYNC}}(t, t + \eta) = \frac{A_k^2}{2T} \sum_{i=-\infty}^{\infty} g_T(t - iT)g_T(t + \eta - iT) \quad (5.27)$$

In this case, the ACF is a periodic function of t with period T and averaging $R_{\mathcal{I}_k}(t, t + \eta)$ over a single period can remove the dependence of the ACF on t [1]. However, this process is not reversible. In other words, we can not use $\mathcal{I}_k(t)$'s PSD to find sample values of the ACF, as the former is only a function of $t_1 - t_2$ whereas the latter depends on both t_1 and t_2 .³ We will show that in a synchronous channel the SINR of the WMF can not exceed that of the CMF and, thus, the WMF can neither maximize nor enhance the SINR. To this end, we first note that in a synchronous channel the variance of the interference term in (5.8) is

$$\sigma_{\mathcal{I}}^2 = E_g E_{\mathcal{I}} \quad (5.28a)$$

where

$$E_g \triangleq \sum_{i=-\infty}^{\infty} g_d^2(i) \quad (5.28b)$$

is $g_d(\cdot)$'s energy and $E_{\mathcal{I}} \triangleq P_{\mathcal{I}}T$ is the total interference energy. Using the Cauchy-Schwarz inequality for integrals one can obtain

$$\left(\frac{1}{2\pi} \int_{-\infty}^{\infty} G_T(\omega)G_R(\omega)d\omega \right)^2 \leq \left(\frac{1}{2\pi} \int_{-\infty}^{\infty} G_T^2(\omega)d\omega \right) \left(\frac{1}{2\pi} \int_{-\infty}^{\infty} G_R^2(\omega)d\omega \right). \quad (5.29)$$

Recalling that $g_T(t)$ has unit energy and σ_n^2 equals $g_R(t)$'s energy (i.e., the second term on the right of (5.29)), one can obtain a lower bound for σ_n^2 from (5.29) as

$$\sigma_n^2 \geq \left(\frac{1}{2\pi} \int_{-\infty}^{\infty} G(\omega)d\omega \right)^2 = g^2(0). \quad (5.30)$$

³When $\{\tau_k\}_{k=1}^K$ are nonzero but deterministic constants, the CCI is not WSS [60]. Such a channel is equivalent to a synchronous channel in which each interfering signal has been time-shifted by its corresponding delay. Thus, a WMF receiver in this channel, can not lead to a larger SINR than a CMF receiver as it can not in a synchronous channel.

Now, using (5.30) and the fact that $\sigma_I^2 = E_g E_I$, one has

$$\begin{aligned}\Gamma &= \frac{\mathcal{E}_0 g^2(0)}{\sigma_n^2 + \sigma_I^2 + \sigma_J^2} \\ &\leq \frac{\mathcal{E}_0}{1 + E_I + (E_I + \mathcal{E}_0) \dot{E}_g / g^2(0)} \\ &\leq \frac{\mathcal{E}_0}{1 + E_I}\end{aligned}\tag{5.31}$$

where $\mathcal{E}_0/(1 + E_I)$ is the SINR of the CMF receiver in synchronous CCI. Note that we did not impose any constraint on $g_R(t)$ when obtaining (5.31). Thus, in a synchronous channel the CMF is optimum in the sense of maximizing the output SINR and is superior to the WMF as opposed to the results given in [4], [16], [56], [58]. When $g(t)$ is not a Nyquist pulse, the WMF may cause significant performance degradation due to both decreasing the SINR and introducing ISI. In this case, the SINR of the ISI-free system can be obtained using (5.14) with \dot{E}_g replaced by 0. In the presence of the ISI, one can average (5.14) over the distribution of \mathcal{E}_0 to obtain

$$\bar{\Gamma} = \frac{m g^2(0)}{\dot{E}_g} \exp\left(\frac{m(\sigma_n^2 + \sigma_I^2)}{\dot{E}_g A_0^2}\right) \mathcal{E}_{1+m}\left(\frac{m(\sigma_n^2 + \sigma_I^2)}{\dot{E}_g A_0^2}\right).\tag{5.32}$$

When the observation interval is limited to $[0, T]$ and the channel is synchronous [4, Section IV], the Cauchy-Schwarz inequality can be exploited to show that the WMF has smaller SINR than the CMF provided that the ISI is negligible.

5.2.3 Discussion

As mentioned earlier, in general, $g(t)$ does not satisfy Nyquist's first criterion. Therefore, the CCI term in (5.8) is not Gaussian, neither for a synchronous nor for an asynchronous channel. For example, in a synchronous channel the PDF of each CCI term in (5.8) is obtained by summing an infinite number of Gaussian PDFs with mean zero and different variances, and this summation does not lead to a Gaussian distribution. Thus, the error probability given in [58, eq. (11)] for the WMF receiver in a synchronous channel is not correct as it is based on the false premise that the noise plus CCI term in (5.8) is a Gaussian process. When the CCI is asynchronous and the desired user transmits only a single information bit (i.e., transmission is ISI-free), a precise error probability

calculation for the WMF receiver has been executed in [58] using the Fourier series method given in [61].

5.3 Derivation of the SINR-Maximizing Filter

The WMF receiver introduced in Section 5.2 maximizes the SINR based on the premise that the ISI power is negligible. This assumption is not necessarily true as in general, $g(t)$ is not a Nyquist pulse and can have significant amplitude at time instants $t = kT$, $k \neq 0$. In this section, we derive a SINRMF receiver using a procedure similar to that used in [62] for the CCI-free case.

5.3.1 IIR Realization

The expression defining the SINR in the presence of the ISI can be written as

$$\text{SINR} = \frac{\frac{\mathcal{E}_0}{2\pi} \left[\int_{-\infty}^{\infty} G(\nu) d\nu \right]^2}{\int_{-\infty}^{\infty} \frac{(1+P_I G_T^2(\nu)) G^2(\nu)}{G_T^2(\nu)} d\nu + \frac{\mathcal{E}_0}{T} \int_{-\frac{\pi}{T}}^{\frac{\pi}{T}} \left| \sum_{n=-\infty}^{\infty} G\left(\nu - \frac{2\pi n}{T}\right) \right|^2 d\nu - \frac{\mathcal{E}_0}{2\pi} \left[\int_{-\infty}^{\infty} G(\nu) d\nu \right]^2} \quad (5.33)$$

where the last two terms in the denominator of (5.33) denote the ISI energy and the second term follows from Parseval's theorem (see Appendix B). It can be seen that maximizing the SINR is equivalent to minimizing the denominator of (5.33) provided that its numerator is a constant, i.e., $g(0)$ is fixed. To this end, we add a nonzero multiplier of $g(0)$ to the denominator of (5.33) and ignore the constant term $\mathcal{E}_0/2\pi \left[\int_{-\infty}^{\infty} G(\nu) d\nu \right]^2$ to obtain an unconstrained functional as

$$\Psi = \int_{-\infty}^{\infty} \frac{[1 + P_I G_T^2(\nu)] G^2(\nu)}{G_T^2(\nu)} d\nu + \frac{\mathcal{E}_0}{T} \int_{-\frac{\pi}{T}}^{\frac{\pi}{T}} \left| \sum_{n=-\infty}^{\infty} G\left(\nu - \frac{2\pi n}{T}\right) \right|^2 d\nu - 2\lambda \int_{-\infty}^{\infty} G(\nu) d\nu \quad (5.34)$$

where λ is a nonzero multiplier to be determined. To obtain $G(\omega)$ that minimizes Ψ we take the derivative⁴ of Ψ with respect to $G(\omega)$ and set the resulting expression to zero.

⁴ The functional derivative is defined as $\frac{\partial \Psi[G(\nu)]}{\partial G(\omega)} = \lim_{\epsilon \rightarrow 0} \frac{\Psi[G(\nu) + \epsilon \delta(\nu - \omega)] - \Psi[G(\nu)]}{\epsilon}$, where $\delta(\cdot)$ is the Dirac delta function [63].

This leads to

$$G(\omega) \left(\frac{1 + P_I G_T^2(\omega)}{G_T^2(\omega)} \right) + \frac{\varepsilon_0}{T} \sum_{n=-\infty}^{\infty} G\left(\omega - \frac{2\pi n}{T}\right) - \lambda = 0. \quad (5.35)$$

Initially, finding $G(\omega)$ seems to be complicated because of the infinite summation in (5.35). However, a closer look at the left side of (5.35) reveals that the multiplier of $G(\omega)$ in the first term is the Fourier transform of a continuous-time signal whereas the second term is the folded spectrum of $G(\omega)$, i.e., the Fourier transform of a discrete-time signal. Motivated by this fact, we can decompose $G(\omega)$ as $G(\omega) = G^{\mathcal{D}}(\omega)G^{\mathcal{C}}(\omega)$, where $G^{\mathcal{D}}(\omega)$ and $G^{\mathcal{C}}(\omega)$ are the discrete and continuous components of $G(\omega)$, respectively. Since $G^{\mathcal{D}}(\omega)$ is a periodic function with period $2\pi/T$, it can be readily seen that $G(\omega - 2\pi n/T) = G^{\mathcal{D}}(\omega)G^{\mathcal{C}}(\omega - 2\pi n/T)$. Thus, $G^{\mathcal{D}}(\omega)$ can be obtained from (5.35) as

$$G^{\mathcal{D}}(\omega) = \frac{\lambda}{G^{\mathcal{C}}(\omega) \left(\frac{1 + P_I G_T^2(\omega)}{G_T^2(\omega)} \right) + \frac{\varepsilon_0}{T} \sum_{n=-\infty}^{\infty} G^{\mathcal{C}}\left(\omega - \frac{2\pi n}{T}\right)}. \quad (5.36)$$

In order for $G^{\mathcal{D}}(\omega)$ to be periodic, the first term in the denominator of (5.36) should be a nonzero constant because neither $G^{\mathcal{C}}(\omega)$ nor $G_T(\omega)$ is a periodic function. Thus, $G^{\mathcal{C}}(\omega)$ is given by

$$G^{\mathcal{C}}(\omega) = \frac{\eta G_T^2(\omega)}{1 + P_I G_T^2(\omega)} \quad (5.37)$$

where η is a nonzero constant. Now, letting $\eta = \lambda = 1$, one obtains

$$G^{\mathcal{D}}(\omega) = \frac{1}{1 + \frac{\varepsilon_0}{T} \sum_{n=-\infty}^{\infty} G^{\mathcal{C}}\left(\omega - \frac{2\pi n}{T}\right)} \quad (5.38)$$

and

$$G_R(\omega) = \frac{G_T(\omega) G^{\mathcal{D}}(\omega)}{1 + P_I G_T^2(\omega)}. \quad (5.39)$$

Thus, the SINRMF is composed of the interference-plus-noise WMF followed by a discrete filter whose Fourier transform is given by (5.38). Note that the foregoing discrete filter is identical to the MMSE equalizer used to remove the ISI caused by the WMF in [58]. In other words, our analysis shows the MMSE equalizer in [58], although proposed there to combat the ISI, is indeed necessary to maximize the output SINR. The SINR of the SINRMF receiver is given by (see Appendix C)

$$\Gamma_{\text{SINRMF}} = \frac{1 - \Lambda_{\text{SINRMF}}}{\Lambda_{\text{SINRMF}}} \quad (5.40a)$$

where

$$\Lambda_{\text{SINRMF}} = \frac{T}{2\pi} \int_{-\frac{\pi}{T}}^{\frac{\pi}{T}} G^{\mathcal{D}}(\omega) d\omega. \quad (5.40b)$$

Note that using the Cauchy-Schwarz inequality for integrals [41] one can obtain

$$1 = \left(\frac{T}{2\pi} \int_{-\frac{\pi}{T}}^{\frac{\pi}{T}} d\omega \right)^2 \leq \Lambda_{\text{SINRMF}} \left(\frac{T}{2\pi} \int_{-\frac{\pi}{T}}^{\frac{\pi}{T}} \frac{1}{G^{\mathcal{D}}(\omega)} d\omega \right) \quad (5.41)$$

or analogously

$$\Lambda_{\text{SINRMF}}^{-1} \leq \frac{T}{2\pi} \int_{-\frac{\pi}{T}}^{\frac{\pi}{T}} \left[1 + \frac{\mathcal{E}_0}{T} \sum_{n=-\infty}^{\infty} \frac{G_T^2(\omega - \frac{2\pi n}{T})}{1 + P_I G_T^2(\omega - \frac{2\pi n}{T})} \right] d\omega. \quad (5.42)$$

Denoting the expression on the right side of (5.42) by χ , one can change the variable ω to $(\omega + 2\pi n/T)$ and interchange the integral and the summation in this expression to obtain

$$\begin{aligned} \chi &= 1 + \frac{\mathcal{E}_0}{2\pi} \sum_{n=-\infty}^{\infty} \int_{\frac{\pi}{T}(2n-1)}^{\frac{\pi}{T}(2n+1)} \frac{G_T^2(\omega)}{1 + P_I G_T^2(\omega)} d\omega \\ &= 1 + \frac{\mathcal{E}_0}{2\pi} \int_{-\infty}^{\infty} \frac{G_T^2(\omega)}{1 + P_I G_T^2(\omega)} d\omega \\ &= 1 + \Gamma_{\text{ISI-free}}. \end{aligned} \quad (5.43)$$

Thus, $\Gamma_{\text{SINRMF}} \leq \Gamma_{\text{ISI-free}}$ and the SINRMF receiver can not entirely remove the ISI.

5.3.2 FIR Realization

The SINR expression given in (5.40) is valid only when $G^{\mathcal{D}}(\omega)$ is implemented using an infinite impulse response (IIR) filter. In practice, we assume that the inverse Fourier transform of $G^{\mathcal{C}}(\omega)$, i.e., $g^{\mathcal{C}}(t)$, is zero outside some interval $[-\mathcal{L}T, \mathcal{L}T]$ (\mathcal{L} integer) and use a finite impulse response (FIR) transversal filter with $\mathcal{N} = 2\mathcal{M} + 1$ tap weights to implement $G^{\mathcal{D}}(\omega)$ in the time domain. Denoting this transversal filter by a $\mathcal{N} \times 1$ vector, \mathbf{C} , it has been shown in [1], [64] that $\mathbf{C} = \mathbf{G}^{-1}\mathbf{z}$ where \mathbf{G} is a $\mathcal{N} \times \mathcal{N}$ matrix whose ij th element is

$$G_{ij} = \begin{cases} \sum_{\ell=-\mathcal{L}}^{\mathcal{L}} g^{\mathcal{C}}(\ell T) g^{\mathcal{C}}((\ell - i + j)T) + \frac{g^{\mathcal{C}}((i-j)T)}{\mathcal{E}_0}, & |i - j| \leq 2\mathcal{L} \\ 0, & \text{otherwise} \end{cases} \quad (5.44a)$$

and \mathbf{z} is a $\mathcal{N} \times 1$ vector whose i th element is

$$z_i = \begin{cases} g^c(iT), & |i| \leq \mathcal{L} \\ 0, & \text{otherwise.} \end{cases} \quad (5.44b)$$

In this case, the SINR is given by

$$\Gamma_{\text{FIR}}^{\text{SINRMF}} = \frac{\xi}{1 - \xi} \quad (5.45a)$$

where

$$\xi = \sum_{\ell=-\mathcal{L}}^{\mathcal{L}} \mathbf{C}_{\ell} z_{\ell}. \quad (5.45b)$$

Note that the denominator of the fraction in (5.45a) is nonnegative and proportional to the mean-square error.

The main drawback of this approach is the computational complexity incurred due to inverting the matrix \mathbf{G} which is $O(\mathcal{N}^3)$ [65]. However, in our problem $g_T(t)$ and, thus, $g^c(t)$ are even functions. Consequently, \mathbf{G} is a symmetric Toeplitz matrix, i.e., $G_{ij} = G_{ji}$ and $G_{ij} = G_{|i-j|}$. For symmetric Toeplitz matrices there are low-complexity inversion algorithms that run in $O(\mathcal{N}^2)$ for small \mathcal{N} [66], and superfast inversion algorithms that run in $O(\mathcal{N} \log_2^2(\mathcal{N}))$ for large \mathcal{N} [65]. Interestingly, when the SNR is large, i.e., $\mathcal{E}_0 \gg 1$, G_{ij} is approximately independent of \mathcal{E}_0 . As a result, \mathbf{G} should be calculated only once, provided that $P_{\mathcal{I}}$ is constant. In this case, if $P_{\mathcal{I}}$ changes, \mathbf{G} should be recalculated as the G_{ij} 's depend on $P_{\mathcal{I}}$ through $g^c(t)$.

5.4 SINR Evaluation

In this section, we evaluate the SINR of the WMF and SINRMF receivers. For the WMF receiver both synchronous and asynchronous channels and the ISI-free and ISI-impaired systems are considered. However, for the SINRMF receiver we only consider the asynchronous channel. We assume that $|G_T(\omega)|^2$ has either a RC spectrum defined as [1]

$$X_{\text{RC}}(\omega) = \begin{cases} T, & |\omega| \leq \frac{\pi(1-\beta)}{T} \\ \frac{T}{2} [1 - \sin(\frac{|\omega T| - \pi}{2\beta})], & \frac{\pi(1-\beta)}{T} \leq |\omega| \leq \frac{\pi(1+\beta)}{T} \\ 0, & \frac{\pi(1+\beta)}{T} \leq |\omega| \end{cases} \quad (5.46)$$

or a BTB spectrum given by [59]

$$X_{\text{BTB}}(\omega) = \begin{cases} T, & |\omega| \leq \frac{\pi(1-\beta)}{T} \\ \frac{T}{2} 2^{-\frac{|\omega T|-\pi}{\pi\beta}}, & \frac{\pi(1-\beta)}{T} \leq |\omega| \leq \frac{\pi}{T} \\ T - \frac{T}{2} 2^{\frac{|\omega T|-\pi}{\pi\beta}}, & \frac{\pi}{T} \leq |\omega| \leq \frac{\pi(1+\beta)}{T} \\ 0, & \frac{\pi(1+\beta)}{T} \leq |\omega| \end{cases} \quad (5.47)$$

where $\beta \in [0, 1]$ denotes the filter's roll-off factor.

5.4.1 WMF Receiver

In this subsection, we evaluate the average SINR and asymptotic signal-to-interference-plus-noise ratio (ASINR) of the ISI-free and ISI-impaired WMF receivers for synchronous and asynchronous channels.

5.4.1.1 Asynchronous Channel

Assume that the channel is asynchronous. Then, using (5.21) the average SINR of the ISI-free system can be readily obtained as

$$\bar{\Gamma}_{\text{ISI-free}} = A_0^2 g(0) \quad (5.48a)$$

where

$$g(0) = \frac{1 + \mathcal{G}}{1 + E_{\mathcal{I}}} \quad (5.48b)$$

and \mathcal{G} equals

$$\mathcal{G}_{\text{RC}} \triangleq \frac{\beta}{E_{\mathcal{I}}} \left(1 - \sqrt{1 + E_{\mathcal{I}}}\right)^2 \quad (5.48c)$$

for the RC pulse and

$$\mathcal{G}_{\text{BTB}} \triangleq \frac{\beta}{E_{\mathcal{I}}} \log_2 \left[\frac{(1 + E_{\mathcal{I}})^{1+E_{\mathcal{I}}}}{(1 + E_{\mathcal{I}}/2)^{2+E_{\mathcal{I}}}} \right] \quad (5.48d)$$

for the BTB pulse and $\log_m(\cdot)$ denotes the base m logarithm. When ISI is present, one should use (5.26a) to obtain the average SINR. The main difficulty with this approach lies in evaluating \dot{E}_g in (5.26a) because a closed-form expression may not exist for $g(t)$. An efficient method for evaluating \dot{E}_g is given in Appendix B.

When a CMF receiver is used, the average SINR for the two pulses is [67, Appendix B]

$$\bar{\Gamma}_{\text{RC}}^{\text{CMF}} = \frac{A_0^2}{1 + E_{\mathcal{I}} \left(1 - \frac{\beta}{4}\right)} \quad (5.49)$$

and

$$\bar{\Gamma}_{\text{BTD}}^{\text{CMF}} = \frac{A_0^2}{1 + E_{\mathcal{I}} \left(1 - \frac{\beta}{4 \log(2)}\right)} \quad (5.50)$$

respectively, where $\log(\cdot)$ denotes the natural logarithm.

Assume now that the ASINR, Υ , is defined as

$$\Upsilon \triangleq \lim_{\gamma_b \rightarrow \infty} \bar{\Gamma}. \quad (5.51)$$

Then, recalling that $\gamma_b = E_{\mathcal{I}} \psi$, one can obtain

$$\Upsilon_{\text{RC, ISI-free}}^{\text{WMF}} = \Upsilon_{\text{BTD, ISI-free}}^{\text{WMF}} = 2(1 + \beta) \psi \quad (5.52)$$

$$\begin{aligned} \Upsilon_{\text{RC}}^{\text{WMF}} &= \Upsilon_{\text{BTD}}^{\text{WMF}} \\ &= \begin{cases} \frac{m(1+\beta)^2}{\beta(1-\beta)} \exp\left(\frac{m(1+\beta)}{2\psi\beta(1-\beta)}\right) \mathcal{E}_{1+m}\left(\frac{m(1+\beta)}{2\psi\beta(1-\beta)}\right), & 0 < \beta < 1 \\ 2(1 + \beta)\psi, & \text{otherwise.} \end{cases} \end{aligned} \quad (5.53)$$

$$\Upsilon_{\text{RC}}^{\text{CMF}} = \frac{8\psi}{4 - \beta} \quad (5.54)$$

$$\Upsilon_{\text{BTD}}^{\text{CMF}} = \frac{8\psi}{4 - \frac{\beta}{\log(2)}}. \quad (5.55)$$

Hence, using the whitening filter in an ISI-free system increases the ASINR by a factor of $(1 + \beta)(4 - \beta)/4$ for the RC pulse and by a factor of $(1 + \beta)(4 - \beta/\log(2))/4$ for the BTD pulse compared to the case when a CMF receiver is used.

5.4.1.2 Synchronous channel

When the channel is synchronous, (5.21) is no longer valid because the CCI is not WSS. In order to find the SINR in this case, we first use (5.10) to obtain the noise variance for the RC and BTD pulses as

$$\sigma_{n,\text{RC}}^2 = \frac{1 - \beta}{(1 + E_{\mathcal{I}})^2} + \frac{\beta}{(1 + E_{\mathcal{I}})^{3/2}} \quad (5.56)$$

$$\sigma_{n,\text{BTD}}^2 = \frac{1 - \beta}{(1 + E_{\mathcal{I}})^2} + \frac{\beta}{(1 + E_{\mathcal{I}})^2} \log_2(2 + E_{\mathcal{I}}) \quad (5.57)$$

respectively. Eqs. (5.56) and (5.57) can then be used along with the fact that $\sigma_I^2 = E_g E_I$ to obtain

$$\sigma_n^2 + \sigma_I^2 = \frac{1}{1 + E_I} \left(1 + \frac{4 + 3E_I}{2 + E_I} \mathcal{G} \right) \quad (5.58)$$

where \mathcal{G} is given by (5.48c) for the RC pulse and by (5.48d) for the BTD pulse. Now, we substitute $g(0)$ and $\sigma_n^2 + \sigma_I^2$ in (5.14) by their equivalent values in (5.48b) and (5.58) to obtain the average SINR of the ISI-free system as

$$\bar{\Gamma}_{\text{ISI-free}} = \frac{A_0^2}{1 + E_I} \left(\frac{(1 + \mathcal{G})^2}{1 + \frac{4+3E_I}{2+E_I} \mathcal{G}} \right). \quad (5.59)$$

For an ISI-impaired system, one can use (5.32) to evaluate the SINR of the WMF receiver.

The ASINR at the output of the WMF receiver for the ISI-free and ISI-impaired systems are

$$\Upsilon_{\text{RC, ISI-free}}^{\text{WMF}} = \Upsilon_{\text{BTD, ISI-free}}^{\text{WMF}} = 2\psi \frac{(1 + \beta)^2}{(1 + 3\beta)} \quad (5.60)$$

and

$$\Upsilon_{\text{RC}}^{\text{WMF}} = \Upsilon_{\text{BTD}}^{\text{WMF}} = \begin{cases} \frac{m(1+\beta)^2}{\beta(1-\beta)} \exp\left(\frac{m(1+3\beta)}{2\psi\beta(1-\beta)}\right) \mathcal{E}_{1+m}^{\mathcal{E}}\left(\frac{m(1+3\beta)}{2\psi\beta(1-\beta)}\right), & 0 < \beta < 1 \\ 2\psi, & \text{otherwise.} \end{cases} \quad (5.61)$$

respectively. It can be easily shown that for a synchronous channel

$$\Upsilon_{\text{RC}}^{\text{CMF}} = \Upsilon_{\text{BTD}}^{\text{CMF}} = 2\psi. \quad (5.62)$$

Thus, the ASINR of the WMF receiver in an ISI-free system decreases by a factor of $(1 + \beta)^2/(1 + 3\beta)$ compared to that of the CMF receiver in a synchronous channel.

5.4.2 SINR-Maximizing Filter

In this section, we evaluate the SINR of the SINRMF to determine how effectively this filter can restore the SINR loss due to the ISI. $g_T(t)$ is either a root RC or a root BTD pulse. To this end, we first use (5.40b) to evaluate Λ for the RC pulse as

$$\Lambda_{\text{RC}} = \frac{1 + E_I}{1 + \mathcal{E}_0 + E_I} - \frac{\mathcal{E}_0\beta(2 + E_I)}{(2\mathcal{E}_0 + E_I)(1 + \mathcal{E}_0 + E_I)} + \frac{2\mathcal{E}_0\beta\sqrt{(2 + E_I)(2 + 2\mathcal{E}_0 + E_I)/(1 + \mathcal{E}_0 + E_I)}}{(2\mathcal{E}_0 + E_I)(2 + 2\mathcal{E}_0 + E_I)} \quad (5.63)$$

and for the BTD pulse as

$$\Lambda_{\text{BTD}} = \frac{(1 + E_{\mathcal{I}})(1 - \beta)}{1 + E_{\mathcal{I}} + \mathcal{E}_0} + \frac{\beta E_{\mathcal{I}}}{2\mathcal{E}_0 + E_{\mathcal{I}}} + \frac{\mathcal{E}_0 \beta (2 + E_{\mathcal{I}})}{2\mathcal{E}_0 + E_{\mathcal{I}}} \log_2 \left[\left(\frac{1 - \zeta_+}{2 - \zeta_+} \right)^{\zeta_+} / \left(\frac{1 - \zeta_-}{2 - \zeta_-} \right)^{\zeta_-} \right] \quad (5.64a)$$

where ζ_+ and ζ_- are given by

$$\zeta_{\pm} = - \frac{E_{\mathcal{I}}(2\mathcal{E}_0 + E_{\mathcal{I}}) \pm \sqrt{E_{\mathcal{I}}(2 + E_{\mathcal{I}})(2\mathcal{E}_0 + E_{\mathcal{I}})(2 + 2\mathcal{E}_0 + E_{\mathcal{I}})}}{2(1 + \mathcal{E}_0 + E_{\mathcal{I}})}. \quad (5.64b)$$

Then, substitute Λ for each pulse in (5.40a) to obtain the maximum SINR. It can be shown that when $\mathcal{E}_0 \ll E_{\mathcal{I}}$, the SINRMF leads approximately to the same SINR as that of the WMF in the ISI-free system. Thus, for small SIR values the SINRMF can eliminate the effect of the ISI caused by the WMF in an ISI-impaired system. The average maximum SINR can be obtained by integrating Γ_{SINRMF} in (5.40a) over the distribution of \mathcal{E}_0 . In this case, the ASINR of the SINRMF is

$$\Upsilon_{\text{RC}}^{\text{SINRMF}} = \Upsilon_{\text{BTD}}^{\text{SINRMF}} = E_{\alpha_0^2} \left\{ \frac{2\psi \alpha_0^2 (1 + \beta + 4\psi \alpha_0^2)}{1 + 2\psi \alpha_0^2 (2 - \beta)} \right\} \quad (5.65)$$

where the last equation follows from the fact that the limit and the ensemble average in (5.51) are interchangeable. Using (5.13), one can obtain

$$\Upsilon_{\text{RC}}^{\text{SINRMF}} = \Upsilon_{\text{BTD}}^{\text{SINRMF}} = \frac{\exp(\delta)}{2 - \beta} \left[m(1 + \beta) \mathcal{E}_{1+m}(\delta) + 4\psi(1 + m) \mathcal{E}_{2+m}(\delta) \right] \quad (5.66a)$$

where

$$\delta = \frac{m}{2\psi(2 - \beta)} \quad (5.66b)$$

and $\mathcal{E}_m(\cdot)$ is given by (5.26b).

5.5 Numerical Results

We have evaluated the SINR of the WMF and the SINRMF receivers and compared them to that of the CMF in several different scenarios. Simulation results have been also presented in some scenarios to verify our analytical results. The BER of the CMF and the WMF receivers have been evaluated in a synchronous channel using computer simulation to highlight the differences between our results and those given in [58]. In the examples, two values of m are usually considered, $m = 0.5$ and $m = \infty$. These

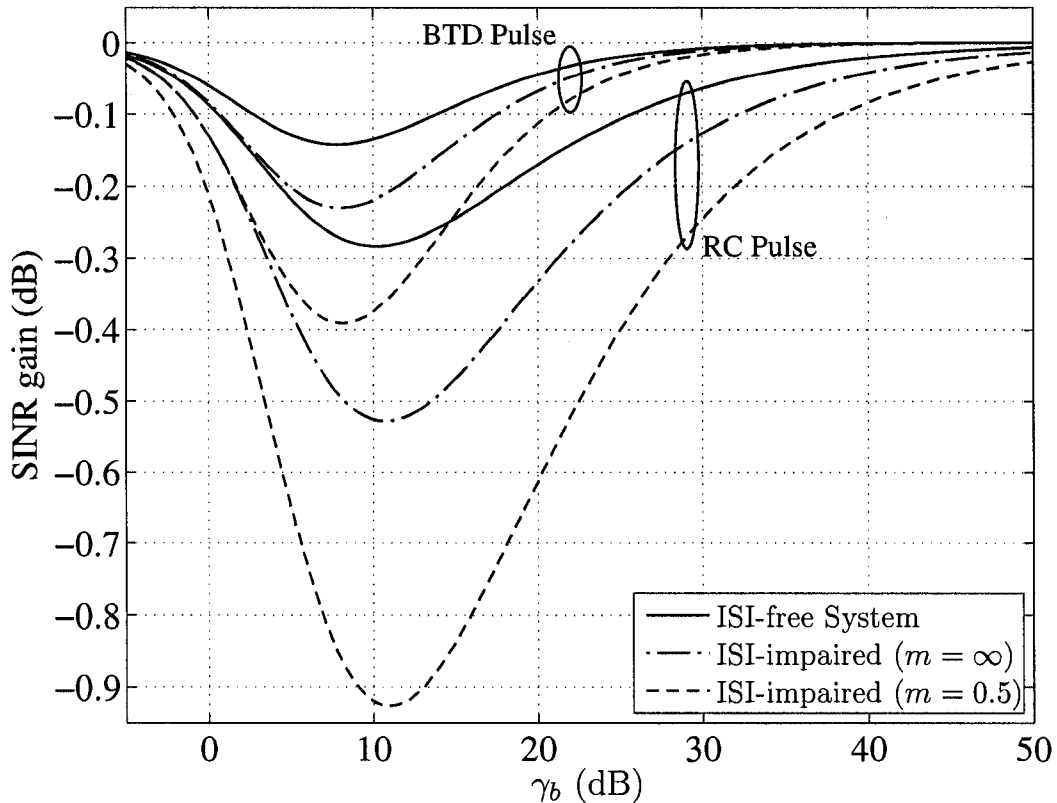


Figure 5.2. The SINR gain achieved by the WMF over the CMF for the RC and BTD pulses, $\beta = 1$, $\psi = 0$ dB for a synchronous channel.

values represent severe fading and no fading, respectively and establish worst case and best case results.

Figs. 5.2 and 5.3 illustrate the SINR gain over the CMF of the ISI-free and ISI-impaired WMF as a function of SNR in synchronous and asynchronous channels. The pulses are assumed to have 100% excess bandwidth and the channel is Nakagami- m fading. When the channel is synchronous, the SINR of both ISI-free and ISI-impaired WMF receivers is smaller than that of the CMF receiver, as shown in Fig. 5.2. Furthermore, when a RC pulse is employed, the WMF receiver suffers from a larger SINR loss than does a WMF receiver with a BTD pulse. Interestingly, when $\gamma_b \rightarrow \infty$, the WMF receiver can achieve the same SINR as can the CMF receiver. This is because for vanishing small background noise, $G_R(\omega)$ approaches $[P_T G_T(\omega)]^{-1}$. Since β is assumed to be unity, one can readily see that $G(\omega)$ tends to a Nyquist pulse spectrum and $\Gamma \rightarrow \mathcal{E}_0/(1 + E_T)$

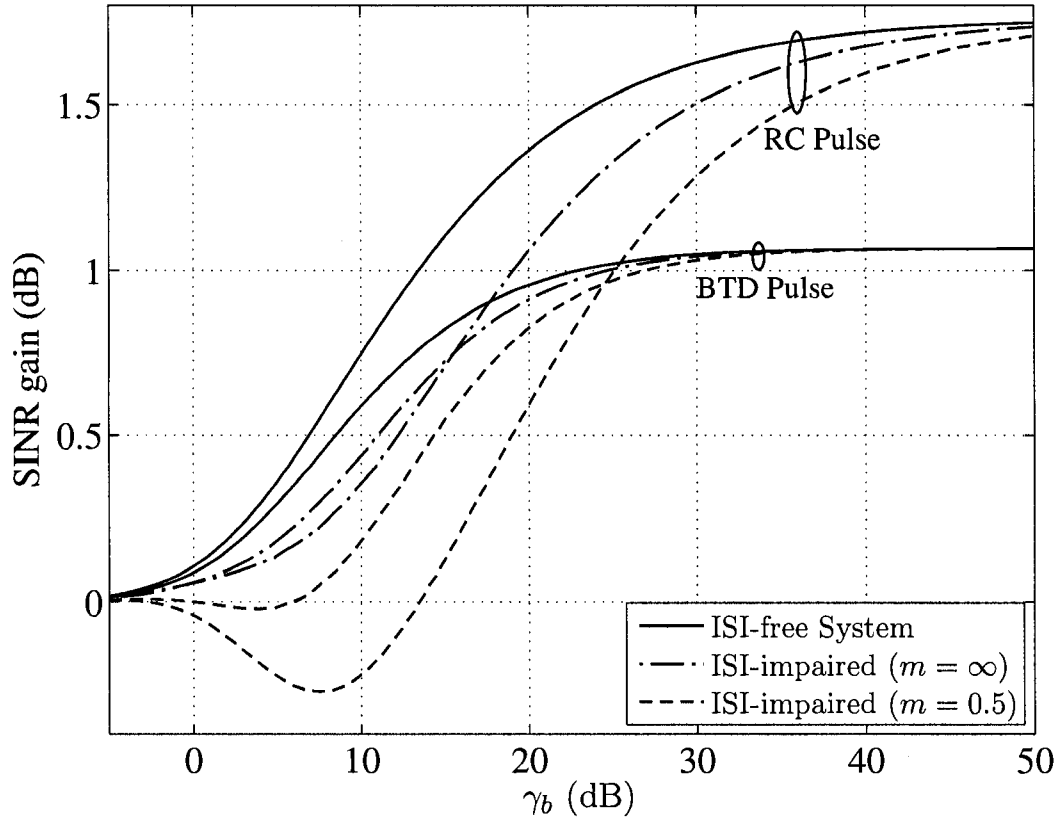


Figure 5.3. The SINR gain achieved by the WMF over the CMF for the RC and BTB pulses, $\beta = 1$, $\psi = 0$ dB for an asynchronous channel.

which is the SINR of the CMF receiver. In the asynchronous channel, however, an ISI-free WMF receiver can achieve a gain as large as $10 \log_{10} [(1 + \beta)(4 - \beta)/4]_{\beta=1} = 1.76$ dB over the CMF receiver when a RC pulse is used. The corresponding gain for the BTB pulse is at most 1.07 dB as shown in Fig. 5.3. Note, however, that for small SNR values and in the presence of ISI and severe fading, the WMF with BTB pulse achieves almost no SINR gain over the CMF, and with a RC pulse its SINR is inferior to that of the CMF.

Fig. 5.4 shows the WMF's SINR gain over the CMF as a function of SNR for the case when $\beta = 0.35$ and $m = 2$. Both analytical and simulation results have been presented. Clearly, the ISI-impaired WMF has smaller SINR than the CMF for both pulses and thus, the superiority of the WMF over the CMF strongly depends on the ISI. Note that in synchronous CCI the SINR of the CMF is the same for all Nyquist pulses and thus,

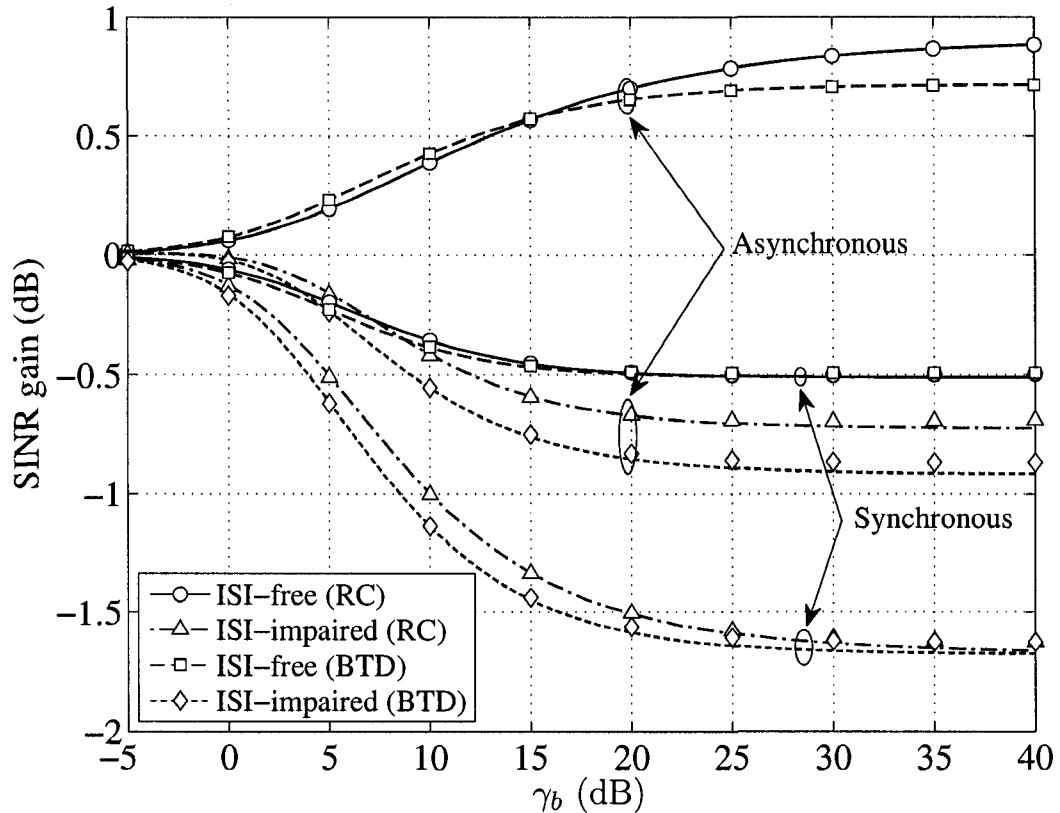


Figure 5.4. The WMF receiver's SINR gain over the CMF receiver for RC and BTD pulses in synchronous and asynchronous CCI for Nakagami- m fading ($m = 2$), with $\beta = 0.35$ and $\psi = 0$ dB. Markers denote simulation results.

the ASINR gain is the same for both RC and BTD pulses. In contrast, in asynchronous CCI the gains are different because $\Gamma_{RC}^{CMF} \neq \Gamma_{BTD}^{CMF}$. Moreover, when $\gamma_b \rightarrow \infty$, the SINR gain does not approach zero in contrast to the case when $\beta = 1$. This is because in this case $G(\omega) \rightarrow P_{\mathcal{I}}^{-1}$ over $[-\pi(1 + \beta)/T, \pi(1 + \beta)/T]$ and Nyquist's criterion is satisfied only if $\beta = 0$ or $\beta = 1$. Note that our simulation results match the analytical results quite well in all the examined cases.

The exact and simulated SINR gains of the WMF over the CMF as a function of β are depicted in Fig. 5.5. The CCI is assumed to be asynchronous and the SNR and SIR are 15 dB and 0 dB, respectively. Although, the SINR gain for the ISI-free WMF is a monotonically increasing function of β , it has some minimum value for the ISI-impaired receiver. For $m = 0.5$, 1 and ∞ the minima occur at $\beta = 0.36$, 0.34 and 0.27 for the RC

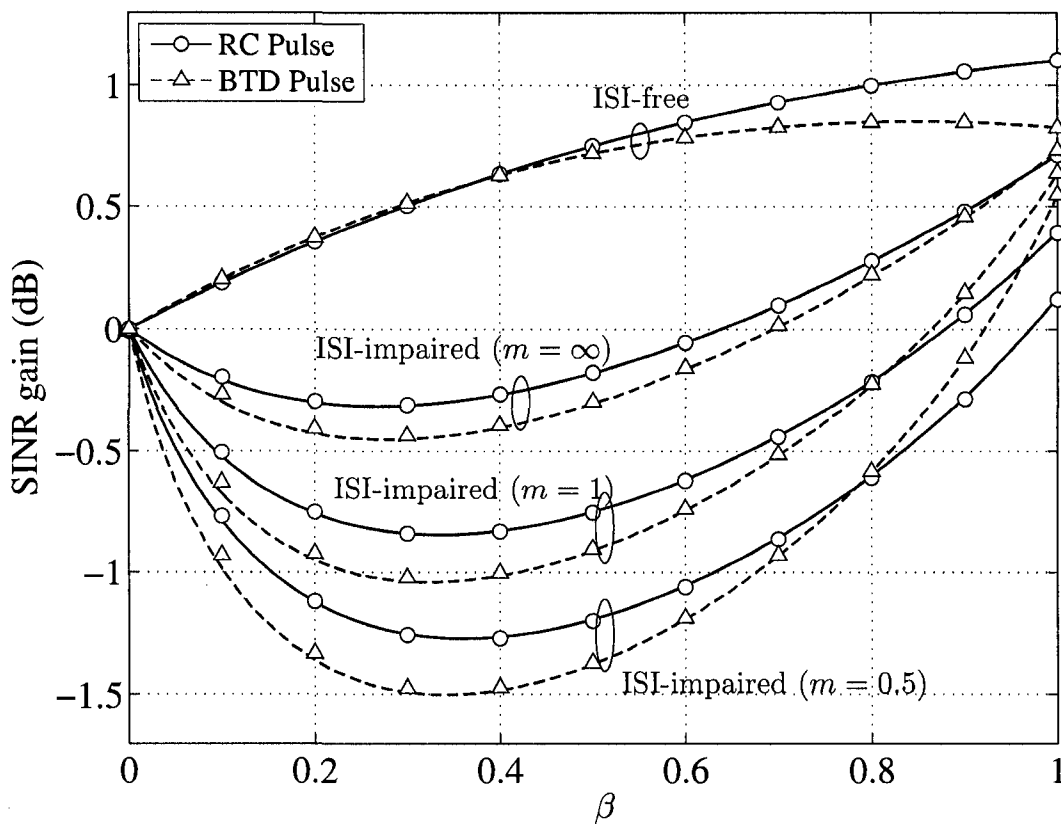


Figure 5.5. The effect of roll-off factor on the SINR gain of the WMF receiver over the CMF receiver for RC and BTM pulses in asynchronous CCI and Nakagami- m fading, for SNR = 15 dB and $\psi = 0$ dB. Markers denote simulation results.

pulse and at $\beta = 0.34$, 0.32 and 0.28 for the BTM pulse, respectively. Furthermore, in the presence of the ISI and severe fading, a slight SINR gain can be achieved only when $\beta > 0.92$ for the BTM pulse and $\beta > 0.97$ for the RC pulse. When $\beta = 1$ and a BTM pulse is used, the SINR gains for $m = 0.5$, 1 and ∞ are approximately 0.55, 0.63 and 0.72 dB, respectively which are close to those achieved by the ISI-free WMF. Note that the simulated SINR gain is in very good agreement with the exact SINR gain for all the cases studied. Thus, for $\beta = 1$, the WMF can achieve ISI-free SINR gain provided that the transmitter pulse has a rectangular spectrum [4], [68]. In this case, close to ISI-free SINR gain can be achieved for sufficiently large SNRs.

Fig. 5.6 shows the WMF's SINR gain over the CMF as a function of SIR evaluated using both theoretical analysis and simulation. The SNR is assumed to be 15 dB, $\beta = 0.35$ and the CCI is asynchronous. When the SIR is large, no SINR gain over the

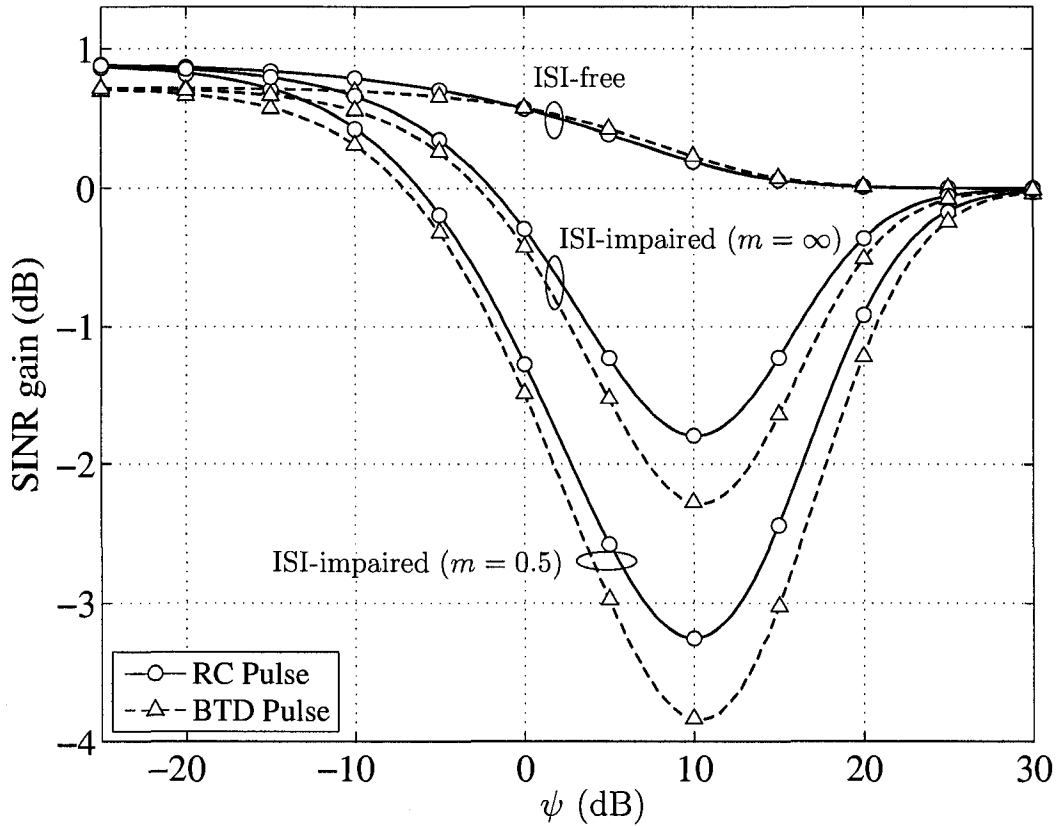


Figure 5.6. The effect of SIR on the SINR gain of the WMF receiver over the CMF receiver for RC and BTD pulses in asynchronous CCI and Nakagami- m fading ($m = 0.5$), for SNR = 15 dB and $\beta = 0.35$. Markers denote simulation results.

CMF can be achieved by the WMF even for an ISI-free system. This is because the WMF receiver approaches the CMF for large values of ψ , and so it has the same SINR as the CMF. For small values of SIR, however, the ISI-impaired WMF exhibits some SINR gain over the CMF even for severe fading. The way to view this is that in the latter case $\sigma_{\mathcal{J}}^2$ is much smaller than $\sigma_{\mathcal{I}}^2$ in (5.14). Hence, the SINR of the ISI-impaired system approaches that of the ISI-free system which, in turn, is superior over the CMF in having larger SINR. Fig. 5.6 also shows that the simulation results compare well with the analytical results for all the examined scenarios.

Fig. 5.7 illustrates the BER performance of the CMF and WMF receivers when the channel is synchronous. To highlight the differences between our results and those given in [58, Fig. 3], we assume that $\beta = 1$ for both pulses. We also assume that the

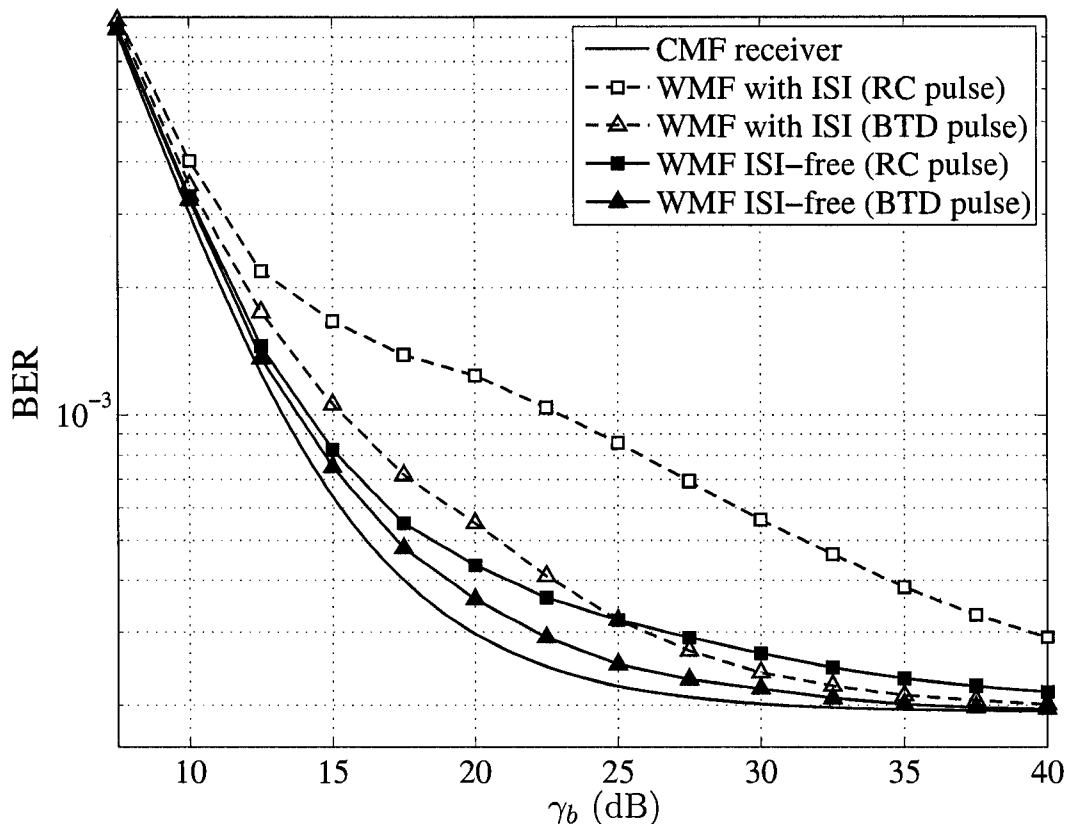


Figure 5.7. Performance of the whitening and the conventional MF receivers in Nakagami- m fading ($m = 8$) with synchronous CCI and AWGN for SIR = 10 dB and BTD and RC pulses with 100% excess bandwidth.

channel is Nakagami- m ($m = 8$) for the desired user and Rayleigh for the interfering users. The BER of the CMF receiver has been obtained using the BER expression given in [67] for synchronous CCI and Nakagami- m fading while for the WMF, it has been evaluated using computer simulation. Fig. 5.7 clearly shows that the WMF receiver can not outperform the CMF receiver even for the ISI-free system in contrast to the results given in [4], [16], [58]. As mentioned in Section 5.2, this is due to the fact that the SINR at the output of the whitening filter is smaller than that of the CMF receiver.

The BER performance of the WMF and SINRMF receivers for asynchronous CCI is shown in Fig. 5.8. Other assumptions are the same as those given for Fig. 5.7. Fig. 5.8 reflects the fact that the ISI can significantly degrade the BER performance of the WMF receiver, especially when a RC pulse is used. Indeed, when $\gamma_b < 30$ dB, the CMF

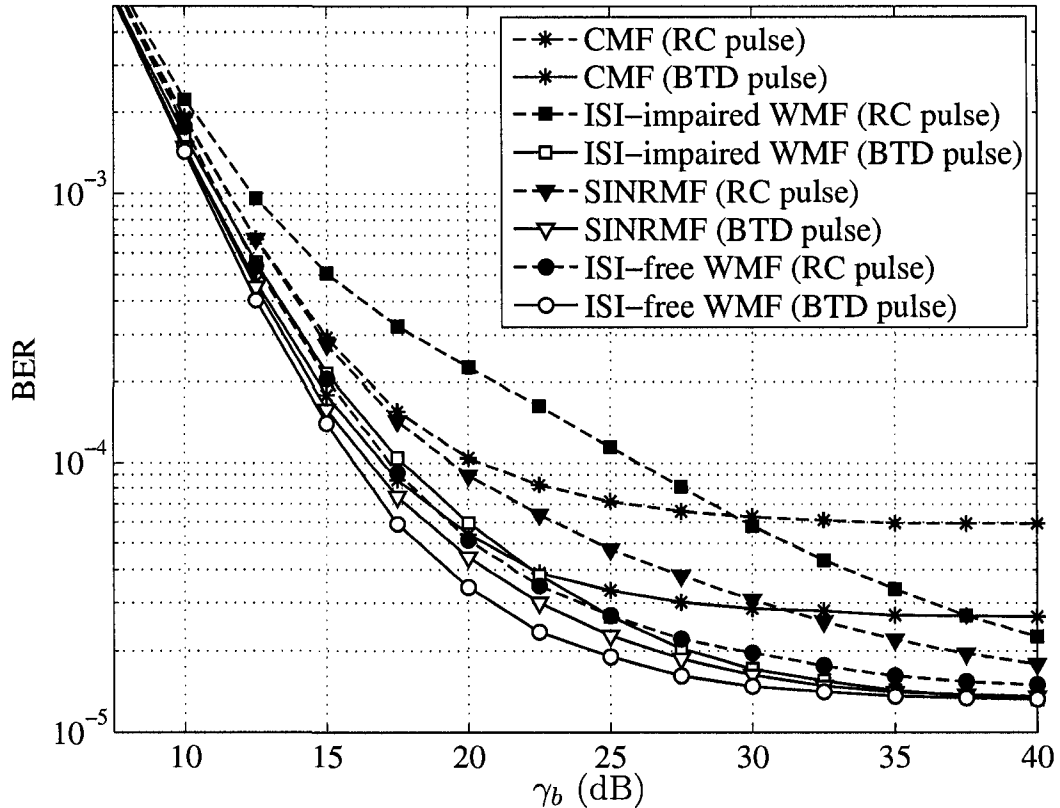


Figure 5.8. Performance of the CMF, WMF and SINRMF receivers in Nakagami- m fading ($m = 8$) with asynchronous CCI and AWGN for SIR = 10 dB and BTD and RC pulses with 100% excess bandwidth.

receiver outperforms the ISI-impaired WMF receiver and makes it ineffective for this SNR range. The SINRMF receiver, however, is superior to the CMF receiver for all the examined values of SNR. Note that our simulation results for the BER of the ISI-free WMF receiver compare quite well with analytical results given in [58, Section III-B].

The ASINR as a function of β of the ISI-free and ISI-impaired WMF as well as the SINRMF receivers are depicted in Fig. 5.9. The channel is Nakagami- m with $m = 0.5$ and the SIR is 0 dB. The ASINR of both the ISI-impaired WMF and the SINRMF receivers approaches that of the ISI-free WMF receiver when β is approaching 0 or 1. This is because for these values of β and vanishing small background noise, the WMF is approximately a Nyquist pulse and does not introduce ISI. Moreover, for $\beta = 1$ the ASINR of the WMF is twice as large as that of the CMF, whereas for $\beta = 0$ the two filters

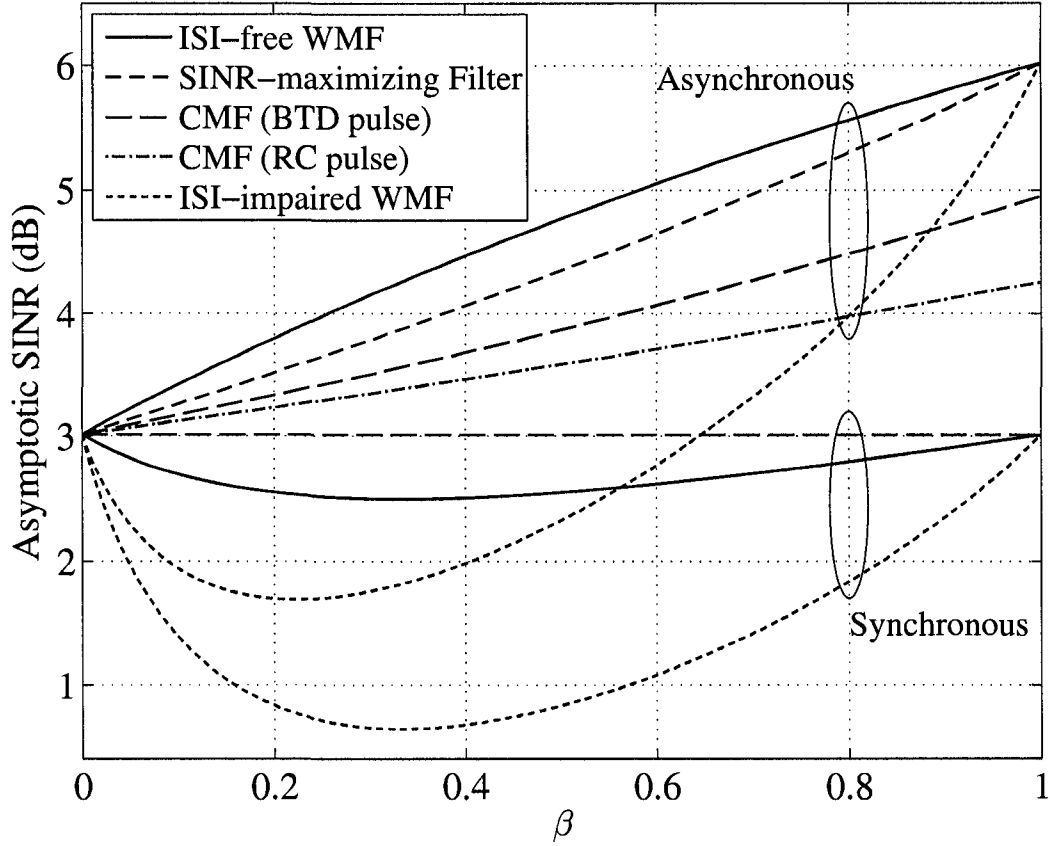


Figure 5.9. The ASINR of the SINRMF, WMF and CMF receivers versus β in Nakagami- m fading ($m = 0.5$) for RC and BTD pulses, with $\psi = 0$ dB.

have the same ASINR. Note that for all values of β , the SINR of the SINRMF closely follows that of the ISI-free WMF. As expected in a synchronous channel, the WMF can not achieve any SINR gain over the CMF even in the absence of ISI. However, in an asynchronous channel, the ISI-impaired SINR is larger than that of the CMF when $\beta > 0.8$ for the RC pulse and when $\beta > 0.88$ for the BTD pulse. To explain this, we note that the ASINR of the ISI-impaired WMF can be expressed as

$$\Upsilon = E_{\alpha_0^2} \left\{ \frac{2(1+\beta)^2 \psi \alpha_0^2}{1 + \beta + 2(1-\beta)\beta \psi \alpha_0^2} \right\}. \quad (5.67)$$

It can be shown that the argument of the expectation in (5.67) is greater than 2ψ (i.e., the instantaneous ASINR of the CMF receiver) when

$$\beta > \max \left\{ 0, \frac{2\psi \alpha_0^2 - 1}{2\psi \alpha_0^2 + 1} \right\}. \quad (5.68)$$

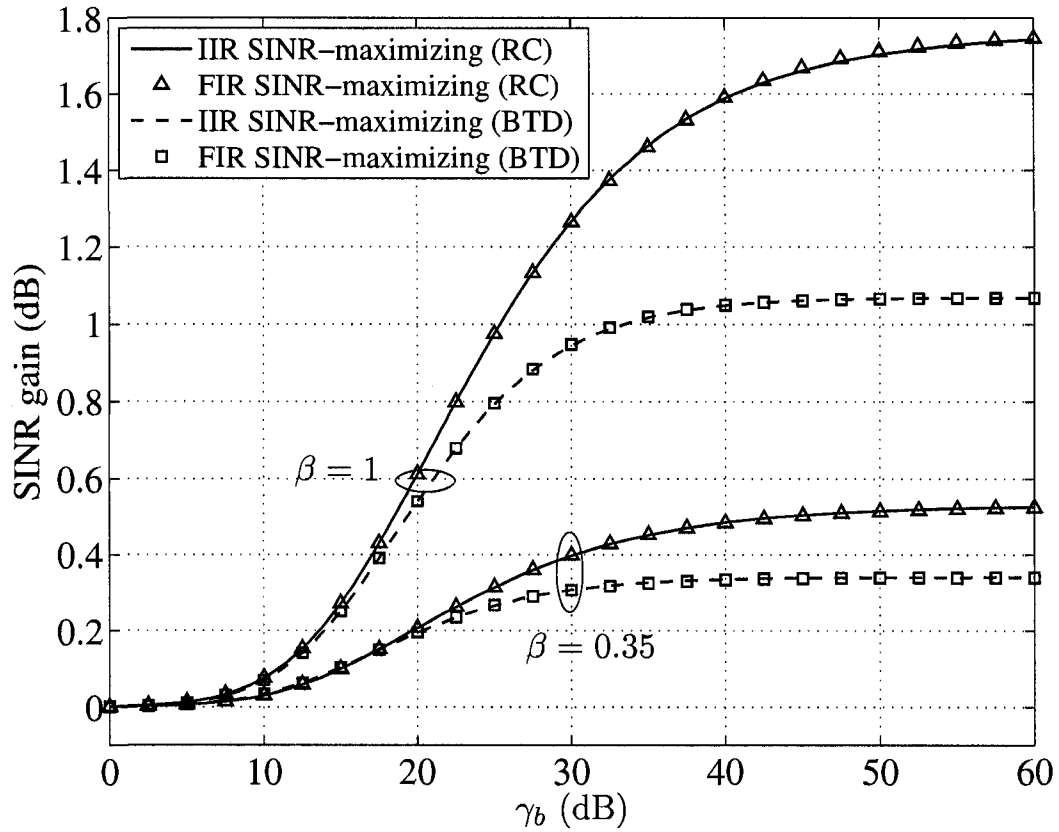


Figure 5.10. The SINR gain over the CMF receiver versus SNR in Nakagami- m fading ($m = 0.5$) and asynchronous CCI, with $\psi = 10$ dB, $\mathcal{M} = 12$, $\beta = 0.35$ and $\beta = 1$ for an SINRMF receiver.

In other words, for very small values of $\psi \alpha_0^2$ the ISI-impaired ASINR is almost certainly larger than that of the CMF. However, when $\psi \alpha_0^2$ is large, the ASINR of the ISI-impaired system can not exceed that of the CMF unless β is very close to unity.

Figs. 5.10 and 5.11 show the SINR gain of the ISI-impaired WMF and the SINRMF over the CMF as a function of SNR. The channel is assumed to be Nakagami- m fading with $m = 0.5$, $\psi = 10$ dB and the pulses have either 35% or 100% excess bandwidth. These values of β , ψ and m can lead to significant SINR loss in the ISI-impaired WMF compared to the CMF, as shown in Fig 5.11. Fig 5.10 shows that the SINRMF always outperforms the CMF even for small SNR values. When the SNR is large and $\beta = 0.35$, the SINRMF can achieve a gain as large as 0.53 dB for the RC pulse and as large as 0.34 dB for the BTD pulse. Comparing these gains with those achieved by the ISI-impaired

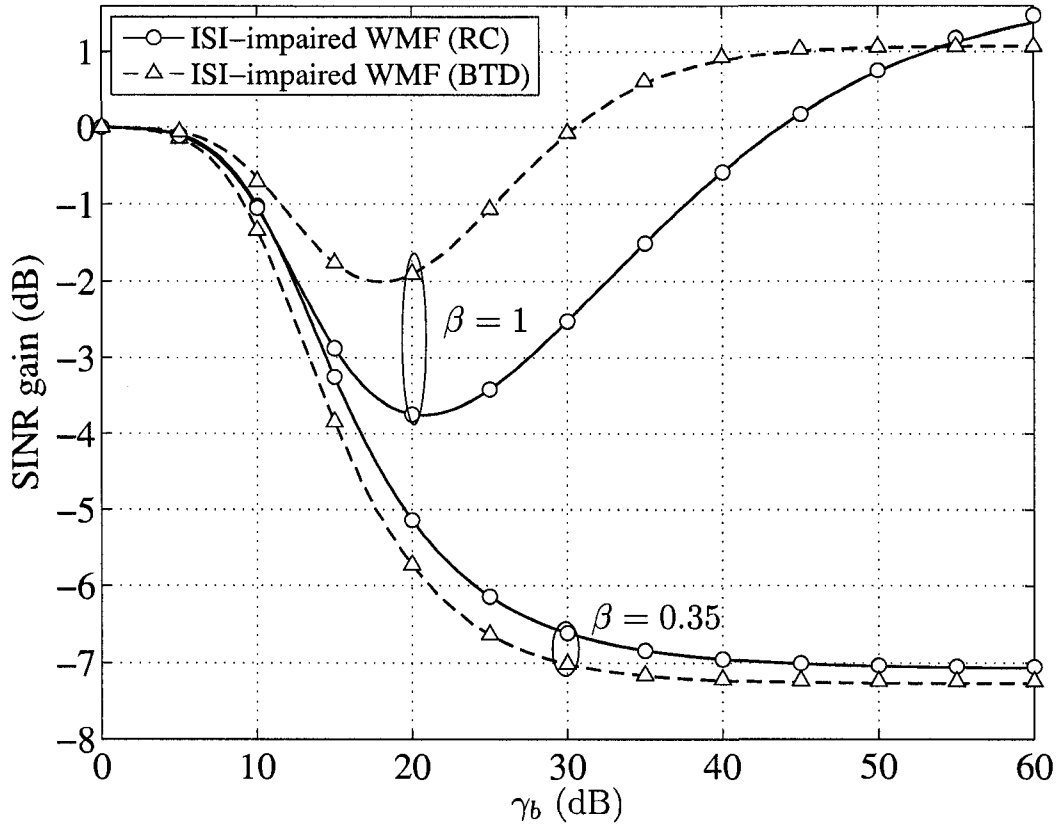


Figure 5.11. The SINR gain over the CMF receiver versus SNR in Nakagami- m fading ($m = 0.5$) and asynchronous CCI, with $\psi = 10$ dB, $\mathcal{M} = 12$, $\beta = 0.35$ and $\beta = 1$ for an ISI-impaired WMF receiver (markers denote simulation results).

WMF, one observes that a SINRMF can increase the SINR of the ISI-impaired WMF by approximately 7.6 dB. Note that in this case the gains achieved by the SINRMF are still 0.38 dB less than the maximum achievable SINR gain for both pulses. For $\beta = 1$ and large SNR values, the SINRMF can achieve the maximum achievable SINR for both pulses even when the SIR is as large as 10 dB. In this case, the SINR of the ISI-impaired WMF approaches that of the SINRMF only when the SNR is sufficiently large. Fig. 5.10 also highlights the fact that the SINR of the FIR SINRMF receiver compares quite well with that of the IIR filter. Note that the analytical results presented in Fig 5.11 match very well with the simulation results.

Chapter 6

ISI-free Transmitter-Receiver Designs for Bandlimited Microcellular Wireless Systems

In this chapter, we derive the T-R filter for bandlimited microcellular systems that can achieve maximum SINR without introducing ISI. In the first design, the transmitter and the receiver filters have flat spectrum with 100% excess bandwidth and can achieve the maximum achievable SINR in a strict sense. In the second design, a more general problem is considered in which the T-R pulses do not have a fixed excess bandwidth and their spectrum is not necessarily flat. In this case, we show that the receiver filter is composed of a WMF receiver followed by a discrete-time filter that removes the ISI caused by the WMF.

6.1 Optimal 100% Excess Bandwidth Signaling in Cochannel Interference

In this section, we show that RC pulse-shaping is suboptimal for 100% excess bandwidth signaling in a CCI environment. This, perhaps surprising, result is revealed by optimizing the transmitter pulse-shaping and receiver pulse-shaping jointly under a transmitted signal power constraint for a channel that corrupts the transmitted signal with AWGN

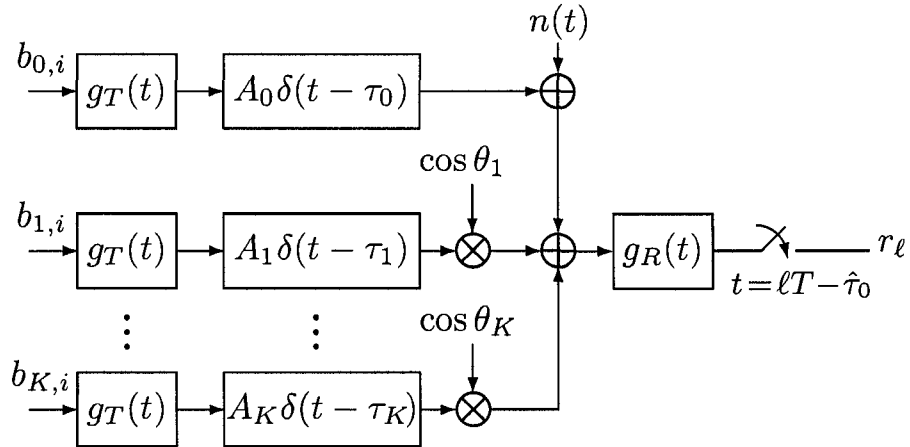


Figure 6.1. The block diagram of the baseband cochannel interference communication system with $(K + 1)$ asynchronous users.

and like-modulated CCI. It is shown that the optimal transmitter and receiver filters that maximize the SINR and minimize the symbol error probability have constant (flat) amplitude across the full available bandwidth for all values of SNR, all values of SIR, and all values of SINR. The gain of optimal 100% excess bandwidth signaling over RC 100% excess bandwidth signaling is a function of the signal power ratios, and is as much as 1.76 dB.

6.1.1 Signal Model

The block diagram of the baseband communication system is illustrated in Fig 6.1. Assume that the desired (i.e., the 0th) and the interfering signals are BPSK modulated. Also assume that carrier phase recovery for the desired user is perfect. Then, the baseband received signal is given by [58]

$$r(t) = A_0 \sum_{i=-\infty}^{\infty} b_{0,i} g_T(t - \tau_0 - iT) + \sum_{k=1}^K A_k \cos \theta_k \sum_{i=-\infty}^{\infty} b_{k,i} g_T(t - \tau_k - iT) + n(t) \quad (6.1)$$

where the parameters of the signal model are defined in Section 5.1. We assume $g_T(t)$'s spectrum is zero outside $[-\mathcal{W}, \mathcal{W}]$ where $\mathcal{W} \triangleq \pi(1 + \beta)/T$ and β is the pulse-shaping excess bandwidth, and $n(t)$ is a zero-mean Gaussian process with unit PSD over $[-\mathcal{W}, \mathcal{W}]$. All random variables are assumed to be mutually independent.

The received signal is passed through the receiver filter, $g_R(t)$, and sampled at $t = \ell T + \hat{\tau}_0$ to obtain the decision statistic for $b_{0,\ell}$, as

$$r_\ell = A_0 \sum_{i=-\infty}^{\infty} b_{0,i} g((\ell - i)T + \delta) + \sum_{k=1}^K A_k \cos \theta_k \sum_{i=-\infty}^{\infty} b_{k,i} g((\ell - i)T + \hat{\tau}_0 - \tau_k) + n_\ell \quad (6.2)$$

where $g(t) = \int_{-\infty}^{\infty} g_T(s) g_R(t - s) ds$, n_ℓ is a zero-mean Gaussian random variable whose variance equals $g_R(t)$'s energy, $\hat{\tau}_0$ is the receiver's estimate of τ_0 , and $\delta \triangleq \hat{\tau}_0 - \tau_0$ is the estimation error.

6.1.2 Filter Design

In this section we design the transmitter and receiver filters to maximize the SINR at the output of $g_R(t)$ subject to the following conditions:

1. $g(t)$ satisfies Nyquist's first criterion [1] for zero ISI.
2. $g_T(t)$ has unit energy, i.e.,

$$\int_{-\infty}^{\infty} g_T^2(t) dt = 1. \quad (6.3)$$

Recalling from Section 5.1, eq. (6.3) implies that the average SNR and the average SIR per symbol at the input of the receiver are given by (5.5) and (5.6), respectively.

Denoting the Fourier transform of $g_T(t)$, $g_R(t)$ and $g(t)$ by $G_T(\omega)$, $G_R(\omega)$ and $G(\omega)$, respectively, and assuming that timing recovery is perfect (i.e., $\delta = 0$), the SINR at the output of $g_R(t)$ is given by

$$\text{SINR} = \frac{A_0^2 \left[\frac{1}{2\pi} \int_{-\mathcal{W}}^{\mathcal{W}} G(\omega) d\omega \right]^2}{\frac{1}{2\pi} \int_{-\mathcal{W}}^{\mathcal{W}} (1 + P_I |G_T(\omega)|^2) |G_R(\omega)|^2 d\omega} \quad (6.4)$$

where $1 + P_I |G_T(\omega)|^2$ is the PSD of the interference-plus-noise term (i.e., the last two terms on the right side of (6.1)) and P_I is the total interference power. Our objective is to find the T-R filters that maximize the expression on the right side of (6.4). To this end, we first note that $G(\omega)$ can be decomposed as

$$G(\omega) = \left[\sqrt{1 + P_I |G_T(\omega)|^2} G_R(\omega) \right] \left[\frac{G_T(\omega)}{\sqrt{1 + P_I |G_T(\omega)|^2}} \right]. \quad (6.5)$$

Then, we use the Cauchy-Schwarz inequality for integrals [69] to obtain

$$\left[\frac{1}{2\pi} \int_{-\mathcal{W}}^{\mathcal{W}} G(\omega) d\omega \right]^2 \leq \frac{1}{2\pi} \int_{-\mathcal{W}}^{\mathcal{W}} \frac{|G_T(\omega)|^2}{1 + P_I |G_T(\omega)|^2} d\omega \times \frac{1}{2\pi} \int_{-\mathcal{W}}^{\mathcal{W}} (1 + P_I |G_T(\omega)|^2) |G_R(\omega)|^2 d\omega \quad (6.6a)$$

or analogously

$$\text{SINR} \leq \frac{A_0^2}{2\pi} \int_{-\mathcal{W}}^{\mathcal{W}} \frac{|G_T(\omega)|^2}{1 + P_I |G_T(\omega)|^2} d\omega. \quad (6.6b)$$

The SINR in (6.6b) is maximized if

$$\sqrt{1 + P_I |G_T(\omega)|^2} G_R(\omega) = \frac{\eta G_T(\omega)}{\sqrt{1 + P_I |G_T(\omega)|^2}} \quad (6.7)$$

or

$$G_R(\omega) = \frac{\eta G_T(\omega)}{1 + P_I |G_T(\omega)|^2} \quad (6.8)$$

where η is some constant. Thus, our problem reduces to finding $G_T(\omega)$ that maximizes the right side of (6.6b). For this purpose, we first rewrite the integral in (6.6b) as

$$\int_{-\mathcal{W}}^{\mathcal{W}} \frac{|G_T(\omega)|^2}{1 + P_I |G_T(\omega)|^2} d\omega = \int_{-\mathcal{W}}^{\mathcal{W}} \frac{1}{P_I} \left[1 - \frac{1}{1 + P_I |G_T(\omega)|^2} \right] d\omega. \quad (6.9)$$

Since P_I is constant, maximizing SINR is equivalent to minimizing

$$\int_{-\mathcal{W}}^{\mathcal{W}} \frac{1}{1 + P_I |G_T(\omega)|^2} d\omega. \quad (6.10)$$

This can be accomplished by recalling the Cauchy-Schwarz inequality for integrals as

$$\left(\frac{1}{2\pi} \int_{-\mathcal{W}}^{\mathcal{W}} d\omega \right)^2 \leq \frac{1}{2\pi} \int_{-\mathcal{W}}^{\mathcal{W}} \frac{1}{1 + P_I |G_T(\omega)|^2} d\omega \frac{1}{2\pi} \int_{-\mathcal{W}}^{\mathcal{W}} [1 + P_I |G_T(\omega)|^2] d\omega. \quad (6.11)$$

Since $g_T(t)$ has unit energy, the second integral on the right side of (6.11) is constant and equals $(1 + \beta + E_I)/T$ where E_I is the total interference energy per symbol. Thus, minimizing (6.10) is equivalent to minimizing the right side of (6.11) and this occurs if

$$\frac{1}{\sqrt{1 + P_I |G_T(\omega)|^2}} = \lambda \sqrt{1 + P_I |G_T(\omega)|^2} \quad (6.12)$$

where λ is some constant. Eq. (6.12) implies that $G_T(\omega)$ should have a flat spectrum over $[-\mathcal{W}, \mathcal{W}]$. Using this fact along with (6.3), one can obtain $G_T(\omega)$ as¹

$$G_T(\omega) = \begin{cases} \sqrt{\frac{T}{1+\beta}}, & -\mathcal{W} \leq \omega \leq \mathcal{W} \\ 0, & \text{otherwise.} \end{cases} \quad (6.13)$$

¹For simplicity of analysis we assume that $G_T(\omega)$ is a zero-phase filter, i.e., $g_T(t) = g_T(-t)$.

In this case, the SINR will be

$$\text{SINR} = \frac{A_0^2}{1 + \frac{E_I}{1+\beta}}. \quad (6.14)$$

A related result was derived in [4] for a direct-sequence CDMA system whose users have equal energy. However, [4] neither examines the SINR gain nor considers the case of imperfect timing recovery. The present work differs in that it examines bandlimited CCI systems (not CDMA system), and in that it considers the SINR gain that can be achieved over the conventional RC system and examines the conditions under which this gain can be maximized. As we will see in the sequel the SINR gain is maximized when the total interference energy approaches infinity. This cannot be concluded from the results in [4].

The SINR of a system whose transmitter and receiver filters each have a root RC spectrum is given by [67, Appendix B]

$$\text{SINR} = \frac{A_0^2}{1 + E_I(1 - \frac{\beta}{4})}. \quad (6.15)$$

It can be readily seen that for $\beta = 1$, the SINR of the optimal system is $A_0^2/(1 + E_I/2)$ whereas the SINR of the conventional system equals $A_0^2/(1 + 3E_I/4)$. Thus, the SINR gain of the optimal filter design over the conventional RC filter design is

$$\mathcal{G} = 1 + \frac{E_I}{2(2 + E_I)}. \quad (6.16)$$

It can be seen from (6.16) that the largest possible SINR gain is 1.5 (or equivalently 1.76 dB). This gain can be achieved only when $E_I \rightarrow \infty$. Numerical examples will be given in the next section to show the gains for finite values of E_I .

6.1.3 Numerical Results

The SINR gain of the optimal T-R filter design over the conventional root RC design as a function of the SNR and the SIR is depicted in Fig. 6.2. Observe that close to maximum SINR gain can be achieved when the SNR to SIR ratio or analogously E_I is large. Fig. 6.2 also shows the fact that the SINR gain is vanishing small only when the SIR is significantly large or when the SNR is very small, and in both cases, impractically so. For practical values of SIR and SNR, for example (SIR, SNR) = (5, 10) dB and (SIR, SNR) = (3, 12) dB the gain is 1.16 dB and 1.46 dB, respectively.

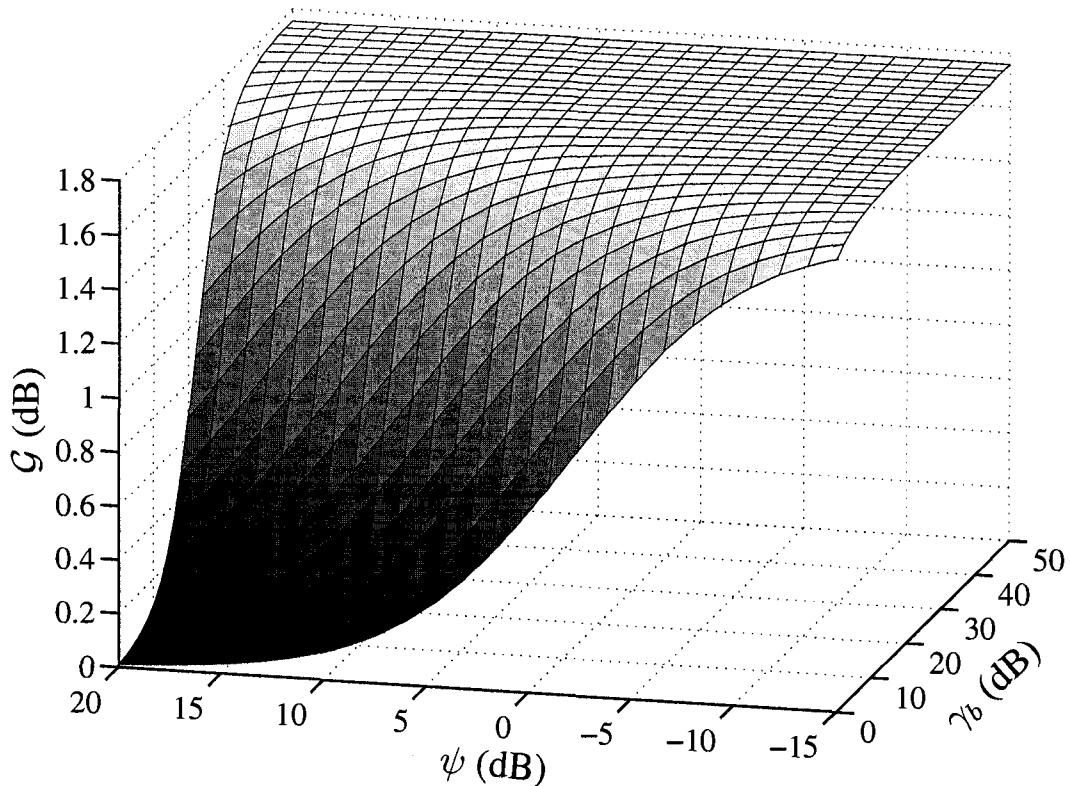


Figure 6.2. The SINR gain of the optimal T-R filter design over the conventional RC design as a function of γ_b and ψ .

A practical issue regarding the optimal T-R filter design is that for this system $g(t)$ is a sinc function whose decay rate is $1/t$ whereas the RC pulse decays as $1/t^3$ when $t \rightarrow \infty$ [1]. Thus, in the presence of timing recovery error the performance of the optimal system may degrade relative to the RC system due to the presence of larger ISI. To examine this issue, we have evaluated the BER performance of the optimal and the conventional systems in perfect and imperfect timing recovery cases. When timing recovery is imperfect, the timing error δ is modeled as a zero-mean Gaussian random variable with standard deviation $\sigma_\delta = 0.05T$ or $\sigma_\delta = 0.1T$. We have also assumed that $g(t)$ is time-limited to $[-6T, 6T]$ as is the case for practical systems [70, Sec. 6.6.2]. The results for SIR = 8 dB and $K = 8$ are shown in Fig. 6.3, where, recall, the SIR is defined in terms of the total interference power. Note that the optimal system substantially outperforms the conventional system even when the standard deviation of the jitter is as large as 5% of a symbol interval. The BER of the optimal system is

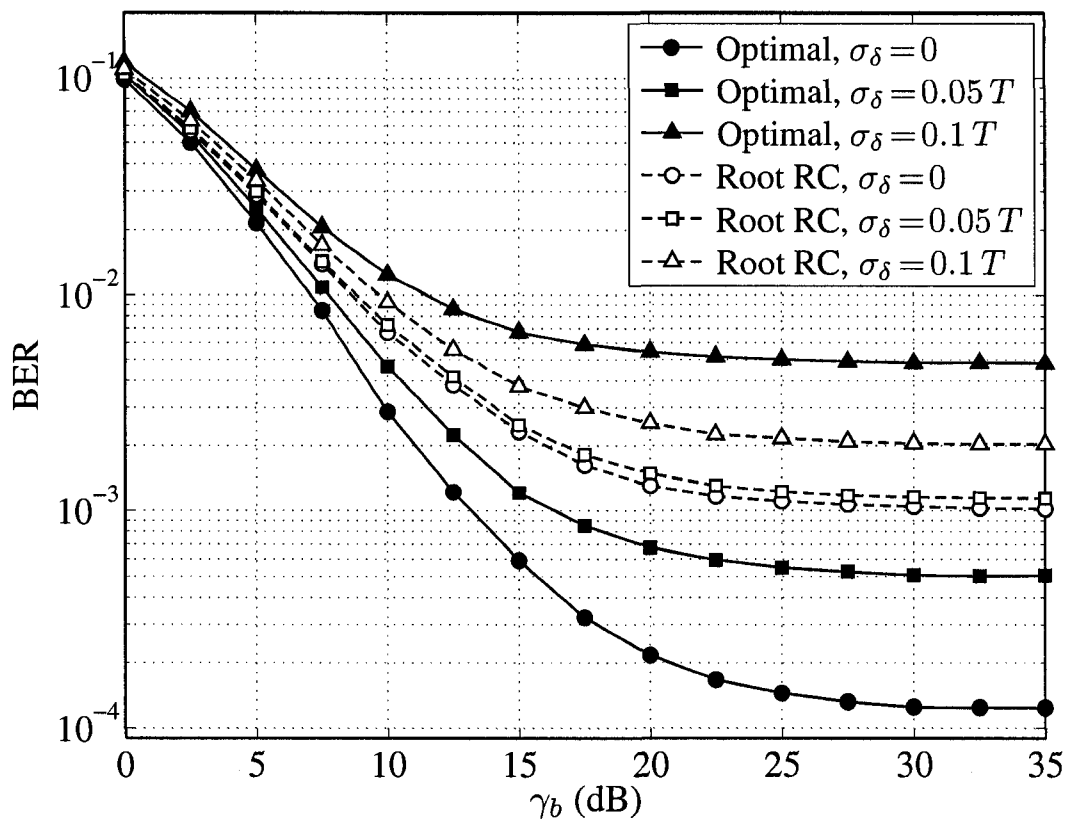


Figure 6.3. The BER versus SNR of the optimal T-R filter design and the conventional root RC design as a function of γ_b for perfect and imperfect timing recovery, SIR = 8 dB and $K = 8$.

inferior to that of the conventional system only when σ_δ is as large as $0.1T$. Expectedly, the conventional filter is more robust to timing recovery error than the optimal filter due to the fact that the time response of the former decays much faster than that of the latter as t increases. However, in receivers with good timing recovery, the optimal pulse-shaping design is superior.

6.2 ISI-Free Cochannel Interference Whitening for Bandlimited Systems

In Chapter 5 we observed that interference-plus-noise whitening is an effective means to mitigate CCI in multiaccess communication systems. Although the interference whitening filter suppresses the CCI, it may deteriorate the receiver's performance through

introducing ISI. To combat ISI, we modified the definition of the SINR to account for the ISI caused by the receiver filter. Then, we showed that the WMF receiver has to be used in conjunction with a discrete time filter in order for the SINR to be maximized.

Although, the SINRMF receiver derived in Section 5 can maximize the output SINR, it needs to know the instantaneous received energy, i.e., \mathcal{E}_0 for each symbol interval. Consequently, in fast time-varying channels the frequency response of the SINRMF receiver changes each time that the channel gain changes. Furthermore, in some environments an accurate estimate of the channel gain may not be available at the receiver. Thus, the SINRMF receiver may not be used for suppressing the ISI caused by the WMF.

Motivated by these facts, in this section we consider the problem of CCI mitigation in bandlimited micro-cellular systems using an ISI-free WMF receiver. For this purpose, we propose two methods in which the cascade of the transmitter and the receiver filters satisfies Nyquist's first criterion for zero ISI [1] while the SINR at the output of the receiver filter is maximized. Then, we analytically compare the SINR of the proposed methods with those of the CMF receiver and the interference whitening receiver in [4]. We derive exact expressions for the SINR of the ISI-free proposed receiver for the cases when the transmitter filter is chosen to have either a root RC [1] or a root BTD [59] spectrum. Note that the analysis presented in this section is different from the works that concurrently suppress CCI and ISI in multipath environments such as [71]. This is because in the latter work the ISI is caused by the multipath channel and is inevitable, whereas in the former the ISI is caused by the whitening filter and can be entirely removed by appropriate receiver design.

6.2.1 Signal Model and Whitening Filter

Consider a multiaccess communication system in which $(K + 1)$ users share an asynchronous channel. Using the system model in Section 5.1, the received signal sampled at $t = \ell T$ is given by

$$r_\ell = A_0\alpha_0 \sum_{i=-\infty}^{\infty} b_{0,i}g((\ell - i)T) + \sum_{k=1}^K A_k\alpha_k \cos \theta_k \sum_{i=-\infty}^{\infty} b_{k,i}g((\ell - i)T - \tau_k) + n_\ell \quad (6.17)$$

where the parameters of the signal model have been defined in Section 5.1. Throughout this section, we assume that $g_T(t)$ is even, i.e.,²

$$g_T(t) = g_T(-t) \quad (6.18a)$$

has unit energy, i.e.,

$$\int_{-\infty}^{\infty} g_T^2(t) dt = \frac{1}{2\pi} \int_{-\infty}^{\infty} G_T^2(\omega) d\omega = 1 \quad (6.18b)$$

and its energy spectrum satisfies Nyquist's first criterion [1], i.e.,

$$\sum_{n=-\infty}^{\infty} G_T^2\left(\omega - \frac{2\pi n}{T}\right) = T. \quad (6.18c)$$

Furthermore, we assume that $G_T(\omega)$ is bandlimited to $[-(1 + \beta)\pi/T, (1 + \beta)\pi/T]$, where $\beta \in [0, 1]$ denotes the filter's roll-off factor [1]. Assuming that the noise PSD equals unity, the average SNR per bit and the average SIR of the system at the input of the receiver are given by (5.5) and (5.6), respectively.

6.2.2 ISI-Free Transmitter-Receiver Design

The ISI introduced by the WMF receiver can dramatically diminish the output SINR and make its performance inferior to the CMF receiver. To address this issue, one can concurrently design the transmitter and the receiver filters to maximize the output SINR while the frequency response of the cascade of the two filters equals a given Nyquist spectrum, $X(\omega)$, i.e.,

$$X(\omega) = G_{T,k}(\omega)G_{R,k}(\omega) \quad (6.19)$$

where $G_{T,k}(\omega)$ and $G_{R,k}(\omega)$ denote the frequency response of the transmitter and the receiver filters for the k th user, respectively. As we observed in Section 6.1, the WMF receiver can achieve the ISI-free SINR gain over the CMF if $\beta = 1$, i.e., a 100% excess bandwidth is used, and the transmitter pulse has a flat spectrum across the entire available bandwidth. However, using the entire excess bandwidth may not be always possible due to practical limitations. Thus, we assume that $\beta < 1$ and derive the T-R filters under this general assumption.

²This implies that $G_T(\omega)$ is real and even.

The PSD of the noise-plus-interference term for the k th user is [4], [58]

$$S_k(\omega) = 1 + \sum_{\substack{\ell=0 \\ \ell \neq k}}^K P_\ell G_{T,\ell}^2(\omega) \quad (6.20)$$

where $P_\ell = A_\ell^2/2T$. It is shown in [72, Section 4.1.2] that the optimum transmitter and receiver filters that maximize the output SINR and their corresponding SINR are given by

$$G_{T,k}(\omega) = X^{\frac{1}{2}}(\omega) S_k^{\frac{1}{4}}(\omega) \quad (6.21)$$

$$G_{R,k}(\omega) = \frac{X^{\frac{1}{2}}(\omega)}{S_k^{\frac{1}{4}}(\omega)} \quad (6.22)$$

$$\Gamma = \frac{2\pi\mathcal{E}_0}{\int_{-\infty}^{\infty} G_{T,k}^2(\omega) d\omega} \quad (6.23)$$

provided that $G_{T,k}(\omega)$ has finite energy. Note that in this case, $G_{T,k}(\omega)$ is not fixed and, thus, it does not necessarily have the properties mentioned in Section 6.2.1. Replacing $S_k(\omega)$ in (6.21) with the expression given in (6.20) one can obtain after some manipulations

$$G_{T,k}^4(\omega) = X^2(\omega) \left[1 + \sum_{\substack{\ell=0 \\ \ell \neq k}}^K P_\ell G_{T,\ell}^2(\omega) \right], \quad \forall k. \quad (6.24)$$

Eq. (6.24) defines $(K + 1)$ polynomial equations that should be solved both at the transmitter and the receiver to obtain the transmitter filter for each user. The receiver filter can then be obtained using (6.19). For the special case when $P_k = \mathcal{P}$, $\forall k$, the transmitter and the receiver filters can be obtained as

$$G_{T,k}(\omega) = \sqrt{\frac{X(\omega)\Theta(\omega)}{2}} \quad (6.25)$$

$$G_{R,k}(\omega) = \sqrt{\frac{2X(\omega)}{\Theta(\omega)}} \quad (6.26)$$

respectively where

$$\Theta(\omega) \triangleq \frac{K\mathcal{P}}{X(\omega)} + \sqrt{4 + \frac{K^2\mathcal{P}^2}{X^2(\omega)}}. \quad (6.27)$$

Since in general the powers are not equal, finding the optimum filters can be computationally complicated, if not impossible, especially when K is large. Furthermore, the transmitted powers of all users should be also known at the transmitters which is not realistic in many practical cases.

6.2.3 ISI-Free SINR-Maximizing Receiver

The transmitter-receiver design method derived in Section 6.2.2 is practically prohibitive as it is rather involved and requires knowledge of transmitted powers both at the transmitter and the receiver sides. In this section, we derive the ISI-free SINRMF receiver based on the premise that the transmitter filter is fixed, and transfer the design problem into the receiver side.

The SINR of the ISI-free system is defined as

$$\text{SINR} = \frac{\mathcal{E}_0}{2\pi} \frac{[\int_{-\infty}^{\infty} G(\omega) d\omega]^2}{\int_{-\infty}^{\infty} \frac{1+P_{\mathcal{I}}G_{\mathcal{T}}^2(\omega)}{G_{\mathcal{T}}^2(\omega)} G^2(\omega) d\omega} \quad (6.28)$$

provided that $g(t)$ satisfies Nyquist's first criterion, i.e.,

$$\sum_{n=-\infty}^{\infty} G\left(\omega - \frac{2\pi n}{T}\right) = T. \quad (6.29)$$

Eq. (6.29) implies that the numerator of (6.28) is constant and, thus, maximizing SINR is equivalent to minimizing

$$\begin{aligned} \Lambda &= \int_{-\infty}^{\infty} \frac{[1 + P_{\mathcal{I}}G_{\mathcal{T}}^2(\omega)] G^2(\omega)}{G_{\mathcal{T}}^2(\omega)} d\omega \\ &= \sum_{n=-\infty}^{\infty} \int_{(2n-1)\frac{\pi}{T}}^{(2n+1)\frac{\pi}{T}} \frac{[1 + P_{\mathcal{I}}G_{\mathcal{T}}^2(\omega)] G^2(\omega)}{G_{\mathcal{T}}^2(\omega)} d\omega. \end{aligned} \quad (6.30)$$

By changing the variable ω to $(\omega + 2\pi n/T)$ and interchanging the integral and the summation in (6.30) we get

$$\Lambda = \int_{-\frac{\pi}{T}}^{\frac{\pi}{T}} \sum_{n=-\infty}^{\infty} \frac{[1 + P_{\mathcal{I}}G_{\mathcal{T}}^2(\omega + \frac{2\pi n}{T})] G^2(\omega + \frac{2\pi n}{T})}{G_{\mathcal{T}}^2(\omega + \frac{2\pi n}{T})} d\omega. \quad (6.31)$$

We can assume without loss of generality that $G(\omega) = G^{\mathcal{D}}(\omega)G^{\mathcal{C}}(\omega)$ where $G^{\mathcal{D}}(\omega)$ and $G^{\mathcal{C}}(\omega)$ are the discrete and continuous components of $G(\omega)$, respectively. Since $G^{\mathcal{D}}(\omega)$ is the Fourier transform of a discrete-time signal, it is periodic with period $2\pi/T$. Hence, using (6.29) one can readily see that

$$G^{\mathcal{D}}(\omega) = \frac{T}{\sum_{\ell=-\infty}^{\infty} G^{\mathcal{C}}(\omega + \frac{2\pi\ell}{T})} \quad (6.32)$$

and thus,

$$G(\omega) = \frac{TG^{\mathcal{C}}(\omega)}{\sum_{\ell=-\infty}^{\infty} G^{\mathcal{C}}(\omega + \frac{2\pi\ell}{T})}. \quad (6.33)$$

Replacing $G(\omega)$ from (6.33) in (6.31) results in

$$\Lambda = T^2 \int_{-\frac{\pi}{T}}^{\frac{\pi}{T}} \left[\sum_{n=-\infty}^{\infty} \frac{[1 + P_I G_T^2(\omega + \frac{2\pi n}{T})] [G^C(\omega + \frac{2\pi n}{T})]^2}{G_T^2(\omega + \frac{2\pi n}{T})} \right] \times \left[\frac{1}{\sum_{\ell=-\infty}^{\infty} G^C(\omega + \frac{2\pi \ell}{T})} \right]^2 d\omega. \quad (6.34)$$

Obviously, Λ is a functional of $G^C(\omega)$ and we need to find $G^C(\omega)$ that minimizes Λ . To this end, we find the derivative of Λ with respect to $G^C(\omega)$, i.e.,

$$\frac{\partial \Lambda}{\partial G^C(\omega)} = \frac{-2T^2}{\left[\sum_{\ell=-\infty}^{\infty} G^C(\omega + \frac{2\pi \ell}{T}) \right]^3} \left[\sum_{n=-\infty}^{\infty} \frac{[1 + P_I G_T^2(\omega + \frac{2\pi n}{T})] [G^C(\omega + \frac{2\pi n}{T})]^2}{G_T^2(\omega + \frac{2\pi n}{T})} - \frac{(1 + P_I G_T^2(\omega)) G^C(\omega)}{G_T^2(\omega)} \sum_{\ell=-\infty}^{\infty} G^C(\omega + \frac{2\pi \ell}{T}) \right]. \quad (6.35)$$

Since the first term on the right side of (6.35) can not be zero, setting $\partial \Lambda / \partial G^C(\omega)$ to zero is equivalent to setting the last expression on the right side of (6.35) to zero, i.e.,

$$\sum_{n=-\infty}^{\infty} \frac{[1 + P_I G_T^2(\omega + \frac{2\pi n}{T})] [G^C(\omega + \frac{2\pi n}{T})]^2}{G_T^2(\omega + \frac{2\pi n}{T})} = \frac{(1 + P_I G_T^2(\omega)) G^C(\omega)}{G_T^2(\omega)} \sum_{\ell=-\infty}^{\infty} G^C(\omega + \frac{2\pi \ell}{T}) \quad (6.36)$$

A thorough examination of (6.36) reveals that the expression on the left of this equation is periodic with period $2\pi/T$ while the expression on the right of (6.36) is not periodic. Thus, the first term on the right of (6.36) should be constant. This yields

$$G^C(\omega) = \frac{G_T^2(\omega)}{1 + P_I G_T^2(\omega)}. \quad (6.37)$$

Thus, $G(\omega)$ equals

$$G(\omega) = T \frac{G_T^2(\omega)}{1 + P_I G_T^2(\omega)} \sum_{n=-\infty}^{\infty} \frac{G_T^2(\omega + \frac{2\pi n}{T})}{1 + P_I G_T^2(\omega + \frac{2\pi n}{T})}. \quad (6.38)$$

By substituting $G^C(\omega)$ from (6.37) in (6.34), one can obtain Λ for the proposed receiver filter as

$$\Lambda_{\text{Prop}} = T^2 \int_{-\frac{\pi}{T}}^{\frac{\pi}{T}} \left[\sum_{n=-\infty}^{\infty} \frac{G_T^2(\omega + \frac{2\pi n}{T})}{1 + P_I G_T^2(\omega + \frac{2\pi n}{T})} \right]^{-1} d\omega. \quad (6.39)$$

Hence, the SINR is given by

$$\Gamma_{\text{Prop}} = \frac{2\pi\mathcal{E}_0}{T^2} \left\{ \int_{-\frac{\pi}{T}}^{\frac{\pi}{T}} \left[\sum_{n=-\infty}^{\infty} \frac{G_T^2(\omega + \frac{2\pi n}{T})}{1 + P_I G_T^2(\omega + \frac{2\pi n}{T})} \right]^{-1} d\omega \right\}^{-1}. \quad (6.40)$$

6.2.4 Optimum Transmitter Filter Design

The analysis given in Subsection 6.2.3 was based on the premise that $G_T(\omega)$ has an arbitrary, but fixed, spectrum. Thus, the SINR of the proposed receiver depends on $G_T(\omega)$. In this subsection, we find the transmitter filter that maximizes the SINR given in (6.40). Note that the analysis in this section is different from the analysis given in Subsection 6.2.2 as in the latter the transmitter and receiver filters are designed concurrently while in the former the transmitter and receiver filters that maximize the SINR are derived individually.

In order to maximize the SINR, we use variational calculus to find the transmitter filter that minimizes the integral term in (6.40) provided that the energy constraint given in (6.18b) is satisfied. Thus, the unconstrained functional of $G_T(\omega)$ to be minimized is given by

$$\Psi(G_T(\nu)) = \int_{-\frac{\pi}{T}}^{\frac{\pi}{T}} \left[\sum_{n=-\infty}^{\infty} \frac{G_T^2(\nu + \frac{2\pi n}{T})}{1 + P_I G_T^2(\nu + \frac{2\pi n}{T})} \right]^{-1} d\nu + \lambda \int_{-\infty}^{\infty} G_T^2(\nu) d\nu \quad (6.41)$$

where λ is a nonzero multiplier whose value will be determined in the sequel. Taking the derivative of $\Psi(G_T(\nu))$ with respect to $G_T(\omega)$ yields

$$\frac{\partial \Psi}{\partial G_T(\omega)} = \frac{-2G_T(\omega)}{[1 + P_I G_T^2(\omega)]^2 \left[\sum_{n=-\infty}^{\infty} \frac{G_T^2(\omega + \frac{2\pi n}{T})}{1 + P_I G_T^2(\omega + \frac{2\pi n}{T})} \right]^2} + 2\lambda G_T(\omega). \quad (6.42)$$

Setting $\partial \Psi / \partial G_T(\omega)$ equal to zero and using the facts that $G_T(\omega) \neq 0$, $\forall \omega \in [-(1 + \beta)\pi/T, (1 + \beta)\pi/T]$, and the expressions inside brackets on the right of (6.42) are both positive, one can obtain

$$\frac{1}{[1 + P_I G_T^2(\omega)]^2} = \lambda \left[\sum_{n=-\infty}^{\infty} \frac{G_T^2(\omega + \frac{2\pi n}{T})}{1 + P_I G_T^2(\omega + \frac{2\pi n}{T})} \right]^2. \quad (6.43)$$

It can be readily seen from (6.43) that λ should be a positive number. Since $G_T^2(\omega)$ satisfies Nyquist's first criterion the summation on the right of (6.43) has only one term

in the $[0, (1 - \beta)\pi/T]$ frequency band. Thus, for this frequency range

$$\frac{\frac{1}{\sqrt{\lambda}} - G_T^2(\omega)}{1 + P_I G_T^2(\omega)} = 0 \quad (6.44)$$

or analogously

$$G_T(\omega) = \frac{1}{\sqrt[4]{\lambda}}. \quad (6.45)$$

For the same reason, the summation on the right of (6.43) has only two terms in the $[(1 - \beta)\pi/T, (1 + \beta)\pi/T]$ frequency range. Thus, for this range $G_T(\omega)$ should satisfy

$$\frac{1}{\sqrt{\lambda}[1 + P_I G_T^2(\omega)]} = \frac{G_T^2(\omega - \frac{2\pi}{T})}{1 + P_I G_T^2(\omega - \frac{2\pi}{T})} + \frac{G_T^2(\omega)}{1 + P_I G_T^2(\omega)}. \quad (6.46)$$

Assume now that $\varphi(\omega)$ is defined as

$$\varphi(\omega) \triangleq \begin{cases} G_T(\omega + \frac{\pi}{T}), & -\frac{\beta\pi}{T} \leq \omega \leq \frac{\beta\pi}{T} \\ 0, & \text{otherwise.} \end{cases} \quad (6.47)$$

By changing ω to $\omega + \pi/T$ in (6.46) and using the fact that $G_T(\omega)$ is an even function, we obtain

$$\frac{1}{\sqrt{\lambda}[1 + P_I \varphi^2(\omega)]} = \frac{\varphi^2(-\omega)}{1 + P_I \varphi^2(-\omega)} + \frac{\varphi^2(\omega)}{1 + P_I \varphi^2(\omega)}. \quad (6.48)$$

A closer look at (6.48) reveals that negating ω in this equation does not change the expression on its right side. Therefore, $\varphi(\omega)$ is an even function. Replacing $\varphi(-\omega)$ with $\varphi(\omega)$ in (6.48) one can easily see that $\varphi^2(\omega) = 1/2\sqrt{\lambda}$. Hence, in the $[(1 - \beta)\pi/T, (1 + \beta)\pi/T]$ frequency range, $G_T(\omega)$ is given by

$$G_T(\omega) = \frac{1}{\sqrt[4]{4\lambda}}. \quad (6.49)$$

Recalling that $G_T(\omega)$ has unit energy, it can be readily shown that $\lambda = T^{-2}$. Using (6.45) and (6.49) along with the fact that $G_T(\omega)$ is an even function, we obtain

$$G_T(\omega) = \begin{cases} \sqrt{T}, & |\omega| \leq \frac{\pi(1-\beta)}{T} \\ \sqrt{\frac{T}{2}}, & \frac{\pi(1-\beta)}{T} \leq |\omega| \leq \frac{\pi(1+\beta)}{T} \\ 0, & \frac{\pi(1+\beta)}{T} \leq |\omega|. \end{cases} \quad (6.50)$$

Using (6.40), the output SINR is given by

$$\Gamma_{\text{Prop}}^{\text{Opt}} = \frac{\mathcal{E}_0}{1 + E_I(1 - \frac{\beta}{2})}. \quad (6.51)$$

Since α_0 has unit energy, the average SINR in this case can be obtained by replacing \mathcal{E}_0 with A_0^2 in (6.51).

Comparing $\Gamma_{\text{Prop}}^{\text{Opt}}$ with that of the CMF receiver with a root RC pulse, one can see that the proposed receiver with an optimum transmitter filter can achieve a gain of

$$\frac{1 + E_{\mathcal{I}}(1 - \frac{\beta}{4})}{1 + E_{\mathcal{I}}(1 - \frac{\beta}{2})} \quad (6.52)$$

over the CMF receiver. In this case, the maximum gain is $1 + \beta/(4 - 2\beta)$ and is achieved when $E_{\mathcal{I}} \rightarrow \infty$.

The optimum transmitter filter can be also derived for the SINRMF receiver using the above procedure and the objective function

$$\Psi(G_T(\nu)) = \int_{-\frac{\pi}{T}}^{\frac{\pi}{T}} \left[1 + \frac{\mathcal{E}_0}{T} \sum_{n=-\infty}^{\infty} \frac{G_T^2(\nu + \frac{2\pi n}{T})}{1 + P_{\mathcal{I}}G_T^2(\nu + \frac{2\pi n}{T})} \right]^{-1} d\nu + \lambda \int_{-\infty}^{\infty} G_T^2(\nu) d\nu. \quad (6.53)$$

In this case, the optimum transmitter filter that minimizes (6.53), can be obtained after some algebraic manipulations as

$$G_T(\omega) = \begin{cases} \sqrt{\frac{T(2\mathcal{E}_0 + E_{\mathcal{I}})}{2\mathcal{E}_0 + E_{\mathcal{I}}(1 + \beta)}}, & |\omega| \leq \frac{\pi(1 - \beta)}{T} \\ \sqrt{\frac{T(\mathcal{E}_0 + E_{\mathcal{I}})}{2\mathcal{E}_0 + E_{\mathcal{I}}(1 + \beta)}}, & \frac{\pi(1 - \beta)}{T} \leq |\omega| \leq \frac{\pi(1 + \beta)}{T} \\ 0, & \frac{\pi(1 + \beta)}{T} \leq |\omega|. \end{cases} \quad (6.54)$$

With this transmitter filter the SINR of the SINRMF receiver will be

$$\Gamma_{\text{SINRMF}}^{\text{Opt}} = \frac{\mathcal{E}_0 [2\mathcal{E}_0 + E_{\mathcal{I}}(1 + \beta)]}{2\mathcal{E}_0 + E_{\mathcal{I}}(1 + \beta + E_{\mathcal{I}} + 2\mathcal{E}_0) - \beta\mathcal{E}_0 E_{\mathcal{I}}}. \quad (6.55)$$

Averaging $\Gamma_{\text{SINRMF}}^{\text{Opt}}$ over the distribution of \mathcal{E}_0 , we obtain

$$\bar{\Gamma}_{\text{SINRMF}}^{\text{Opt}} = \frac{\exp(\delta)}{2 + E_{\mathcal{I}}(2 - \beta)} [mE_{\mathcal{I}}(1 + \beta)\mathcal{E}_{1+m}(\delta) + 2(1 + m)A_0^2\mathcal{E}_{2+m}(\delta)] \quad (6.56a)$$

where

$$\delta = \frac{mE_{\mathcal{I}}(1 + \beta + E_{\mathcal{I}})}{A_0^2 [2 + E_{\mathcal{I}}(2 - \beta)]} \quad (6.56b)$$

and $\mathcal{E}_{\nu}(\cdot)$ is given by (5.26b).

6.2.5 SINR Analysis

In this section we compare the SINR of the ISI-free proposed receiver with that of the CMF, ISI-free WMF and the SINRMF filter derived in Section 5.3. Then, the SINR of the proposed receiver is evaluated for the RC and BTB pulses.

6.2.5.1 SINR Comparison

The SINR expression given in (6.40) does not provide any insight as to whether the proposed filter is superior to the CMF in having larger SINR or not. Furthermore, comparing the SINR of the proposed receiver with that of the SINRMF receiver might be of particular interest. We first show that Γ_{Prop} is greater than Γ_{CMF} . To this end, we use the Cauchy-Schwarz inequality [41]

$$\left(\sum_{n=-\infty}^{\infty} \zeta_n \eta_n \right)^2 \leq \left(\sum_{n=-\infty}^{\infty} \zeta_n^2 \right) \left(\sum_{n=-\infty}^{\infty} \eta_n^2 \right) \quad (6.57)$$

with $\zeta_n = G_T^2(\omega + 2\pi n/T) [1 + P_I G_T^2(\omega + 2\pi n/T)]$ and $\eta_n = G_T^2(\omega + 2\pi n/T) / [1 + P_I G_T^2(\omega + 2\pi n/T)]$ to obtain

$$\left[\sum_{n=-\infty}^{\infty} G_T^2\left(\omega + \frac{2\pi n}{T}\right) \right]^2 \leq \sum_{n=-\infty}^{\infty} G_T^2\left(\omega + \frac{2\pi n}{T}\right) \left[1 + P_I G_T^2\left(\omega + \frac{2\pi n}{T}\right) \right] \times \sum_{n=-\infty}^{\infty} \frac{G_T^2\left(\omega + \frac{2\pi n}{T}\right)}{1 + P_I G_T^2\left(\omega + \frac{2\pi n}{T}\right)}. \quad (6.58)$$

Since $G_T^2(\omega)$ satisfies Nyquist's first criterion, i.e., eq. (6.18c), the expression on the left of (6.58) equals T^2 . Thus, (6.58) can be written as

$$\int_{-\frac{\pi}{T}}^{\frac{\pi}{T}} \left[\sum_{n=-\infty}^{\infty} \frac{G_T^2\left(\omega + \frac{2\pi n}{T}\right)}{1 + P_I G_T^2\left(\omega + \frac{2\pi n}{T}\right)} \right]^{-1} d\omega \leq \frac{1}{T^2} \int_{-\frac{\pi}{T}}^{\frac{\pi}{T}} \sum_{n=-\infty}^{\infty} G_T^2\left(\omega + \frac{2\pi n}{T}\right) \left[1 + P_I G_T^2\left(\omega + \frac{2\pi n}{T}\right) \right] d\omega \quad (6.59)$$

Dividing both sides of (6.59) by $T^2/2\pi\mathcal{E}_0$ and changing the variable ω to $\omega - 2\pi n/T$ results in

$$\begin{aligned} \frac{1}{\Gamma_{\text{Prop}}} &\leq \frac{1}{2\pi\mathcal{E}_0} \sum_{n=-\infty}^{\infty} \int_{(2n-1)\frac{\pi}{T}}^{(2n+1)\frac{\pi}{T}} G_T^2(\omega) [1 + P_I G_T^2(\omega)] d\omega \\ &= \frac{1}{\mathcal{E}_0} \left[1 + \frac{P_I}{2\pi} \int_{-\infty}^{\infty} G_T^4(\omega) d\omega \right] \end{aligned} \quad (6.60)$$

where the last equation follows from the fact that $g_T(t)$ has unit energy. Using (5.22), one can see

$$\Gamma_{\text{CMF}} \leq \Gamma_{\text{Prop}}. \quad (6.61)$$

We now show that Γ_{Prop} is upper-bounded by Γ_{SINRMF} (defined in (5.40)). For this purpose, we first define $\mathcal{H}(\omega)$ as

$$\mathcal{H}(\omega) \triangleq \frac{\mathcal{E}_0}{T} \sum_{n=-\infty}^{\infty} \frac{G_T^2(\omega + \frac{2\pi n}{T})}{1 + P_I G_T^2(\omega + \frac{2\pi n}{T})}. \quad (6.62)$$

Using Cauchy-Schwarz inequality for integrals [41], one can see

$$\begin{aligned} 1 &\leq \left[\frac{T}{2\pi} \int_{-\frac{\pi}{T}}^{\frac{\pi}{T}} \frac{\mathcal{H}(\omega)}{1 + \mathcal{H}(\omega)} d\omega \right] \left[\frac{T}{2\pi} \int_{-\frac{\pi}{T}}^{\frac{\pi}{T}} \left(1 + \frac{1}{\mathcal{H}(\omega)} \right) d\omega \right] \\ &= (1 - \Lambda_{\text{SINRMF}}) \left[1 + \frac{T}{2\pi} \int_{-\frac{\pi}{T}}^{\frac{\pi}{T}} \frac{1}{\mathcal{H}(\omega)} d\omega \right] \end{aligned} \quad (6.63)$$

After rearranging, (6.63) can be simplified to

$$\frac{T}{2\pi} \int_{-\frac{\pi}{T}}^{\frac{\pi}{T}} \frac{1}{\mathcal{H}(\omega)} d\omega \leq \frac{1 - \Lambda_{\text{SINRMF}}}{\Lambda_{\text{SINRMF}}} \quad (6.64)$$

or analogously

$$\Gamma_{\text{Prop}} \leq \Gamma_{\text{SINRMF}}. \quad (6.65)$$

Recalling that Γ_{SINRMF} is upper-bounded by the SINR of the ISI-free WMF receiver, i.e., $\Gamma_{\text{ISI-free}}$, it is clear that $\Gamma_{\text{Prop}} \leq \Gamma_{\text{ISI-free}}$.

6.2.5.2 SINR Evaluation for the RC and BTB Pulses

In this section, we find exact expressions for the SINR of the proposed receiver for the cases when $|G_T(\omega)|^2$ has either a RC [1] or a BTB spectrum [59]. Since both pulses are bandlimited to $[-(1 + \beta)\pi/T, (1 + \beta)\pi/T]$ and the integration in (6.40) is over $[-\pi/T, \pi/T]$, only three terms (corresponding to $n = -1, 0$ and 1) in the summation on the right of (6.40) contribute to the integral in this equation. Thus, for the RC pulse eq. (6.40) becomes

$$\Gamma_{\text{Prop}}^{\text{RC}} = \frac{2\pi\mathcal{E}_0}{T^2} \left\{ \int_{-\frac{\pi}{T}}^{\frac{\pi}{T}} \left[\frac{X_{\text{RC}}(\omega - \frac{2\pi}{T})}{1 + P_I X_{\text{RC}}(\omega - \frac{2\pi}{T})} + \frac{X_{\text{RC}}(\omega)}{1 + P_I X_{\text{RC}}(\omega)} + \frac{X_{\text{RC}}(\omega + \frac{2\pi}{T})}{1 + P_I X_{\text{RC}}(\omega + \frac{2\pi}{T})} \right]^{-1} d\omega \right\}^{-1}. \quad (6.66)$$

where, recall, $X_{\text{RC}}(\omega)$ denotes the Fourier transform of a RC pulse given by (5.46). By substituting $X_{\text{RC}}(\omega)$ from (5.46) into (6.66), one can obtain after some algebraic

manipulations

$$\begin{aligned}\Gamma_{\text{Prop}}^{\text{RC}} &= \mathcal{E}_0 \left[2T \int_0^{\frac{1-\beta}{2T}} (1 + E_I) dx \right. \\ &\quad \left. + \frac{2\beta}{\pi} \int_0^{\frac{\pi}{2}} \left(\frac{1 + \cos x}{2 + E_I(1 + \cos x)} + \frac{1 - \cos x}{2 + E_I(1 - \cos x)} \right) dx \right]^{-1} \\ &= \frac{2\mathcal{E}_0}{2 + E_I(2 - \beta) + (\sqrt{4 + 2E_I} - 2)\beta}\end{aligned}\quad (6.67)$$

where E_I is the total interference energy. Averaging $\Gamma_{\text{Prop}}^{\text{RC}}$ over the distribution of \mathcal{E}_0 and rearranging results in

$$\bar{\Gamma}_{\text{Prop}}^{\text{RC}} = \frac{A_0^2}{1 + E_I + \beta \left(\sqrt{1 + E_I/2} - 1 - E_I/2 \right)}.\quad (6.68)$$

Similarly, the average SINR of the ISI-free proposed filter for the BTD pulse can be obtained as

$$\bar{\Gamma}_{\text{Prop}}^{\text{BTD}} = A_0^2 \left\{ 1 + E_I + \frac{\beta}{4} \log_2 \left[\frac{(1 + E_I/2)^{2+E_I}}{\left(1 + E_I + \sqrt{E_I(2 + E_I)}\right) \sqrt{E_I(2+E_I)}} \right] \right\}^{-1}.\quad (6.69)$$

In this case, the ASINR for both pulses is the same and is given by

$$\begin{aligned}\bar{\Upsilon}_{\text{Prop}}^{\text{RC}} &= \bar{\Upsilon}_{\text{Prop}}^{\text{BTD}} \\ &= \frac{4\psi}{2 - \beta}.\end{aligned}\quad (6.70)$$

6.2.6 Numerical Results

The SINR gain of the proposed, ISI-free WMF and ISI-impaired WMF receivers over the CMF receiver has been numerically evaluated for several different scenarios and asynchronous CCI. Similar to Chapter 5, we have considered two values of m , $m = 0.5$ and $m = \infty$ corresponding to severe fading and no fading, respectively.

The SINR gain over the CMF of the ISI-free and ISI-impaired WMF receivers as well as the proposed receiver as a function of SIR is illustrated in Fig. 6.4. The SNR is assumed to be 10 dB and β equals 0.35. When the SIR is large, no SINR gain over the CMF can be achieved by any of the receivers even by the ISI-free WMF receiver. This is because, when SIR is large, i.e., interference power is very small, both the WMF and the

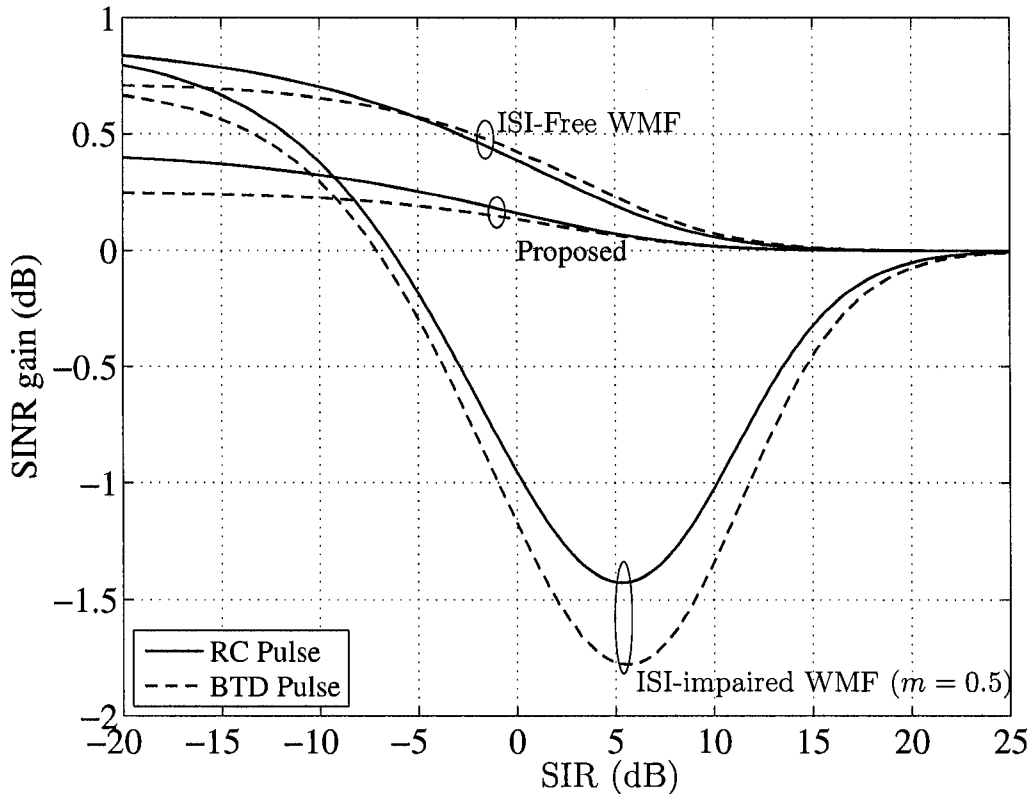


Figure 6.4. The effect of SIR on the SINR gain over the CMF receiver for RC and BTD pulses in asynchronous CCI and Nakagami- m fading, for SNR = 10 dB and $\beta = 0.35$.

proposed receivers approach the CMF. Thus, their SINR is the same as that of the CMF receiver. When the SIR is impractically small, the ISI-impaired WMF can achieve some SINR gain over the CMF even for severe fading. To explain this, we note that in the latter case $\hat{E}_g \mathcal{E}_0$ is much smaller than σ_T^2 in (5.14). Thus, the SINR of the ISI-impaired WMF approaches that of the ISI-free WMF receiver which, in turn, is superior to the CMF in having larger SINR. Also observe that the SINR of the proposed receiver is superior to that of the CMF receiver for all values of the examined SIR.

Fig. 6.5 shows the SINR gain over the CMF as a function of SNR for the case when $\beta = 0.35$ and $m = \infty$, i.e., there is no fading for the desired signal. Both the RC and BTD pulses have been considered. As observed in Section 5, the ISI-impaired WMF receiver has smaller SINR than the CMF receiver for both pulses and, thus, ISI reduces the SINR

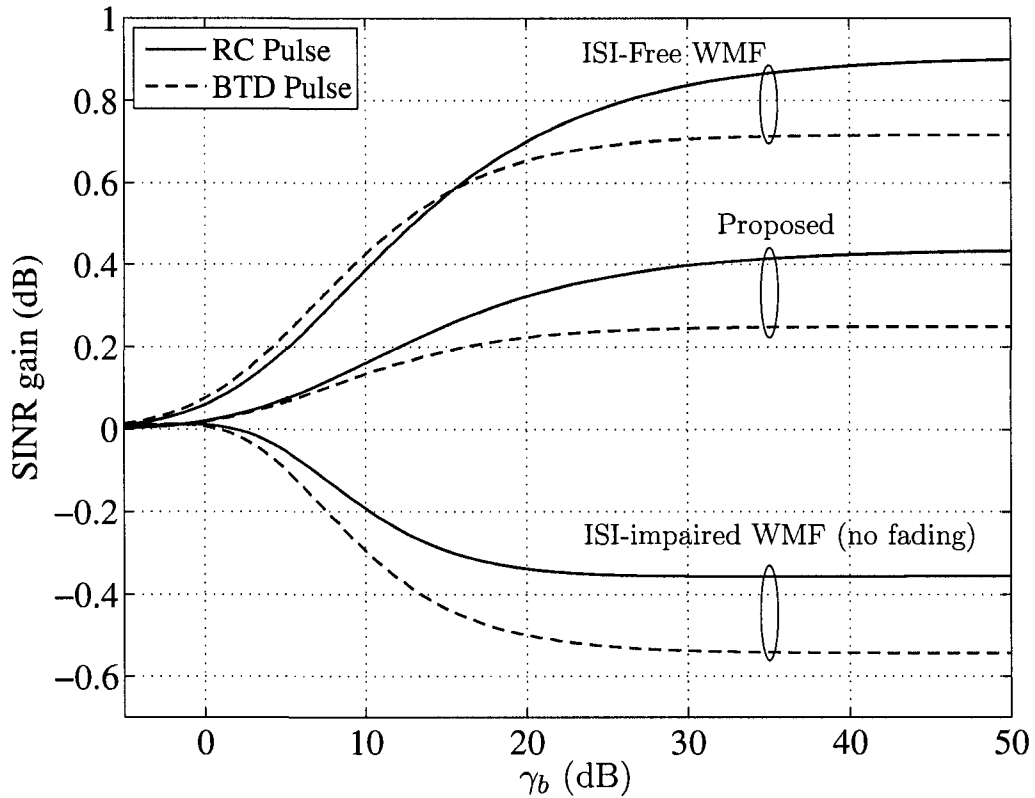


Figure 6.5. The SINR gain over the CMF receiver as a function of SNR for RC and BTD pulses in asynchronous CCI and Nakagami- m fading, with $\beta = 0.35$ and SIR = 0 dB.

of the WMF receiver with respect to the CMF receiver. This is significant because there is no fading for the desired user. The proposed receiver, however, is superior to the CMF receiver for all examined values of SNR. For vanishing small background noise, i.e., $\text{SNR} \rightarrow \infty$, the SINR of the proposed receiver is approximately 0.5 dB less than that of the ISI-free WMF both for the RC and the BTD pulses. This is because the proposed receiver enhances the CCI power even though it entirely removes the ISI component from the received signal.

The SINR gain over the CMF as a function of β is depicted in Fig. 6.6. The SNR and SIR are assumed to be 10 dB and 0 dB, respectively. Although, the SINR gain for the ISI-free WMF is a monotonically increasing function of β , it has some minimum value for the ISI-impaired receiver. For $m = 0.5$ and ∞ the minima occur at $\beta = 0.42$

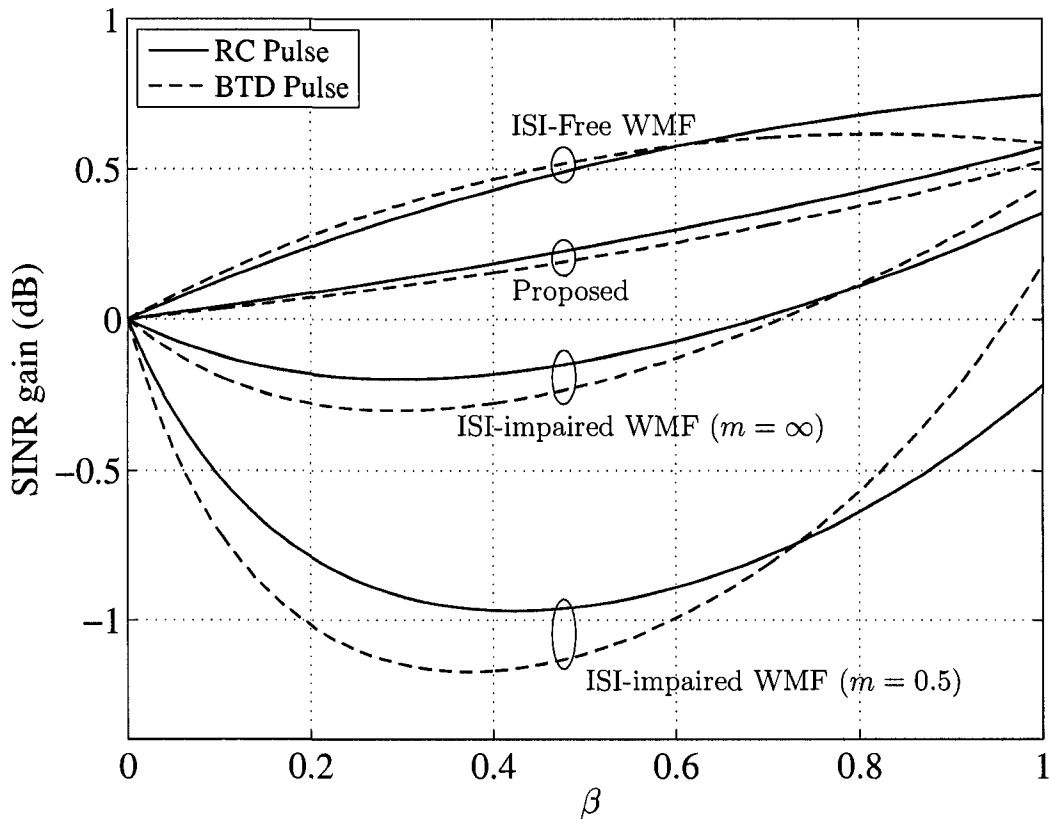


Figure 6.6. The effect of roll-off factor on the SINR gain over the CMF receiver for RC and BTD pulses in asynchronous CCI and Nakagami- m fading, for SNR = 10 dB and SIR = 0 dB.

and 0.3 for the RC pulse and at $\beta = 0.37$ and 0.29 for the BTD pulse, respectively. Furthermore, in the presence of the ISI and severe fading (i.e., $m = 0.5$), a slight SINR gain can be achieved only when $\beta > 0.96$ for the BTD pulse. When there is no fading a SINR gain can be achieved only when $\beta > 0.69$ for the RC pulse and $\beta > 0.71$ for the BTD pulse. Furthermore, the larger the roll-off factor the larger SINR gain can be achieved by the ISI-free WMF and the proposed receiver.

Fig. 6.7 shows the ASINR gain of the ISI-free WMF, the SINRMF and the proposed receivers over the CMF receiver as a function of the roll-off factor. The SIR equals 10 dB and the channel is Nakagami- m fading with $m = 0.5$. Both the RC and BTD pulses have been considered. For both pulses the ASINR gain of the proposed receiver is very close to that of the SINRMF receiver and for most values of β the difference between the ASINR gains is less than 0.1 dB. Using (5.65) one can show that for large SIR values the

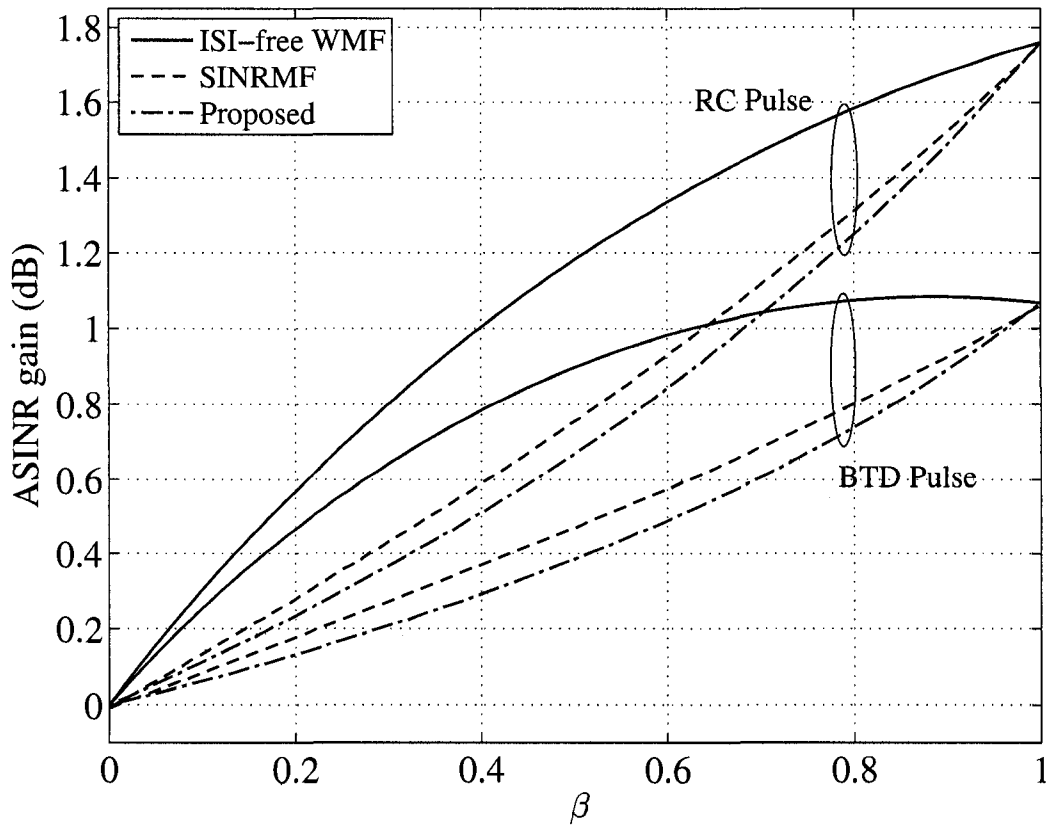


Figure 6.7. The ASINR gain of the ISI-free WMF, SINRMF and proposed receivers over the CMF receiver for RC and BTD pulses in asynchronous CCI and Nakagami- m fading ($m = 0.5$), for SIR = 0 dB.

ASINR of the SINRMF receiver approaches $4\psi/(2 - \beta)$, i.e., the ASINR of the proposed receiver. Using eqs. (5.52) with (6.70) one can readily obtain the ASINR gain of the ISI-free WMF receiver over the ASINR of the proposed receiver as

$$10 \log_{10} \left(\frac{(2 - \beta)(1 + \beta)}{2} \right). \quad (6.71)$$

This gain has a maximum of 0.5115 dB at $\beta = 0.5$ as seen in Fig. 6.7.

The SINR gain achieved by the proposed receiver with an optimum transmitter filter over a CMF receiver with a root RC is depicted in Fig. 6.8. The channel is Nakagami- m fading with $m = 0.5$ and the roll-off factor is 0.35. When the $E_I \gg 1$, the proposed receiver with the optimum transmitter filter can achieve the maximum possible SINR

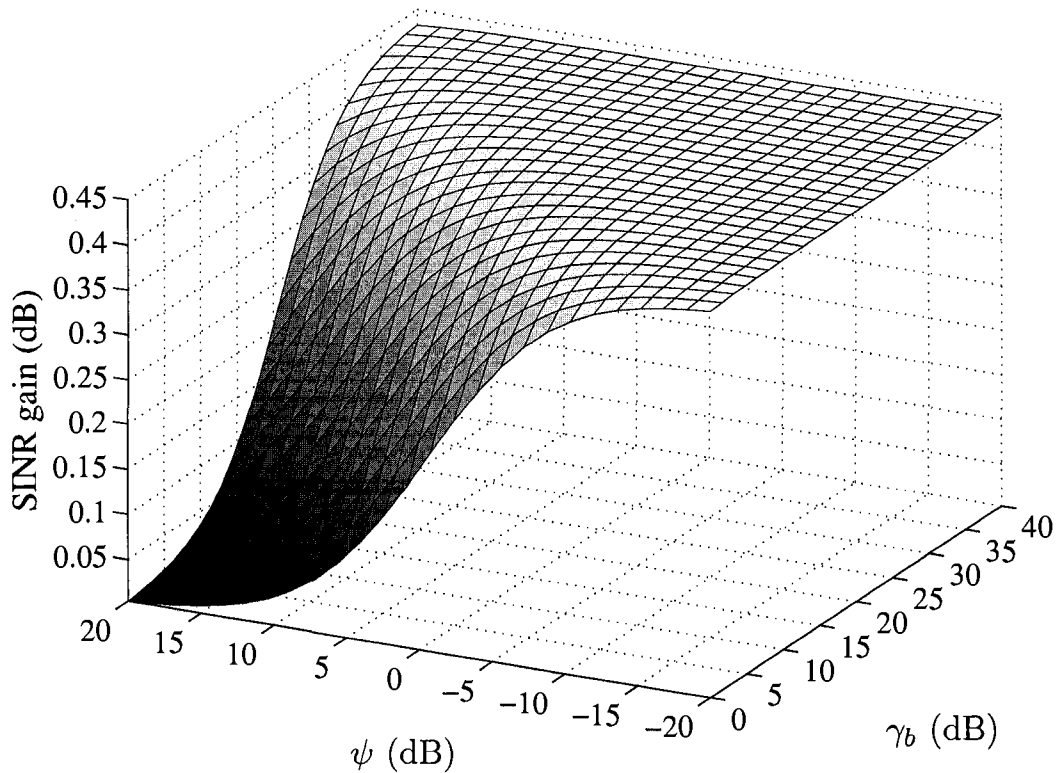


Figure 6.8. The SINR gain achieved by the proposed receiver with an optimum transmitter filter over the CMF receiver with a root RC filter for Nakagami- m fading ($m = 0.5$), asynchronous CCI and $\beta = 0.35$.

gain, i.e.,

$$10 \log_{10} \left(\frac{4 - \beta}{4 - 2\beta} \right) \Big|_{\beta=0.35} = 0.44 \text{ dB} \quad (6.72)$$

over the CMF receiver. Note that the SINR gain achieved by the proposed receiver in this case has a similar pattern to that of the optimal T-R design depicted in Fig. 6.2. However, our proposed T-R design does not need to utilize a pulse with 100% excess bandwidth.

Fig. 6.9 illustrates the SINR gain of a system employing an optimum transmitter filter (eq. (6.54)) over a system using a root RC pulse at the transmitter side, when both systems use a SINRMF receiver. The channel is the same as that of Fig. 6.8 and the excess bandwidth is 100%. As seen in the figure, the optimum transmitter filter can increase the output SINR of the system by up to 1 dB. The gain is negligible when the SNR \gg SIR. Note that both systems use the same receiver and have the same

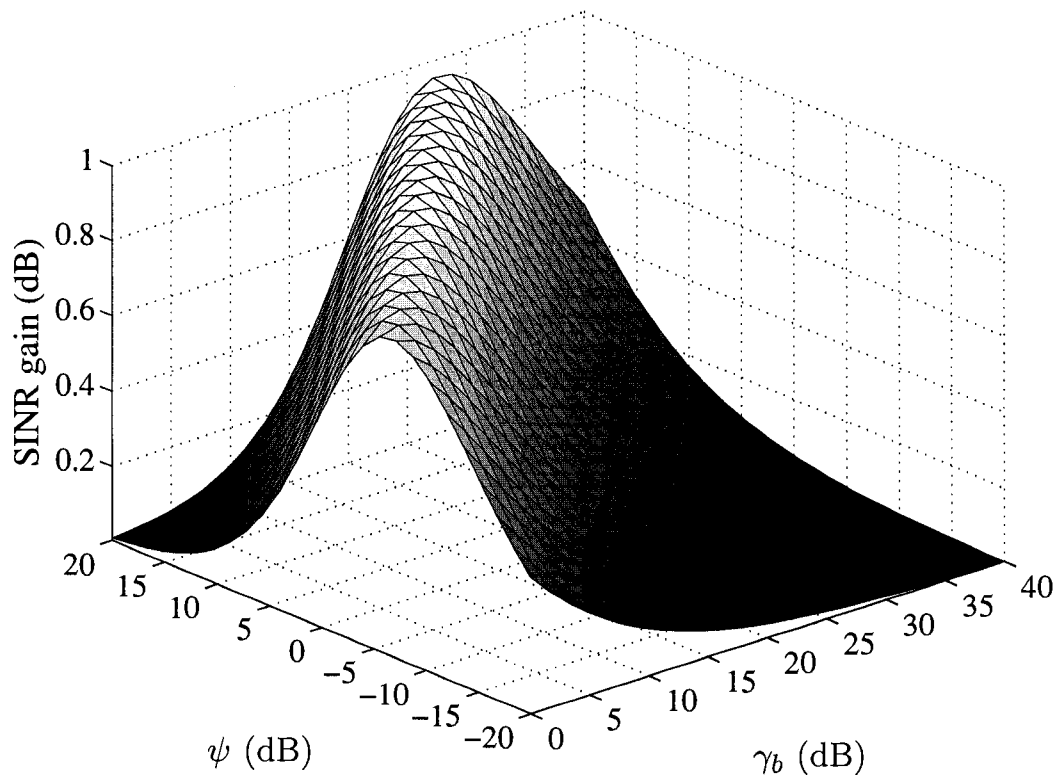


Figure 6.9. The SINR gain achieved by the SINRMF receiver with an optimum transmitter filter over the SINRMF receiver with a root RC filter for Nakagami- m fading ($m = 0.5$), asynchronous CCI and $\beta = 1$.

amount of complexity. In other words, the SINR gain is achieved without increasing the computational complexity. Fig. 6.9 also shows that the maximum SINR gain is achieved when the ratio of SIR and SNR is neither too large nor too small.

Fig. 6.10 shows the SINR gain of a system employing an optimum transmitter filter (eq. (6.50)) and the proposed receiver, over a system using a root RC filter along with the proposed receiver. The SNR is assumed to be 10 dB and the channel is Nakagami- m fading with $m = 0.5$. For all examined values of the SIR, the maximum gain is achieved when $\beta = 1$. Furthermore, the SINR gain decreases when the SIR is significantly larger or smaller than the SNR, i.e., when $P_{\mathcal{I}} \gg 1$ or $P_{\mathcal{I}} \ll 1$, respectively. To explain this we note that the SINR of the proposed receiver (eq. (6.40)) is approximately constant and independent of the transmitter pulse-shaping when $P_{\mathcal{I}}$ is very large or very small.

The SINR gain of the SINRMF receiver over the proposed receiver when the receivers

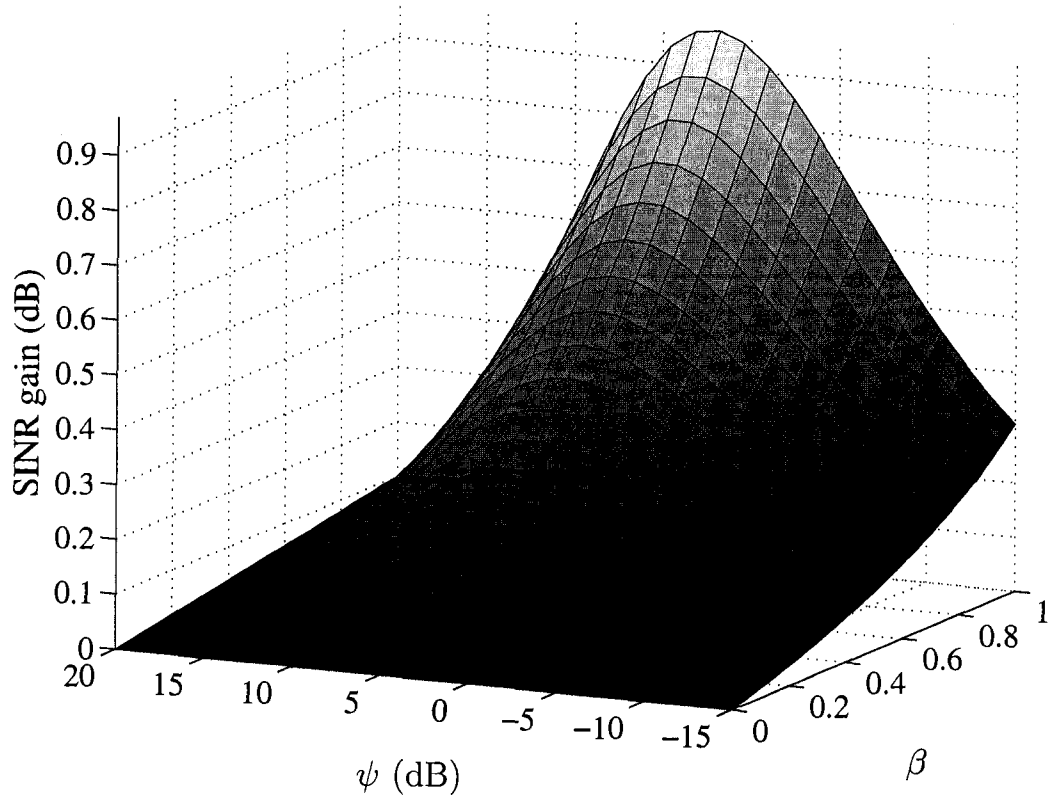


Figure 6.10. The SINR gain achieved by the proposed receiver with an optimum transmitter filter over the proposed receiver with a root RC filter for Nakagami- m fading ($m = 0.5$), asynchronous CCI and SNR = 10 dB.

are used with their corresponding optimum transmitter filters is illustrated in Fig. 6.11. The channel is again Nakagami- m with $m = 0.5$ and the excess bandwidth is 35%. As seen in Fig. 6.11, the maximum SINR gain is approximately 0.47 dB which is achieved when the SIR is small or when the SNR is large, i.e., when $\mathcal{E}_0 \ll E_{\mathcal{I}}$. This is because when $\mathcal{E}_0 \gg E_{\mathcal{I}}$, the SINRMF receiver and its corresponding optimum transmitter filter, i.e., eq. (6.54) are essentially the same as the proposed receiver filter and its corresponding optimum transmitter filter given in (6.50). Hence, we do not expect a large SINR gain in this case. However, when $\mathcal{E}_0 \ll E_{\mathcal{I}}$, the SINR at the output of the SINRMF receiver is approximately

$$\Gamma_{\text{SINRMF}}^{\text{Opt}} \approx \frac{\mathcal{E}_0}{E_{\mathcal{I}}}(1 + \beta) \quad (6.73)$$

which is $(1 + \beta)(1 - \beta/2)$ times larger than the SINR of the proposed receiver with

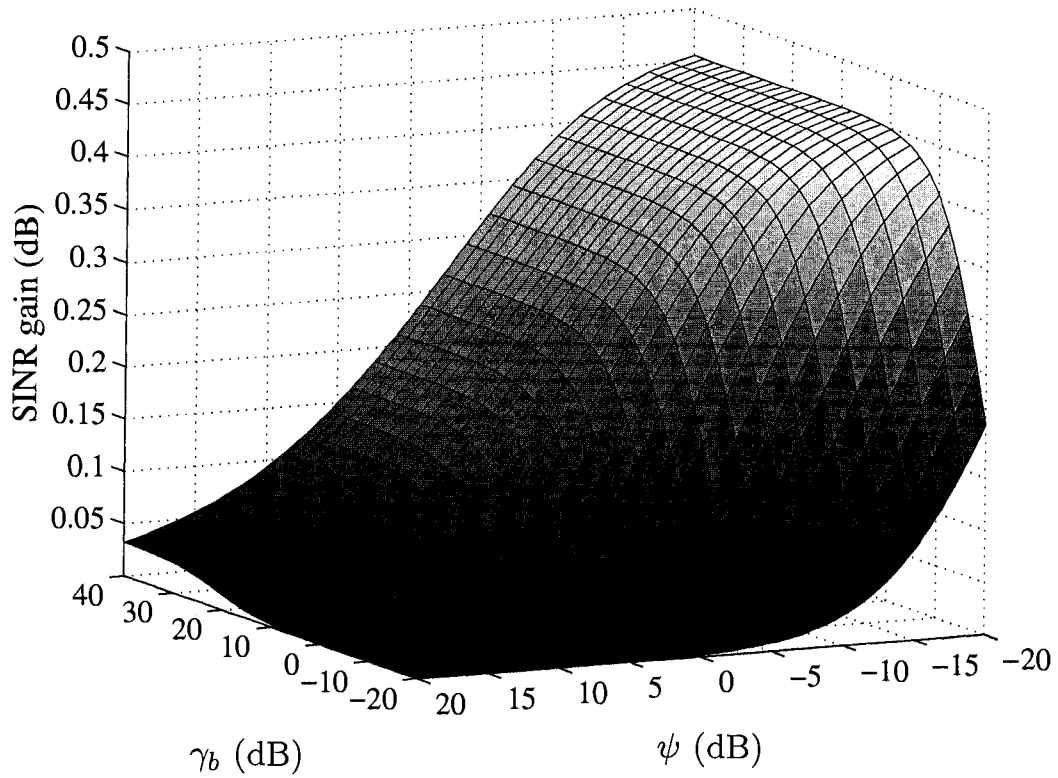


Figure 6.11. The SINR gain achieved by the SINRMMF receiver with an optimum transmitter filter over the proposed receiver with its corresponding optimum transmitter filter for Nakagami- m fading ($m = 0.5$), asynchronous CCI and $\beta = 0.35$.

optimum transmitter filter. This gain is approximately 0.47 dB for $\beta = 0.35$ as seen in Fig. 6.11. In this case, the maximum gain is achieved when $\mathcal{E}_0 \ll E_T$ and $\beta = 0.5$, and equals $9/8$ or equivalently 0.5115 dB.

Chapter 7

Conclusion and Future Work

7.1 Concluding Remarks

In this thesis, we studied the structure and performance of several well-known linear and nonlinear multiuser receivers. It was observed that the ML multiuser detector can achieve the best error probability performance among all multiuser receivers. The ML receiver is practically prohibited due to its large computational complexity. However, the performance of the ML receiver is important as it can be used as a reference of comparison for suboptimal multiuser receivers.

Jointly and individually optimal detectors were introduced and new analytical solutions for their exact bit error probability were derived and compared for a two-user synchronous Gaussian channel. It was observed that the IOD can outperform the JOD for small SNRs whereas for moderate and large SNRs the two receivers perform approximately the same. Consequently, using an IOD instead of a JOD for practical SNR values yields small performance improvement at the expense of substantially increased complexity. Thus, an IOD may not be desirable in many practical scenarios. We also analyzed the performance of the JOD in the presence of carrier phase errors for a bandlimited two-user channel, and showed that the jointly optimal detector can not achieve near single-user performance at very small values of SIR for sufficiently large carrier phase errors. In other words, we showed that the JOD receiver is near-far resistant if the carrier phase recovery is perfect or close to perfect, and substantial performance

improvements over the CMF receiver can not be achieved when SIR is small and phase recovery error is large.

Although optimal combining is an effective method to concurrently combat multiaccess interference and multipath fading in wireless communication systems, it is not the best detection strategy in the sense of minimizing the bit error probability. We showed that the ML and the optimal diversity receivers are both superior to the OC in having smaller error probability. The ML diversity receiver was shown to be composed of a bank of maximal ratio combiners, one for each matched filter, followed by an ML detector. We also showed that minimum error probability for a desired user can be achieved if the ML detector in the foregoing structure is replaced by an appropriate likelihood ratio test that picks the globally best hypothesis. The main advantage of the better than optimum combining receivers is that they can exploit the multipath fading to achieve a performance that is almost independent of the interference power and is very close to that of an optimum single-user receiver which makes use of MRC. We observed that the benefit is quite substantial, particularly for interference-dominated systems.

An interference-plus-noise whitening receiver was shown to degrade the performance of a microcellular wireless system in synchronous CCI due to the fact that in a synchronous channel the cochannel interference is a cyclostationary process rather than a wide-sense stationary process. This receiver, however, can improve the performance of a bandlimited microcellular system by increasing the SINR, provided that the CCI is asynchronous and under the impractical assumption that the transmission is ISI-free. We showed that in practical systems, the ISI generated by the whitening receiver can deteriorate both the SINR and the error probability performance of the receiver and make the whitening ineffective. We also showed that the whitening receiver can no longer maximize the SINR due to the ISI. In this case, the SINR-maximizing filter was derived and it was shown that a gain in SINR can be achieved in an asynchronous channel, particularly when the SIR is small. The improvement due to interference whitening depends crucially on the interference power or the choice of the excess bandwidth, both when the desired signal is not subject to fading and when it is subject to fading. Both FIR and IIR realizations of the SINR-maximizing receiver were shown to outperform the CMF receiver.

An ISI-free SINR-maximizing transmitter-receiver filter design for a BPSK signal corrupted with like-modulated interference and Gaussian noise was shown to have a flat spectrum across the entire available frequency spectrum with 100% excess bandwidth. We showed that this transmitter-receiver set can achieve a SINR gain as large as 1.76 dB over the conventional filter design without adding any additional complexity. The BER performance of the optimal system was compared to that of the conventional system when timing recovery is imperfect. It was observed that the optimal system is superior to the conventional system for practical values of the timing jitter. When the available excess bandwidth is less than 100%, we proposed two ISI-free techniques to design the transmitter-receiver filters for maximizing the output SINR. In both techniques the ISI-free transmission is achieved by setting the cascade of the transmitter and the receiver filters equal to a given Nyquist spectrum. In the first technique, each user was assumed to have its own transmitter and receiver filters, and these filters were concurrently designed to maximize the SINR for each user. In the second technique, all users were assumed to have the same transmitter filter and only their receiver filters were designed to achieve the maximum SINR. The ISI-free SINR-maximizing receiver filter designed based on the second method was shown to effectively restore much of the SINR loss due to ISI and is always superior to the CMF receiver in having larger SINR. We also observed that interference whitening is more beneficial when the SNR and the excess bandwidth are large, or when the SIR is small.

7.2 Suggestions for Future Work

- It would be highly useful to extend the BEP analysis presented in Chapter 3 to cases where there are more than two users in the channel and to cases where higher order modulation schemes, such as QPSK or MQAM, are used in the system. This appears to be a very challenging task.
- The BEP versus SIR curves depicted in Fig. 3.5 show that for some SIR ranges, reducing the signal power can improve the performance provided that the INR is fixed. This fact can be used to develop novel power control techniques for multiuser systems that make use of a JOR.

- In Section 3.3 we evaluated the BEP of the JOR in the case where carrier phase recovery was not perfect. The analysis given in this section can be readily executed for the case where there is frequency mismatch between the transmitter and receiver carriers.
- The BEP performance analysis of the ML receiver proposed in Section 4 has out-reaching interest. In particular, when all users employ the same signature waveforms, it is insightful to compare the performance of the ML receiver with that of the single-user receiver when the number of receiver antennae is large.
- MAI suppression is an important problem in ultra-wideband (UWB) systems [73]. An interference whitening receiver is an effective means to combat the MAI in UWB systems when only the total interference power is known at the receiver. Importantly, the whitening receiver can coexist with the receivers which exploit the multipath diversity of the UWB channels (e.g., RAKE receivers [74]). Indeed, in some cases, it can decrease the complexity of the latter receivers by reducing the number of their processing branches. This is a promising topic for investigation.
- It may be productive to investigate the efficacy of the interference whitening technique for mitigating the MAI in nonorthogonal cooperative communication systems where the source and the relay may transmit simultaneously over nonorthogonal subspaces [31].
- The optimum transmitter filters derived for the ISI-free and ISI-impaired SINR-maximizing receivers in Section 6.2 were analyzed based on the premise that the synchronization is perfect. The SINR analysis of these filters in the presence of synchronization errors is of great interest, because the timing recovery in practical systems is imperfect.

References

- [1] J. G. Proakis, *Digital Communications*, 3rd ed. New York: McGraw-Hill, 2000.
- [2] G. L. Stüber, *Principles of Mobile Communications*, 2nd ed. Norwell, MA: Kluwer Academic Publishers, 2001.
- [3] S. Verdú, *Multiuser Detection*, 1st ed. New York: Cambridge University Press, 1998.
- [4] A. M. Monk, M. Davis, L. B. Milstein, and C. W. Helstrom, "A noise-whitening approach to multiple access rejection—part I: theory and background," *IEEE J. Select. Areas Commun.*, vol. 12, no. 5, pp. 817–827, Jun. 1994.
- [5] Z. Xie, R. T. Short, and C. K. Rashforth, "A family of suboptimum detectors for coherent multi-user communications," *IEEE J. Select. Areas Commun.*, vol. 8, no. 4, pp. 683–690, May 1990.
- [6] K. S. Schneider, "Optimum detection of code division multiplexed signals," *IEEE Trans. Aerosp. Electron. Syst.*, vol. AES-15(1), no. 4, pp. 181–185, Jan. 1979.
- [7] S. Moshavi, E. G. Kanterakis, and D. L. Schilling, "Multistage linear receivers for DS-CDMA systems," *Int'l J. Wireless Info. Networks*, vol. 3, no. 1, pp. 1–17, Jan. 1996.
- [8] S. Verdú, "Minimum probability of error for asynchronous multiple access communication channels," in *IEEE Military Commun. Conf. (MILCOM)*, vol. 1, Nov. 1983, pp. 213–219.

- [9] S. Verdú, "Minimum probability of error for asynchronous Gaussian multiple-access channels," *IEEE Trans. Inform. Theory*, vol. IT-32, no. 1, pp. 85–96, Jan. 1986.
- [10] S. Moshavi, "Multi-user detection for DS-CDMA communication," *IEEE Commun. Mag.*, vol. 34, no. 10, pp. 124–136, Oct. 1996.
- [11] R. Kohno, H. Imai, M. Hatori, and S. Pasupathy, "Combination of an adaptive array antenna and a canceller of interference for direct-sequence spread-spectrum multiple-access system," *IEEE J. Select. Areas Commun.*, vol. 8, no. 4, pp. 675–682, May 1990.
- [12] A. J. Viterbi, "Very low-rate convolutional codes for maximum theoretical performance of spread-spectrum multiple-access channels," *IEEE J. Select. Areas Commun.*, vol. 8, no. 4, pp. 641–649, May 1990.
- [13] P. Patel and J. Holtzman, "Analysis of a simple successive interference cancellation scheme in a DS/CDMA system," *IEEE J. Select. Areas Commun.*, vol. 12, no. 5, pp. 796–807, Jun. 1994.
- [14] M. K. Varanasi and B. Aazhang, "Multistage detection in asynchronous code-division multiple access communications," *IEEE Trans. Commun.*, vol. 38, no. 4, pp. 509–519, Apr. 1990.
- [15] H. V. Poor and S. Verdú, "Single-user detectors for multiuser channels," *IEEE Trans. Commun.*, vol. 36, no. 1, pp. 50–60, Jan. 1988.
- [16] Y. C. Yoon and H. Leib, "Matched filters with interference suppression capabilities for DS-CDMA," *IEEE J. Select. Areas Commun.*, vol. 14, no. 8, pp. 1510–1521, Oct. 1996.
- [17] J. Cheng and N. C. Beaulieu, "Accurate DS-CDMA bit-error probability calculation in Rayleigh fading," *IEEE Trans. Wireless Commun.*, vol. 1, no. 1, pp. 3–15, Jan. 2002.
- [18] A. Papoulis and S. U. Pillai, *Probability, Random Variables and Stochastic Processes*, 4th ed. New York: McGraw-Hill, 2000.

- [19] R. Lupas and S. Verdú, "Linear multiuser detectors for synchronous code-division multiple-access channels," *IEEE Trans. Inform. Theory*, vol. 35, no. 1, pp. 123–136, Jan. 1989.
- [20] R. Lupas-Golaszewski and S. Verdú, "Asymptotic efficiency of linear multiuser detectors," in *IEEE Conf. on Decision and Control*, vol. 3, Athens, Greece, Dec. 1986, pp. 2094–2100.
- [21] H. V. Poor and S. Verdú, "Probability of error in MMSE multiuser detection," *IEEE Trans. Inform. Theory*, vol. 43, no. 3, pp. 858–871, May 1997.
- [22] R. R. Müller and S. Verdú, "Design and analysis of low-complexity interference mitigation on vector channels," *IEEE J. Select. Areas Commun.*, vol. 19, no. 8, pp. 1429–1441, Aug. 2001.
- [23] Z. Zvonar and D. Brady, "Multiuser detection in single-path fading channels," *IEEE Trans. Commun.*, vol. 42, no. 2/3/4, pp. 1729–1739, Feb./Mar./Apr. 1994.
- [24] Y. Z. Mohasseb, U. Mitra, and M. P. Fitz, "Bounding the performance of a narrow-band MUD receiver," in *IEEE Global Telecommun. Conf.*, vol. 2, San Antonio, TX, Nov. 2001, pp. 832–837.
- [25] Y. Mohasseb, M. P. Fitz, and U. Mitra, "An improved bound on the performance of maximum-likelihood multiuser detection receivers in Rayleigh fading," *IEEE Trans. Inform. Theory*, vol. 52, no. 3, pp. 1184–1196, Mar. 2006.
- [26] R. Kohno, H. Imai, M. Hatori, and S. Pasupathy, "An adaptive canceller of cochannel interference for spread-spectrum multiple-access communication networks in a power line," *IEEE J. Select. Areas Commun.*, vol. 8, no. 4, pp. 691–699, May 1990.
- [27] M. K. Varanasi and B. Aazhang, "Near-optimum detection in synchronous code-division multiple-access systems," *IEEE Trans. Commun.*, vol. 39, no. 5, pp. 725–736, May 1991.

- [28] A. Duel-Hallen, "Decorrelation decision-feedback multi-user detector for synchronous code-division multiple access channel," *IEEE Trans. Commun.*, vol. 41, no. 2, pp. 285–290, Feb. 1993.
- [29] A. Duel-Hallen, "A family of multi-user decision-feedback detectors for asynchronous code-division multiple access channels," *IEEE Trans. Commun.*, vol. 43, no. 2/3/4, pp. 421–434, Feb./Mar./Apr. 1995.
- [30] A. Hafeez, K. J. Molnar, H. Arslan, G. E. Bottomley, and R. Ramésh, "Adaptive joint detection of cochannel signals for TDMA handsets," *IEEE Trans. Commun.*, vol. 52, no. 10, pp. 1722–1732, Oct. 2004.
- [31] K. Azarian, H. El Gamal, and P. Schniter, "On the achievable diversity-multiplexing tradeoff in half-duplex cooperative channels," *IEEE Trans. Inform. Theory*, vol. 51, no. 12, pp. 4152–4172, Dec. 2005.
- [32] R. Kwan and C. Leung, "Optimal detection of a BPSK signal contaminated by interference and noise," *IEEE Commun. Lett.*, vol. 6, no. 2, pp. 225–227, Jun. 2002.
- [33] T. V. Poon and N. C. Beaulieu, "Performance analysis of a jointly optimal BPSK receiver in cochannel interference," in *IEEE Global Telecommun. Conf.*, vol. 3, San Francisco, CA, Dec. 2003, pp. 1721–1725.
- [34] T. V. Poon and N. C. Beaulieu, "Jointly and individually optimum receivers for BPSK signals in cochannel interference plus noise," in *IEEE Pacific Rim Conf. on Commun., Comput., Signal Processing*, vol. 2, Victoria, Canada, Aug. 2003, pp. 530–532.
- [35] T. V. Poon and N. C. Beaulieu, "Error performance analysis of a jointly optimal single-cochannel-interferer BPSK receiver," *IEEE Trans. Commun.*, vol. 7, no. 52, pp. 1051–1054, Jul. 2004.
- [36] J. W. Craig, "A new simple and exact result for calculating the probability of error for two-dimensional signal constellations," in *IEEE Military Commun. Conf. (MILCOM)*, vol. 2, Boston, MA, Nov. 1991, pp. 571–575 (25.5.1–25.5.5).

- [37] M. Moretti, E. Nostrato, S. Piagneri, and G. J. M. Janssen, "Performance analysis of a narrowband two-signal receiver based on joint detection," in *IEEE Veh. Technol. Conf.*, vol. 5, Boston, Sep. 2000, pp. 2312–2316.
- [38] S. J. Grant and J. K. Cavers, "Performance enhancement through joint detection of cochannel signals using diversity arrays," *IEEE Trans. Commun.*, vol. 46, no. 8, pp. 1038–1049, Aug. 1998.
- [39] G. J. K. Janssen, "Receiver structure for simultaneous reception of two BPSK modulated cochannel signals," *IEE Elect. Lett.*, vol. 29, no. 12, pp. 1095–1097, Jun. 1993.
- [40] A. M. Rabiei and N. C. Beaulieu, "A simple, intuitive expression for the BER of a jointly optimal single cochannel interferer BPSK receiver," *IEEE Commun. Lett.*, vol. 9, no. 3, pp. 201–203, Mar. 2005.
- [41] I. S. Gradshteyn and I. M. Ryzhik, *Tables of Integrals, Series, and Products*, 6th ed. San Diego, CA: Academic Press, 2000.
- [42] U. Mengali and A. N. D'Andrea, *Synchronization Techniques for Digital Receivers*, 1st ed. New York: Plenum Press, 1997.
- [43] J. H. Winters, "Optimum combining in digital mobile radio with cochannel interference," *IEEE J. Select. Areas Commun.*, vol. SAC-2, no. 4, pp. 528–539, Jul. 1984.
- [44] H. Gao, P. J. Smith, and M. V. Clark, "Theoretical reliability of MMSE linear diversity combining in Rayleigh-fading additive interference channels," *IEEE Trans. Commun.*, vol. 46, no. 5, pp. 666–672, May 1998.
- [45] W. C. Jakes, Ed., *Microwave Mobile Communications*. New York: IEEE Press, 1994.
- [46] E. Villier, "Performance analysis of optimum combining with multiple interferers in flat Rayleigh fading," *IEEE Trans. Commun.*, vol. 47, no. 10, pp. 1503–1510, Oct. 1999.

- [47] M. Chiani, M. Z. Win, A. Zanella, R. K. Mallik, and J. H. Winters, "Bounds and approximations for optimum combining of signals in the presence of multiple cochannel interferers and thermal noise," *IEEE Trans. Commun.*, vol. 51, no. 2, pp. 296–307, Feb. 2003.
- [48] A. Shah and A. M. Haimovich, "Performance analysis of optimum combining in wireless communications with Rayleigh fading and cochannel interference," *IEEE Trans. Commun.*, vol. 46, no. 4, pp. 473–479, Apr. 1998.
- [49] A. Shah and A. M. Haimovich, "Performance analysis of maximal ratio combining and comparison with optimum combining for mobile radio communications with cochannel interference," *IEEE Trans. Veh. Technol.*, vol. 49, no. 4, pp. 1454–1463, Jul. 2000.
- [50] C. Chayawan and V. A. Aalo, "On the outage probability of optimum combining and maximal ratio combining schemes in an interference-limited Rice fading channel," *IEEE Trans. Commun.*, vol. 50, no. 4, pp. 532 – 535, Apr. 2002.
- [51] Q. T. Zhang and X. W. Cui, "Outage probability for optimum combining of arbitrarily faded signals in the presence of correlated Rayleigh interferers," *IEEE Trans. Veh. Technol.*, vol. 53, no. 4, pp. 1043–1051, Jul. 2004.
- [52] Y. A. Chau and S.-H. Yu, "Optimal diversity for multiuser detection with soft-decision decoding in fading channels," in *IEEE Veh. Technol. Conf.*, vol. 1, Amsterdam, Netherlands, Sep. 1999, pp. 603–607.
- [53] A. J. Viterbi, *CDMA: Principles of Spread Spectrum Communication*. MA: Addison-Wesley, 1995.
- [54] M. K. Simon and M.-S. Alouini, *Digital Communication over Fading Channels*, 2nd ed. New York: Wiley, 2005.
- [55] A. M. Rabiei and N. C. Beaulieu, "Exact error probability of a bandlimited single-interferer maximum-likelihood BPSK receiver in AWGN," *IEEE Trans. Wireless Commun.*, vol. 6, no. 1, pp. 30–34, Jan. 2007.

- [56] M. Davis, A. Monk, and L. B. Milstein, "A noise-whitening approach to multiple access rejection—part II: implementation issues," *IEEE J. Select. Areas Commun.*, vol. 14, no. 8, pp. 1488–1499, Oct. 1996.
- [57] K. Sivanesan and N. C. Beaulieu, "Interference whitening receivers for CCI mitigation in micro-cellular BPSK systems," in *IEEE Veh. Technol. Conf.*, vol. 4, Los Angeles, CA, Sep. 2004, pp. 2330–2334.
- [58] N. C. Beaulieu and K. Sivanesan, "CCI mitigation using interference whitening in bandlimited micro-cellular BPSK systems," in *IEEE Global Telecommun. Conf.*, vol. 5, Dallas, TX, Nov./Dec. 2004, pp. 3083–3087.
- [59] N. C. Beaulieu, C. C. Tan, and M. O. Damen, "A "better than" Nyquist pulse," *IEEE Commun. Lett.*, vol. 5, no. 9, pp. 367–368, Sep. 2001.
- [60] T. F. Wong, T. M. Lok, and J. S. Lehnert, "Asynchronous multiple-access interference suppression and chip waveform selection with aperiodic random sequences," *IEEE Trans. Commun.*, vol. 47, no. 1, pp. 103–114, Jan. 1999.
- [61] N. C. Beaulieu, "The evaluation of error probabilities for intersymbol and cochannel interference," *IEEE Trans. Commun.*, vol. 39, no. 12, pp. 1740–1749, Dec. 1991.
- [62] D. A. George, "Matched filters for interfering signals," *IEEE Trans. Inform. Theory*, vol. 11, no. 1, pp. 153–154, Jan. 1965.
- [63] C. Fox, *An Introduction to the Calculus of Variations*. New York: Dover, 1988.
- [64] S. U. H. Qureshi, "Adaptive equalization," *Proc. IEEE*, vol. 73, no. 9, pp. 1349–1387, Sep. 1985.
- [65] G. S. Ammar and W. B. Gragg, "Superfast solution of real positive definite Toeplitz systems," *SIAM J. Matrix Anal. Appl.*, vol. 9, no. 1, pp. 61–76, Jan. 1988.
- [66] N. Levinson, "The Wiener RMS (root mean square) error criterion in filter design and prediction," *J. Math. Phys.*, vol. 25, no. 4, pp. 261–278, 1947.

- [67] N. C. Beaulieu and J. Cheng, "Precise error-rate analysis of bandwidth-efficient BPSK in Nakagami fading and cochannel interference," *IEEE Trans. Commun.*, vol. 52, no. 1, pp. 149–158, Jan. 2004.
- [68] A. M. Rabiei, N. C. Beaulieu, and P. D. Rahmizadeh, "Optimal 100% excess bandwidth signaling in cochannel interference," *IEEE Commun. Lett.*, vol. 11, no. 5, pp. 375–377, May 2007.
- [69] M. Abramowitz and I. A. Stegun, Eds., *Handbook of Mathematical Functions with Formulas, Graphs, and Mathematical Tables*. New York: Dover, 1974.
- [70] T. S. Rappaport, *Wireless Communications: Principles and Practice*, 2nd ed. New Jersey: Prentice-Hall, 2001.
- [71] N. W. K. Lo, D. D. Falconer, and A. U. H. Sheikh, "Adaptive equalization for cochannel interference in a multipath fading environment," *IEEE Trans. Commun.*, vol. 43, no. 2/3/4, pp. 1441–1453, Feb./Mar./Apr. 1995.
- [72] R. W. Lucky, J. Salz, and E. J. Weldon Jr., *Principles of Data Communication*. New York: McGraw-Hill, 1968.
- [73] M. Z. Win and R. A. Scholtz, "Ultra-wide bandwidth time-hopping spread-spectrum impulse radio for wireless multiple-access communications," *IEEE Trans. Commun.*, vol. 48, no. 4, pp. 679–689, Apr. 2000.
- [74] M. Z. Win and R. A. Scholtz, "On the energy capture of ultrawide bandwidth signals in dense multipath environments," *IEEE Commun. Lett.*, vol. 2, no. 9, pp. 245–247, Sep. 1998.
- [75] J. G. Proakis and D. G. Manolakis, *Digital Signal Processing: Principles, Algorithms, and Applications*, 3rd ed. New Jersey: Prentice-Hall, 1996.

Appendix A

Proof of Fact 1

We first assume θ to be in each of the second, third and fourth quadrants. For each case we express θ in terms of a $\theta_0 \in [0, \pi/2)$ and then show that the receiver's BEP in each case is the same as the BEP for the case where the phase difference between desired and interfering unmodulated carriers is θ_0 .

A.1 $\theta \in [\frac{\pi}{2}, \pi)$

In this case, θ can be expressed as $\theta = \pi - \theta_0$. If we replace θ in (3.9) with $\pi - \theta_0$, we conclude that the ordinates of all constellation points remain unchanged but the abscissas of C_0 and C_2 must be exchanged with those of C_1 and C_3 , respectively. This causes the new constellation points¹ and decision boundaries to be the reflection in the y -axis of the constellation points and decision boundaries of the case when θ is in the first quadrant, as shown in Fig. A.1. Using the facts that n_0 and n_1 are i.i.d. Gaussian RVs and the information bits are equiprobable, one concludes that the BEP in this case is the same as the BEP for the case that the unmodulated carriers of the users have a phase difference equal to θ_0 . Note that the probability of error expression given in (3.25) is only valid for θ_0 and should be revised for $\theta \in [\pi/2, \pi)$. Since $\theta = \pi - \theta_0$, $\sin \theta$ is equal to $\sin \theta_0$ while $\cos \theta = -\cos \theta_0$. Thus, $\cos \theta$ in (3.25) should be replaced by $-\cos \theta$ to get the correct expression for the BEP in this case.

¹In this case, C_0 , C_1 , C_2 and C_3 are the reflection in the y -axis of C_2 , C_3 , C_0 and C_1 of the case where $\theta \in [0, \pi/2)$, respectively.

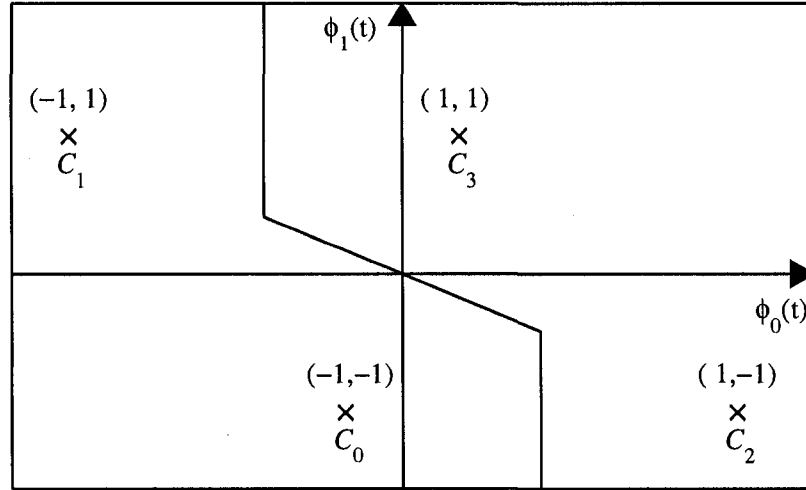


Figure A.1. The received signal constellation points and decision boundaries for $\pi/2 \leq \theta < \pi$.

A.2 $\theta \in [\pi, \frac{3\pi}{2})$

Clearly, θ can be expressed as $\theta = \pi + \theta_0$. Replacing θ in (3.9) with $\pi + \theta_0$, one concludes that in this case the locations of the constellation points will be the same as those in Fig. 3.1, with C_0 and C_2 exchanged with C_1 and C_3 , respectively. These exchanges, however, do not affect the decision regions and boundaries as shown in Fig. A.2. Thus, the receiver's BEP is the same as that of the case when the phase difference between unmodulated carriers is θ_0 . Furthermore, in this case $\cos \theta$ and $\sin \theta$ are the negatives of $\cos \theta_0$ and $\sin \theta_0$, respectively. Therefore, one has to negate both $\sin \theta$ and $\cos \theta$ in (3.25) to obtain a correct expression for the BEP in this case.

A.3 $\theta \in [\frac{3\pi}{2}, 2\pi)$

In this case, one can express θ as $\theta = 2\pi - \theta_0$. Replacing θ in (3.9) with $2\pi - \theta_0$ does not change the abscissas of the constellation points while it causes the ordinates of C_0 and C_2 to be exchanged with those of C_1 and C_3 , respectively. Thus, the new constellation points and decision boundaries (shown in Fig. A.3) are the reflection in the x-axis of those shown in Fig. 3.1. For the same reasons as mentioned for A.1, the receiver's BEP in this case is the same as that of the case where unmodulated carriers of the users

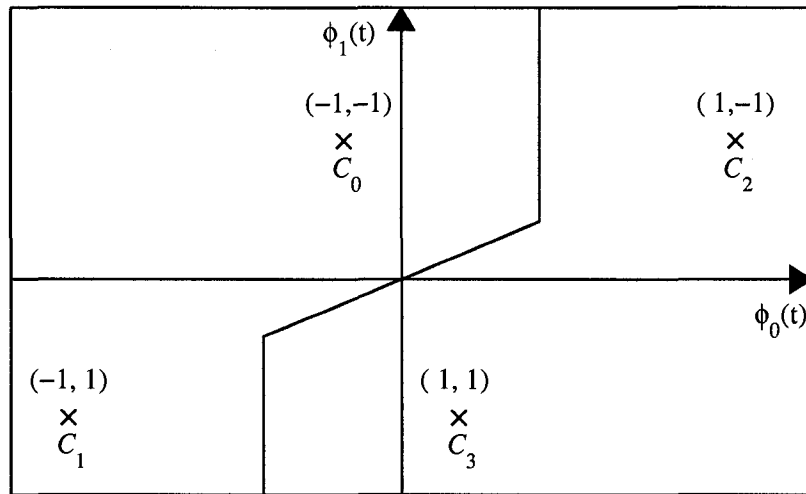


Figure A.2. The received signal constellation points and decision boundaries for $\pi \leq \theta < 3\pi/2$.

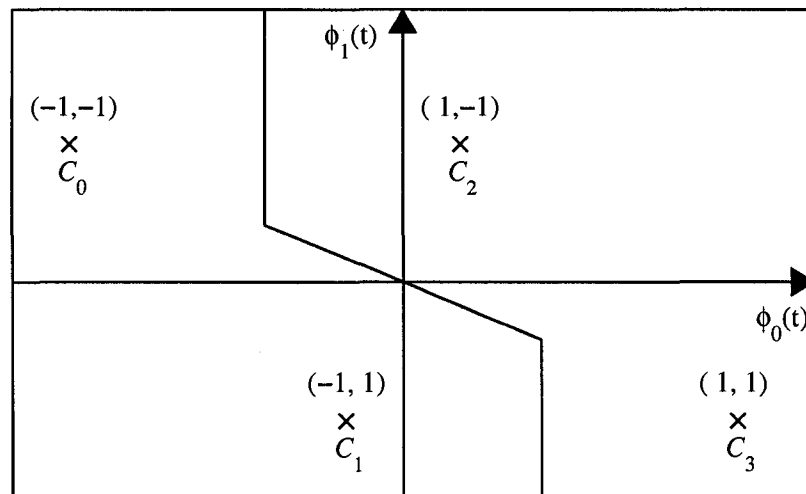


Figure A.3. The received signal constellation points and decision boundaries for $3\pi/2 \leq \theta < 2\pi$.

sharing the channel, have a phase difference equal to θ_0 . Moreover, in this case $\sin \theta$ is the negative of $\sin \theta_0$. Hence, one has to negate $\sin \theta$ in (3.25) to get the appropriate expression for the BEP when $\theta \in [3\pi/2, 2\pi)$.

Appendix B

Evaluating \mathring{E}_g

In order to evaluate \mathring{E}_g , one can use the fact that $\mathring{E}_g = E_g - g^2(0)$, where E_g is $g_d(\cdot)$'s energy and $g(0)$ is given by (5.48b). Using Parseval's theorem [75], one can obtain

$$E_g = \frac{T}{2\pi} \int_{-\pi}^{\pi} |G_d(e^{j\omega T})|^2 d\omega \quad (\text{B.1})$$

$$= \frac{1}{2\pi T} \int_{-\frac{\pi}{T}}^{\frac{\pi}{T}} \left| \sum_{n=-\infty}^{\infty} G\left(\omega - \frac{2\pi n}{T}\right) \right|^2 d\omega \quad (\text{B.2})$$

where $G_d(e^{j\omega})$ is the Fourier transform of $g_d(i)$. Note that the summation in (B.2) denotes the folded (aliased) spectrum of $g(t)$ when the sampling rate is $1/T$ [75]. Since in our problem, $G(\omega)$ is bandlimited to $[-\pi(1 + \beta)/T, \pi(1 + \beta)/T]$ and the integration in (B.2) is over $[-\pi/T, \pi/T]$, only three terms of the summation on the right of (B.2) (corresponding to $n = -1, 0$ and 1) contribute to the integral in this equation. By expanding this integrand, one can obtain

$$\begin{aligned} E_g = \frac{1}{2\pi T} & \left[\int_{-\frac{\pi}{T}}^{\frac{\pi}{T}} G^2\left(\omega - \frac{2\pi}{T}\right) d\omega + \int_{-\frac{\pi}{T}}^{\frac{\pi}{T}} G^2(\omega) d\omega + \int_{-\frac{\pi}{T}}^{\frac{\pi}{T}} G^2\left(\omega + \frac{2\pi}{T}\right) d\omega \right. \\ & + 2 \int_{-\frac{\pi}{T}}^{\frac{\pi}{T}} G(\omega) G\left(\omega + \frac{2\pi}{T}\right) d\omega + 2 \int_{-\frac{\pi}{T}}^{\frac{\pi}{T}} G(\omega) G\left(\omega - \frac{2\pi}{T}\right) d\omega \\ & \left. + 2 \int_{-\frac{\pi}{T}}^{\frac{\pi}{T}} G\left(\omega + \frac{2\pi}{T}\right) G\left(\omega - \frac{2\pi}{T}\right) d\omega \right]. \quad (\text{B.3}) \end{aligned}$$

The last integral on the right of (B.3) is zero because $G(\omega + 2\pi/T)$ and $G(\omega - 2\pi/T)$ do not overlap. Now, we change ω to $\omega + 2\pi/T$ in the first integral and ω to $\omega - 2\pi/T$ in the third and fourth integrals in (B.3) and use the fact that $G(\omega)$ is an even function

to obtain

$$E_g = \frac{1}{2\pi T} \left[\int_{-\frac{(1+\beta)\pi}{T}}^{\frac{(1+\beta)\pi}{T}} G^2(\omega) d\omega + 4 \int_{\frac{(1-\beta)\pi}{T}}^{\frac{\pi}{T}} G(\omega) G\left(\omega - \frac{2\pi}{T}\right) d\omega \right]. \quad (\text{B.4})$$

Thus, after some algebraic manipulations, E_g for the RC and BTD pulses can be obtained as

$$E_{g,\text{RC}} = \frac{1-\beta}{(1+E_I)^2} + \frac{\beta}{E_I^2} \left[4 - \frac{E_I^2}{(1+E_I)^2} - \frac{8+E_I(16+7E_I)}{(1+E_I)^{3/2}(2+E_I)} \right] \quad (\text{B.5})$$

$$E_{g,\text{BTD}} = \frac{1-\beta}{(1+E_I)^2} + \frac{\beta}{E_I^2} \log_2 \left[\frac{(1+E_I)^{\frac{4+3E_I}{2+E_I}}}{(1+E_I/2)^{\frac{3E_I^2+8E_I+4}{(1+E_I)^2}}} \right] \quad (\text{B.6})$$

respectively. Now, we use eqs. (5.48b)–(5.48d) along with (B.5) and (B.6) to obtain \dot{E}_g for the RC and BTD pulses as

$$\dot{E}_{g,\text{RC}} = \frac{\beta}{E_I^2} \left[4 - \frac{E_I^2}{(1+E_I)^2} - \frac{8+E_I(16+7E_I)}{(1+E_I)^{3/2}(2+E_I)} \right] - \frac{\mathcal{G}_{\text{RC}}(\mathcal{G}_{\text{RC}}+2)}{(1+E_I)^2} \quad (\text{B.7})$$

$$\dot{E}_{g,\text{BTD}} = \frac{\beta}{E_I^2} \log_2 \left[\frac{(1+E_I)^{\frac{4+3E_I}{2+E_I}}}{(1+E_I/2)^{\frac{3E_I^2+8E_I+4}{(1+E_I)^2}}} \right] - \frac{\mathcal{G}_{\text{BTD}}(\mathcal{G}_{\text{BTD}}+2)}{(1+E_I)^2} \quad (\text{B.8})$$

respectively. Clearly, when $\beta = 0$, \dot{E}_g and, thus, the ISI become zero for both pulses.

Appendix C

Evaluating the SINR of the SINRMF Receiver

In order to find the SINR of the SINRMF filter, we evaluate each of the integrals given in eq. (5.33). To this end, we first use eqs. (5.37)–(5.39) to write the first integral in the denominator of (5.33) as

$$\begin{aligned} \mathcal{I}_1 &= \int_{-\infty}^{\infty} \frac{(1 + P_T G_T^2(\omega)) G^2(\omega)}{G_T^2(\omega)} d\omega \\ &= \int_{-\infty}^{\infty} G^C(\omega) [G^D(\omega)]^2 d\omega \\ &= \sum_{n=-\infty}^{\infty} \int_{\frac{\pi}{T}(2n-1)}^{\frac{\pi}{T}(2n+1)} G^C(\omega) [G^D(\omega)]^2 d\omega \end{aligned} \quad (\text{C.1})$$

$$= \sum_{n=-\infty}^{\infty} \int_{-\frac{\pi}{T}}^{\frac{\pi}{T}} G^C\left(\omega - \frac{2\pi n}{T}\right) \left[G^D\left(\omega - \frac{2\pi n}{T}\right)\right]^2 d\omega \quad (\text{C.2})$$

where the last equation obtained by changing the variable ω to $\omega - 2\pi n/T$ in (C.1). Now, using the fact that integration and summation in (C.2) are interchangeable along with the fact that $G^D(\omega)$ is a periodic function with period $2\pi/T$, one can obtain

$$\mathcal{I}_1 = \int_{-\frac{\pi}{T}}^{\frac{\pi}{T}} \left[G^D(\omega)\right]^2 \sum_{n=-\infty}^{\infty} G^C\left(\omega - \frac{2\pi n}{T}\right) d\omega. \quad (\text{C.3})$$

Using (5.38), it can be shown that

$$\sum_{n=-\infty}^{\infty} G^C\left(\omega - \frac{2\pi n}{T}\right) = \frac{T}{\mathcal{E}_0} \left[\frac{1 - G^D(\omega)}{G^D(\omega)} \right] \quad (\text{C.4})$$

Thus (C.3) can be rewritten as

$$\mathcal{I}_1 = \frac{T}{\mathcal{E}_0} \int_{-\frac{\pi}{T}}^{\frac{\pi}{T}} G^{\mathcal{D}}(\omega) [1 - G^{\mathcal{D}}(\omega)] d\omega. \quad (\text{C.5})$$

The second and third integrals in the denominator of (5.33) can be obtained in a similar manner as

$$\begin{aligned} \mathcal{I}_2 &= \int_{-\frac{\pi}{T}}^{\frac{\pi}{T}} \left| \sum_{n=-\infty}^{\infty} G\left(\omega - \frac{2\pi n}{T}\right) \right|^2 d\omega \\ &= \frac{T^2}{\mathcal{E}_0^2} \int_{-\frac{\pi}{T}}^{\frac{\pi}{T}} [1 - G^{\mathcal{D}}(\omega)]^2 d\omega. \end{aligned} \quad (\text{C.6})$$

and

$$\begin{aligned} \mathcal{I}_3 &= \int_{-\infty}^{\infty} G(\omega) d\omega \\ &= \int_{-\frac{\pi}{T}}^{\frac{\pi}{T}} G^{\mathcal{D}}(\omega) \sum_{n=-\infty}^{\infty} G^{\mathcal{C}}\left(\omega - \frac{2\pi n}{T}\right) d\omega \\ &= \frac{T}{\mathcal{E}_0} \int_{-\frac{\pi}{T}}^{\frac{\pi}{T}} [1 - G^{\mathcal{D}}(\omega)] d\omega. \end{aligned} \quad (\text{C.7})$$

respectively. Thus, the SINR of the SINRMF receiver in (5.33) can be evaluated as

$$\begin{aligned} \Gamma_{\text{SINRMF}} &= \frac{\frac{\mathcal{E}_0}{2\pi} \mathcal{I}_3^2}{\mathcal{I}_1 + \frac{\mathcal{E}_0}{T} \mathcal{I}_2 - \frac{\mathcal{E}_0}{2\pi} \mathcal{I}_3^2} \\ &= \frac{\frac{T}{2\pi} \int_{-\frac{\pi}{T}}^{\frac{\pi}{T}} [1 - G^{\mathcal{D}}(\omega)] d\omega}{1 - \frac{T}{2\pi} \int_{-\frac{\pi}{T}}^{\frac{\pi}{T}} [1 - G^{\mathcal{D}}(\omega)] d\omega} \\ &= \frac{1 - \frac{T}{2\pi} \int_{-\frac{\pi}{T}}^{\frac{\pi}{T}} G^{\mathcal{D}}(\omega) d\omega}{\frac{T}{2\pi} \int_{-\frac{\pi}{T}}^{\frac{\pi}{T}} G^{\mathcal{D}}(\omega) d\omega} \\ &= \frac{1 - \Lambda_{\text{SINRMF}}}{\Lambda_{\text{SINRMF}}} \end{aligned} \quad (\text{C.8})$$

where Λ_{SINRMF} is defined in (5.40b).